ATMIRE

Title	Integrated seismic and geologic analysis of Waddle Creek field in southeastern Moffat County, Colorado
Item Type	Text
Authors	Lin, Vivian
Publisher	Colorado School of Mines. Arthur Lakes Library
Rights	Copyright of the original work is retained by the author.
Download date	2026-11-27 23:13:30
Link to Item	https://hdl.handle.net/11124/78995

INTEGRATED SEISMIC AND GEOLOGIC ANALYSIS OF WADDLE CREEK FIELD IN SOUTHEASTERN MOFFAT COUNTY, COLORADO

by

Vivian Lin

A thesis submitted to the Faculty and the Board of Trustees of the Colorado School of Mines in partial fulfillment of the requirements for the degree of a Master of Science (Geology).

Golden, Colorado

Date_____

Signed: _____

Vivian Lin

Signed: _____

Dr. J. Frederick Sarg

Thesis Advisor

Golden, Colorado

Date _____

Signed: _____

Dr. John D. Humphrey

Department Head

Department of Geology and Geological Engineering

ABSTRACT

The Niobrara Formation is a self-sourced resource play and unlike in conventional reservoirs, key production can occur in "sweet spots" that may extend down-dip off structure. Mapping the location and orientations of high-density fracture zones is key to identifying these productive areas in tight petroleum systems. This study integrates a 3D seismic interpretation with well log analysis and forward modeling in order to determine how high density fracture and fault zones in the Niobrara relate to regional structures and paleo-tectonic controls. Seismic curvature, variance, and ant-tracking attribute maps show 5 major thrust faults, several smaller reverse faults, a few normal faults, and a number of linear features below seismic resolution. The features identified on these attribute maps suggest transpressional tectonics with an overall WSW-ENE direction of shortening from the Laramide orogeny. During compression, the rigid Colorado Plateau to the southwest reinforced the orientation of pre-existing NW-SE trending faults in the study area resulting in strain partitioning. This formed a complex transition zone between two major NW-trending thrust faults. Production distribution suggests the existence of fracture swarms associated with this transition zone with the best production occuring along linear features that align with expected orientations for conjugate fracture sets in a left lateral strike-slip fault system.

Isochrons of key time intervals highlight three major tectonic periods: Precambrian extension, Pennsylvanian uplift and erosion, and Late Cretaceous to Middle Tertiary compression. These tectonic periods are separated by intervals of quiescence and widespread, horizontal deposition. Forward modeling of the study area tests the validity of the structural history interpretation and highlights areas of high strain that may have resulted in fracture formation. The strain analysis suggests that medium amounts of strain help improve production but extremely high strains result in dry holes. One possible explanation is that overly intense fracturing allows water to flow easily through the area resulting in cementation whereas too little fracturing prevents production and thus a "medium" amount of strain is necessary to allow for production but avoid cementation.

This integrated approach using seismic and well log analyses may be applied to explore other trends within the Sand Wash basin and nearby regions particularly where pre-existing

structures affected stress and strain distributions during the Laramide orogeny. The relationships identified in this study between current stress regimes and paleo-tectonic controls allow for better identification and prediction of "sweet spots" when pre-existing structures affect the distribution of stress and strain. In areas where good seismic and well log data are available, the same procedures conducted in this study may be applied to produce potential high-density fracture and fault zone maps that may then be analyzed to determine the most prospective locations. Even in areas where seismic and well log data may be limited, these relationships permit exploration play trends to be high-graded for further data acquisition and analyses.

TABLE OF CONTENTS

ABSTRACT iii
LIST OF FIGURES vi
LIST OF TABLES ix
ACKNOWLEDGMENTS x
CHAPTER 1 INTRODUCTION 1
1.1 Importance 1
1.2 Objectives 2
CHAPTER 2 BACKGROUND 3
2.1 Regional setting 3
2.1.1 General stratigraphy and lithology 3
2.1.2 Niobrara petroleum system 11
2.1.3 Regional structure 15
2.1.4 Local structure 15
2.2 Predicting fracture orientations 19
2.3 Basics of seismic curvature attributes 23
CHAPTER 3 METHODOLOGY 24
3.1 Well log top picks 24
3.2 Seismic well tie 26
3.3 Seismic analysis 26
3.3.1 Durham Ranch 3D seismic volume dataset 28
3.3.2 Digitizing horizons 29
3.3.3 Seismic attribute analysis 30
3.3.4 Convert two-way time horizon to depth horizon 31
3.4 Forward model 32
3.5 Production data 33
CHAPTER 4 RESULTS 34
4.1 Well log results 34
4.2 Production data 35
4.3 Seismic data 36
4.3.1 Present-day subsurface structure 36
4.3.2 Seismic Attributes 51
4.3.3 Isochron maps 59
4.4 3D Move model 64
CHAPTER 5 DISCUSSION 66
5.1 Fracture prediction 66
5.1.1 Curvature anomalies and production trends 66
5.1.2 Strain analysis 70
5.2 Paleo-tectonic history 71
CHAPTER 6 CONCLUSIONS 74
6.1 Conclusions 74
6.2 Recommended future work 74
REFERENCES CITED 76

LIST OF FIGURES

Figure 2.1	Location map of southwestern Wyoming, northeastern Utah, and northwestern Colorado showing the location of the Southwestern Wyoming Province, structural configuration, intrabasin uplifts, and subbasins (modified Finn and Johnson,1995).	4
Figure 2.2	Surface geologic map of the Northwest quarter of Colorado with survey area outlined (modified Tweto,1979).	5
Figure 2.3	General stratigraphic column for the Uranium Peak area, about 15 mi southwest of the study area (modified Robertson et al., 1995).	6
Figure 2.4	A type log and subsurface cross section show the gamma ray and induction log characteristics of the Niobrara Formation in northwestern Colorado (modified from modified Vincelette and Foster, 1992, in Finn and Johnson, 2005).	7
Figure 2.5	Paleogeographic reconstruction of the Western Interior Seaway during Coniacian-Santonian time (modified Finn and Johnson, 1995, after Longman et al., 1998).	9
Figure 2.6	Plots of data from Rock-Eval analysis of kerogen of 28 Niobrara Formation samples, USGS Organic Geochemistry Database (Finn and Johnson, 1995).	12
Figure 2.7	Eastern part of the Southwestern Wyoming Province showing variations in levels of thermal maturity based on extrapolated vitrinite reflectance (R_o) for the Niobrara Formation and equivalent rocks (modified Finn and Johnson, 2005).	13
Figure 2.8	Simplified map of the Greater Green River basin with SH_{max} superimposed on the geologic map (S.M. Larson from E.A. Erslev, 2013, personal communication).	16
Figure 2.9	Surface structure map of the Beaver Creek Anticline and Pagoda anticline (modified Morel et al., 1986).	17
Figure 2.10	Two-dimensional seismic line SE of the study area showing the deep, basement-involved Indian Run fault associated with the Beaver Creek Anticline (Morel et al., 1986).	18
Figure 2.11	Geologic map of Craig with stereonets of joint planes superimposed on the geologic map (S.M. Larson from E.A. Erslev, 2013, personal communication).	20

Figure 2.12 Fold model for fracture intensity on fold along high-angle fault (Zahm and Hennings, 2009). 21

Figure 2.13 Reference three-D Move model of the Big Snowy Mountains showing high strain (green) in regions with highest curvature, including on the steep wall of the anticline, at the crest of the anticline, and near the bend in the anticlinal axis (Angster, 2010). 22

Figure 3.1 Type log picks on right for study area based on reference log on left from Finn and Johnson (2005). 25

Figure 3.2 Seismic well tie for well 0508105148000, the deepest well drilled in the survey area. 27

Figure 4.1 Top Niobrara structure map generated from top picks on forty-six well logs in the study area. 34

Figure 4.2 Vertical thickness map, in feet, generated from the top Niobrara to top Carlile, top picks from 23 wells. 35

Figure 4.3 True vertical depths of all wells within the Niobrara.. 40

Figure 4.4 Bubble map of the fourteen Niobrara wells with initial production test data. 41

Figure 4.5 Bubble map of cumulative production from the Niobrara. 42

Figure 4.6 Bubble map of first 12 months production from the Niobrara. 42

Figure 4.7 Inline 100 showing Transition Fault Zone 1 (TFZ1) and Transition Fault Zone 2 (TFZ2) forming three fault blocks. 43

Figure 4.8 Inline 170 showing the complex faulting between TFZ2 and Major Fault 2. 44

Figure 4.9 Crossline 270 showing the Indian Run Fault, TFZ1, and Major Fault 3. 45

Figure 4.10 Crossline 40 showing the Indian Run Fault and Major Fault 2. 46

Figure 4.11 Three-dimensional view from the south of the five major faults with the transparent Niobrara horizon on top for reference. 47

Figure 4.12 Structure map of top Niobrara. 48

Figure 4.13 Closeup of crossline 370 showing the truncation of the Precambrian wedge and the rotated parallel bedding within the wedge. 50

Figure 4.14	Minimum curvature attribute on the Top Niborara horizon run in Kingdom.	52
Figure 4.15	Similarity attribute map on the top Niobrara horizon generated in Kingdom.	53
Figure 4.16	Map of maximum curvature on the top Niobrara horizon generated in Petrel.	54
Figure 4.17	Map of maximum curvature on the top Tow Creek bench horizon generated in Petrel with left lateral strain ellipse diagram at bottom.	55
Figure 4.18	Close up of crossline 120 showing that the NNW-SSE trending linear features are reverse faults.	56
Figure 4.19	Close-up of inline 230 showing that the three linear features at the tip of TFZ1 are normal faults.	58
Figure 4.20	Mapped linear features from maximum curvature on Tow Creek bench overlain on the Petra isopach map.	60
Figure 4.21	Isochron maps of five key intervals.	61
Figure 4.22	Isochron maps from Petrel of the Weber-Minturn and Minturn-Leadville intervals.	63
Figure 4.23	Isochron maps from Petrel of the Buck Peak to Tow Creek bench interval.	63
Figure 4.24	Strain analysis run from 3D Move on the forward modeled top Niobrara surface.	65
Figure 4.25	Curvature analysis run from 3D Move on the forward modeled top Niobrara surface.	65
Figure 5.1	Wells targeting the Niobrara Formation superimposed on the top Niobrara structure map with IP data overlain.	67
Figure 5.2	Cumulative production (bbls) mapped on top of the Top Tow Creek Bench maximum curvature attribute map with mapped linear features.	69
Figure 5.3	First 12 months production (bbls) mapped on top of the Top Tow Creek Bench maximum curvature attribute map with mapped linear features.	70
Figure 5.4	Wells that targeted the Niobrara Formation superimposed on the 3D Move strain analysis map.	71

LIST OF TABLES

Table 4.1 A list of wells targeting the Niobrara Formation within the survey area with initial production, cumulative production, and first 12 months production. .. 37

Table 5.1 Comparison of local tectonic events within larger regional context. ……..72

ACKNOWLEDGEMENTS

First and foremost, I wish to thank my advisor, Rick Sarg, for his patience, guidance, and feedback throughout my studies and research work. His advice has helped me develop the geologic skills necessary to tackle this research project, and his feedback has insured the integrity of the interpretations.

I am also grateful to the rest of my committee members: Steve Sonnenberg for feedback on numerous presentations, Chuck Kluth for his insight on structure and tectonic controls, and Mark Chapin for his help with keeping the project relevant to the petroleum industry.

A special thanks to ION Geophysical for providing the 3D seismic survey dataset that made this entire project possible. Also, thanks to the companies of the Niobrara Consortium for supporting my studies and research and to my fellow graduate students at CSM for their feedback.

I would like to acknowledge Martin Krueger for sharing his work on the Piceance basin for comparison with my well log top picks within the Niobrara interval. Also, thanks to Doug Klepacki, Long Wu, and Carlos Perez for their help with using the Kingdom and Petrel programs. Finally, thanks to my family and Kevin Yu for always supporting and motivating me throughout my studies.

CHAPTER 1
INTRODUCTION

1.1 Importance

Unlike conventional reservoirs, the Niobrara Formation is a low porosity, low permeability, self-sourced resource play with key production occurring in fracture-rich "sweet spots" that may extend down dip off structure. Recent interest in expanding the limits of the Niobrara play has renewed interest in the Sand Wash basin of northwestern Colorado and south-central Wyoming. Due to the fine-grained lithology, low matrix porosity and permeability of the Niobrara, production from its reservoir rocks relies heavily on the presence of open natural fracture swarms. These natural swarms provide fracture permeability that allows hydrocarbons to flow through the formation more easily thus resulting in better production.

The unconventional Niobrara continuous oil accumulation in NW Colorado is poorly understood because past productive Niobrara wells in the region primarily targeted "conventional" structural traps. Due to the relatively sparse well data, companies have yet to identify the key components of a productive unconventional Niobrara target in the Sand Wash basin. This study will help shed light on the structural component of a successful Niobrara target in the Sand Wash basin.

In order to predict the location of high-density fracture zones, it is important to understand the changes in stresses through time. The Sand Wash basin is broken up into various compressional features formed during the Laramide Orogeny, which began soon after the deposition of the Niobrara Formation. This study aims to determine the relationship between paleo-tectonic controls and high-density fracture zones by comparing the structural history of the study area with faults and disruptions identified on seismic attribute maps. This relationship will provide a model for predicting locations of high-density fracture zones on similar structures in the region and thus facilitate discovery of productive fields and support well planning. The seismic dataset provides an opportunity to assess structural controls on fracture production.

The study area is defined by the limits of a 25 mi^2 3D seismic survey and covers a complex transition zone as one major NW-trending thrust fault dies out and another offset NW-trending thrust fault begins. The large asymmetrical anticline that runs along the major thrust

fault is broken into three fault blocks downstepping to the NW suggesting that the structures are dominated by transpressional tectonics rather than pure dip-slip movement.

Situated in the center of the study area is the "conventional" Waddle Creek Oil Field, which targets the middle fault block of the faulted anticline at a dome-like structure bounded on three sides by faults and on the fourth side by an anticlinal limb. The field's discovery well was drilled in 1963 and completed on January 6, 1964. Activity in the field hit its peak in the 1980's then trailed off until 2010 when companies began to re-explore the field as an unconventional target. The cumulative production to date for the Waddle Creek Field is 664,402 bbls.

It should be noted that the model produced from this study may not apply directly to other structures in the region due to its location in a complex structural transition zone, however, it does illustrate that understanding structural history may help predict fracture formation that could not be predicted from present-day structure alone.

1.2 Objectives

The four main objectives for this study are to:

1. Map subsurface structures and faults in the study area using seismic horizons, seismic attributes, and well log data and compare them to regional stress regimes and surface fracture trends within the Sand Wash basin.
2. Assess the paleo-tectonic controls on the structures based on structure and isochron maps to develop a 3D forward model of the study area. Using this model, generate high strain and curvature maps to understand localized fracturing in this complex transition zone.
3. Compare past production to locations of structural features and potential high-density fracture zones to help determine controls on productivity in the area.
4. Develop an interpretation of structural and potential diagenetic controls on the presence of open fractures based on the maps, model, and production data.

CHAPTER 2
BACKGROUND

2.1 Regional setting

The Niobrara Formation was deposited within the Western Interior Cretaceous Seaway in a broad asymmetric foreland basin during the Late Cretaceous. During the Laramide orogeny, this large foreland basin was broken up into smaller basins, one of which was the Greater Green River basin. Several intra-basin uplifts further subdivide the Greater Green River basin into smaller basins (Fig. 2.1), including the Sand Wash basin, which contains the study area. This section summarizes the stratigraphy, Niobrara petroleum system, and regional/local structure in southern Sand Wash basin, as it has been characterized in literature and other previous work.

2.1.1 General stratigraphy and lithology

Surface geology maps of Northwestern Colorado show that Mancos Shale outcrops over most of the study area with some Iles Formation and Williams Fork Formation of the Mesaverde Group cropping out in the synclinal and monoclinal areas to the SW and NE (Fig. 2.2). There are some pockets of Pliocene/Miocene basalt flows at the surface of the study area, but no intrusions within the study area as indicated by the seismic data. There is a large Miocene-age intrusion ~30mi SSE of the study area that does not appear large enough based on the size of the intrusion on the surface geology map to have affected the thermal history of the study area (Fig. 2.2).

The general stratigraphy of the local region is shown in the general stratigraphic column for the Uranium Peak area, which is ~15mi southwest of the study area. It includes the stratigraphic breakdown of the Niobrara Formation itself (Fig. 2.3). A type log and subsurface cross section from Finn and Johnson (2005) modified from Vincelette and Foster (1992) illustrate the gamma ray and induction log characteristics of the Niobrara Formation in northwestern Colorado (Fig. 2.4). They identify three “calcareous-rich” marl benches separated by marly shales. The Texas Knolton 14 and Malco 1 Kowach wells in the cross section are each only 5 miles away from the study area. Malco 1 Kowach has oil production from the Buck Peak and Tow Creek benches.

The Niobrara Formation was deposited in the Western Interior Cretaceous Seaway during the Coniacian to Santonian ages of the Cretaceous (Hale, 1961, in Finn and Johnson, 2005) when

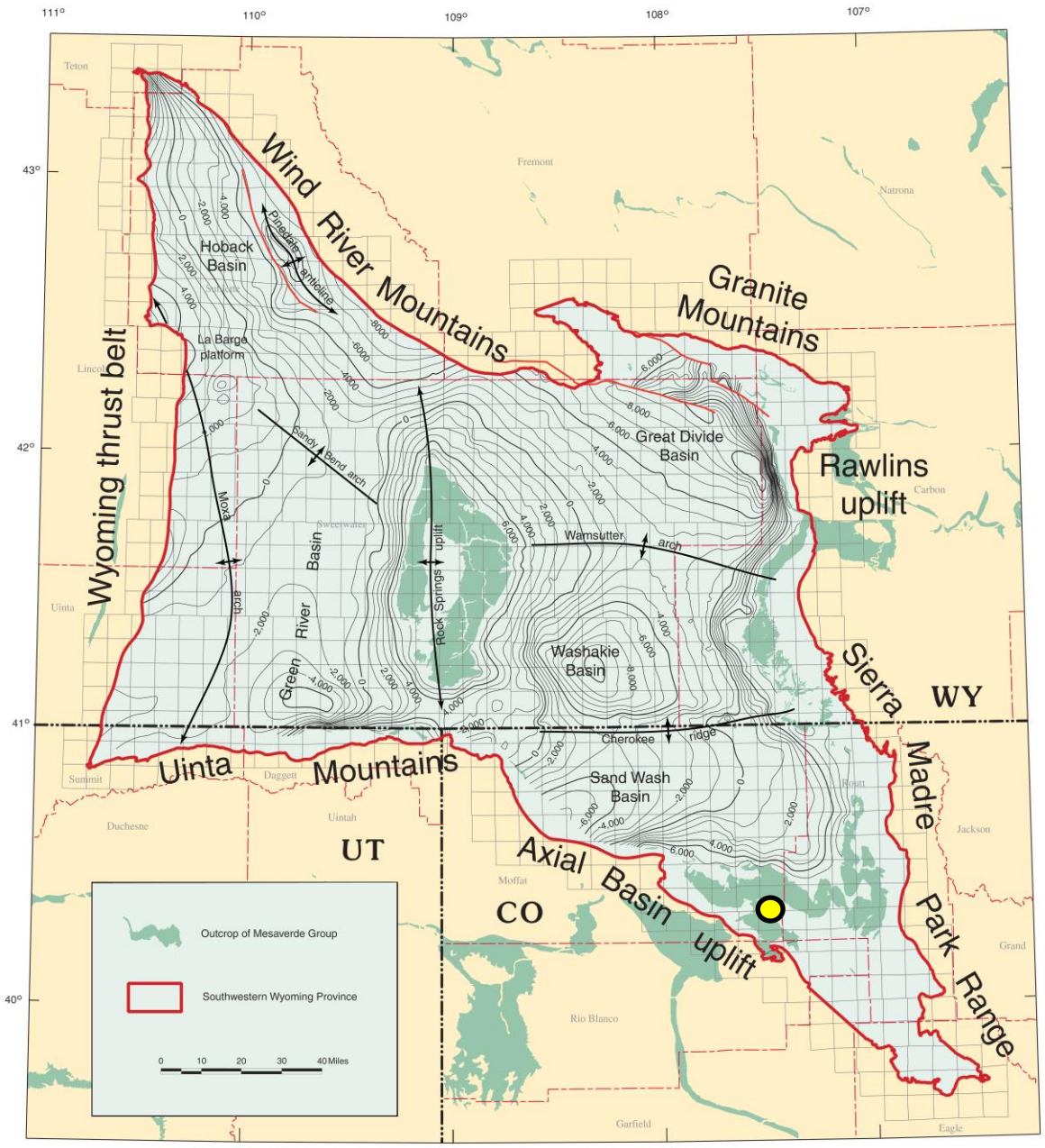

Figure 2.1. Location map of southwestern Wyoming, northeastern Utah, and northwestern Colorado showing the location of the Southwestern Wyoming Province, structural configuration, intrabasin uplifts, and subbasins (modified Finn and Johnson, 1995). Structure contours drawn on top of the Mesaverde Group. Countour interval = 1,000 feet. The Sand Wash basin is in the southeastern part of the Greater Greenriver basin and is bounded to the south by the Axial basin uplift and the eastern part of the Uinta Mountains. The study area is denoted by a yellow dot.

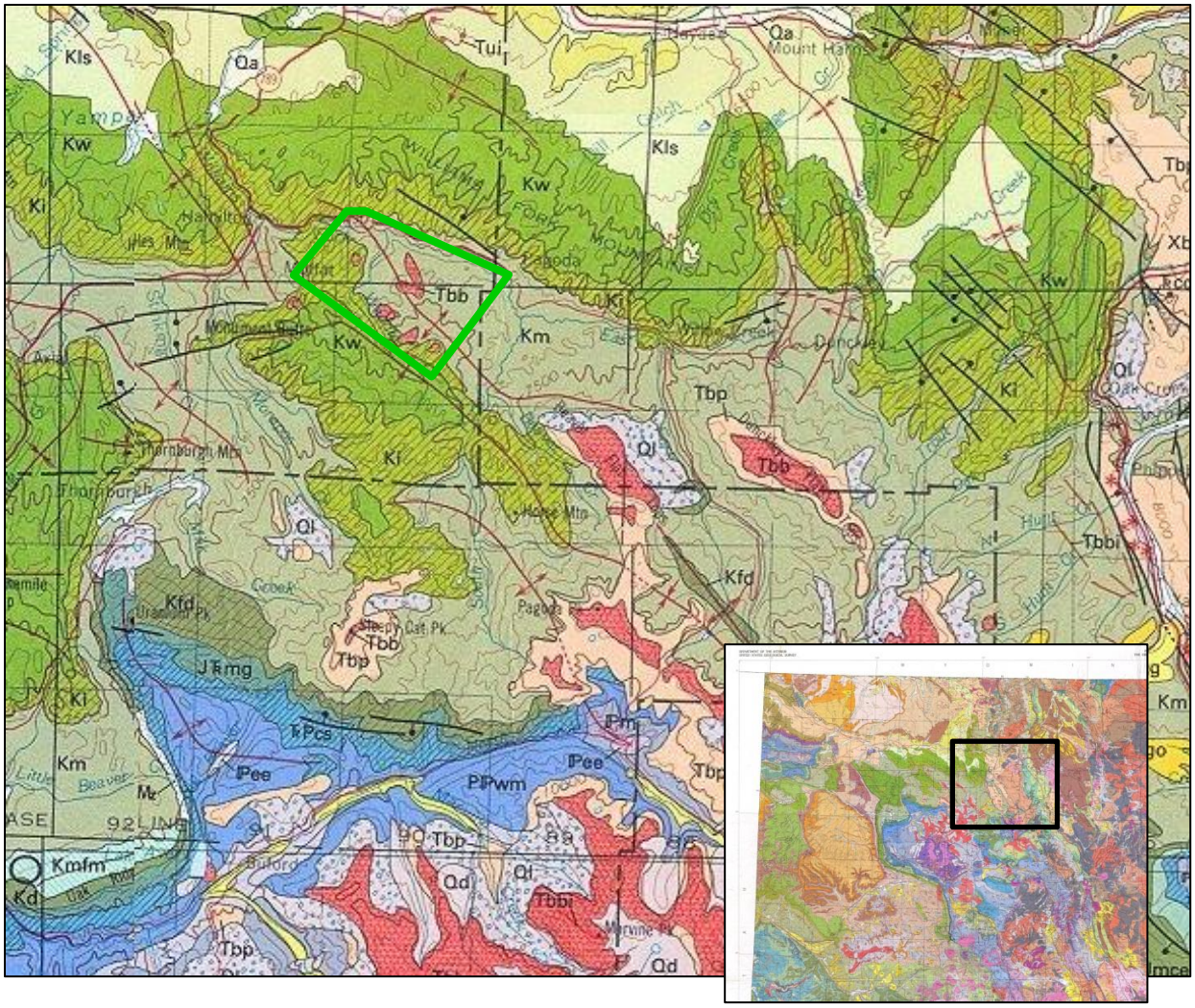

Figure 2.2 The seismic survey area is denoted by the green outline on this section of the northwest quarter of a surface geologic map of Colorado (modified Tweto, 1979). The map shows primarily Cretaceous Mancos Shale (Km) cropping out in the study area with some Iles Formation (Ki) and Williams Fork Formation (Kw) of the Mesaverde Group cropping out in the synclinal and monoclinal areas to the SW and NE. The light red areas in the study area are Pliocene/Miocene basalt flows (Tbb) and intrustion (Tbbi).

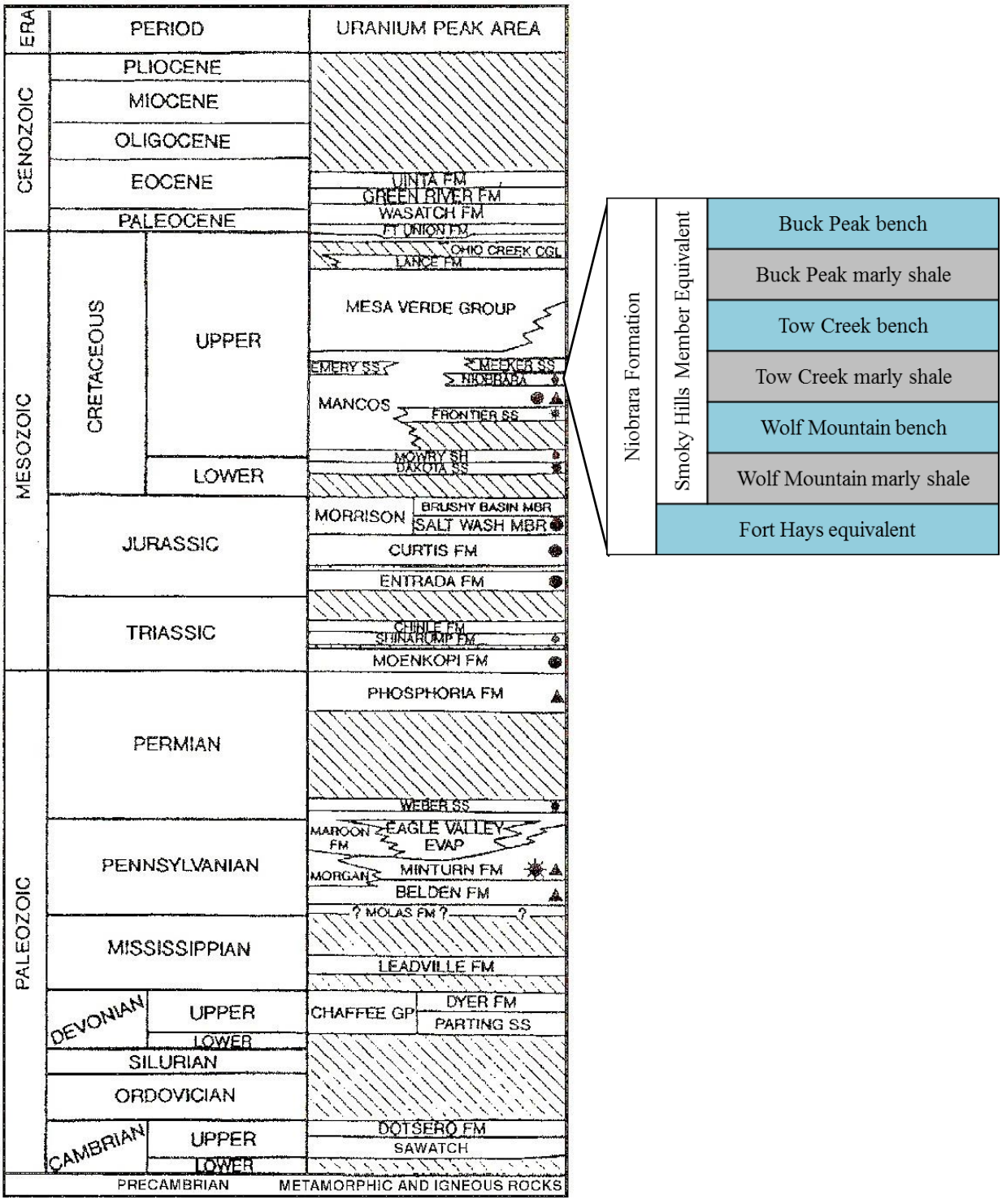

Figure 2.3 General stratigraphic column for the Uranium Peak area ~15mi southwest of the study area (modified Robertson et al., 1995). Known regional source rocks in the area denoted by triangle, producing oil horizons denoted by black circles, and producing gas horizons denoted by black gas well symbols. On the right the Sand Wash basin nomenclature used for the benches and shales within the Niobrara is shown.

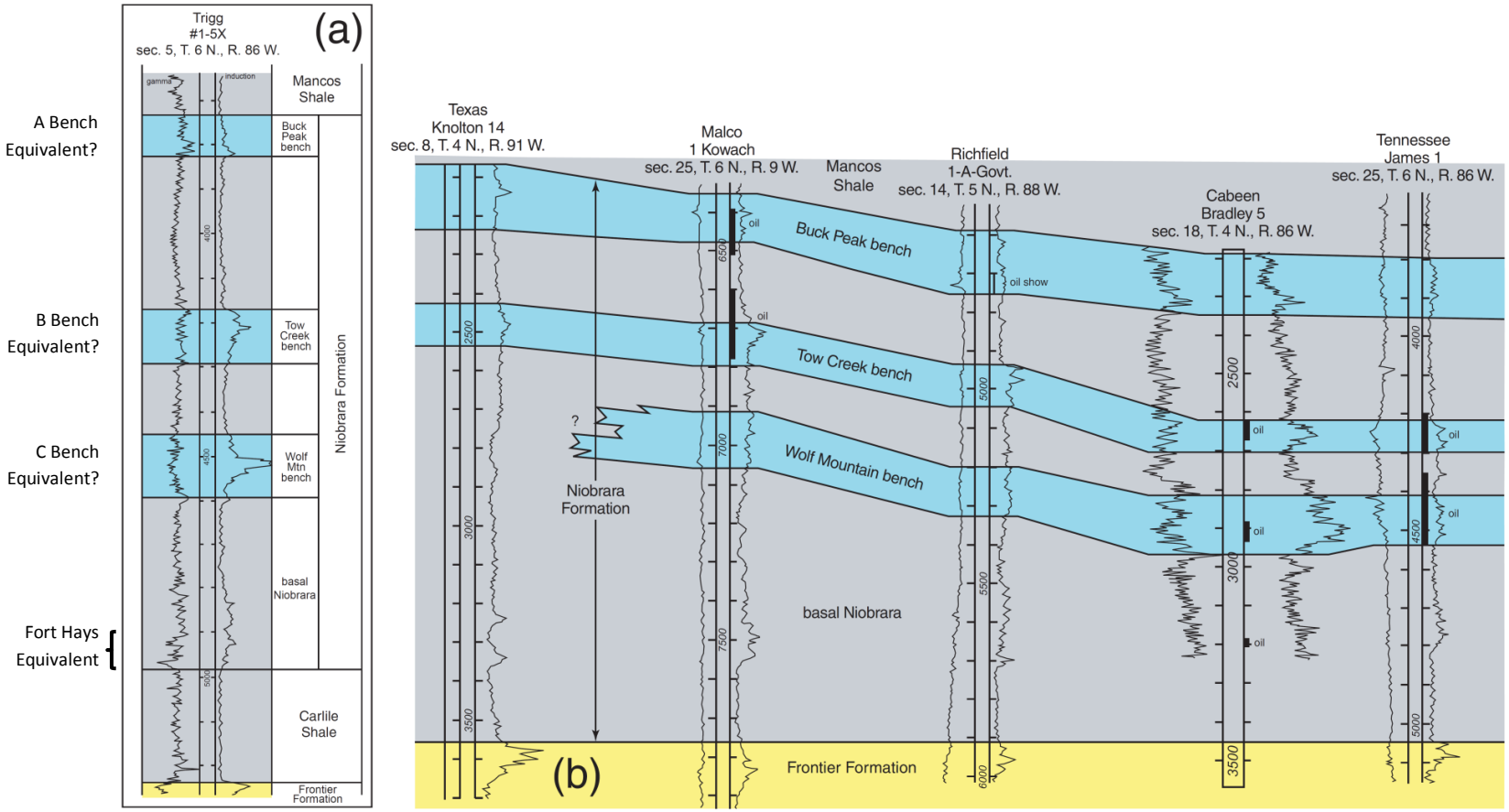

Figure 2.4. A type log and subsurface cross section show the gamma ray and induction log characteristics of the Niobrara Formation in northwestern Colorado (modified from modified Vincelette and Foster, 1992, in Finn and Johnson, 2005). The Niobrara Formation is subdivided into three calcareous-rich benches and three marly shales. The more calcareous-rich benches highlighted in light blue are more brittle and likely more prone to fracturing. Unlike in the Denver basin where the benches are true chalks, the benches in the Sand Wash basin are marls (<65% carbonate content). Heavy vertical black bars indicate oil-producing zones coinciding with the benches. The Texas Knolton #14 and Malco #1 Kowach wells are 5 miles from the study area and are the closest wells to the study area. Location of these logs shown in Figure 2.7.

the epicontinental Western Interior Seaway extended from the Arctic Ocean to the Gulf of Mexico (Fig. 2.5). This seaway covered a broad asymmetric foreland basin adjacent to the Sevier orogenic belt to the west. The stable cratonic platform to the east of the seaway supplied little sediment, occasionally allowing carbonate platforms to form in the shallow eastern waters and resulting in the deposition of limestones and chalks (Longman et al., 1998).

In the Denver basin, the Niobrara Formation is composed of a lower Fort Hays Member and an upper Smoky Hill Member (Longman et al., 1998). The Fort Hays in the Denver basin is limestone and the Smoky Hill Member has three chalk benches alternating with three marl intervals. The basal Fort Hays limestone equivalent in northwestern Colorado is an interbedded chalk and limestone interval, which is referred to as the Fort Hays equivalent in this study. The upper Smoky Hill Member equivalent appears to be diluted by siliciclastics and includes three marl benches alternating with three marly shales identified by Vincelette and Foster. They are locally referred to as the Wolf Mountain bench, Tow Creek bench, and Buck Peak bench in ascending order. It is possible that these three benches are time equivalent to the C, B, and A chalk benches, respectively, in the Denver basin, although more work on regional correlations would be needed to confirm this. Similarly the more siliciclastic-rich marly shales below each bench may correlate with the C Marl, B Marl, and A Marls of the Denver basin but are referred to in this study by the proposed nomenclature of Wolf Mountain marly shale, Tow Creek marly shale, and Buck Peak marly shale.

Siliciclastic input was supplied primarily from the active Sevier orogenic belt to the west during this time. Carbonate deposition occurred across the Western Interior Cretaceous basin and the sediment supply from the Sevier orogeny diluted carbonate content in the west, accounting for the lower carbonate content of the Niobrara bench equivalents in the study area. Due to the lower carbonate content to the west, the Smoky Hill Member equivalent in northwestern Colorado does not have any true chalks but more calcareous-rich marls and marly shales. Thin section petrography of nine samples from a core in the nearby Piceance basin showed that the Wolf Mountain marly shale interval has 15-26% carbonate content and would be classified as a marly shale (<35% carbonate content) by the simplified nomenclature suggested by Longman et al. (1998). It also showed the Tow Creek bench to have 25-52% carbonate content, which would be classified as marl (<65% carbonate content) to marly shale (Strasen, 2012). Similarly, Bruchez (2013) describes mainly calcareous shale with some intervals of platy chalk at a

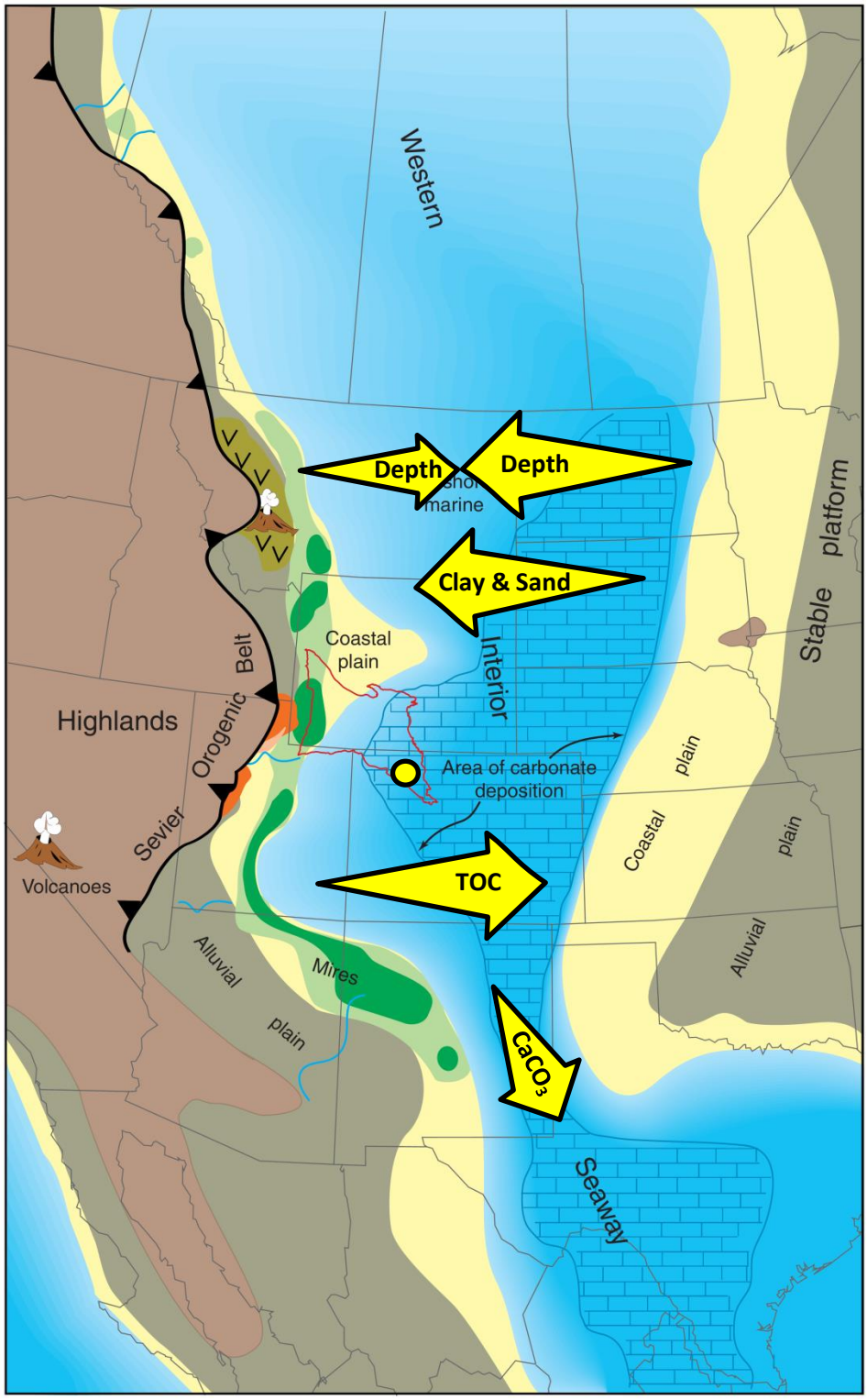

Figure 2.5 Paleogeographic reconstruction of the Western Interior Seaway during Coniacian-Santonian time (modified Finn and Johnson, 1995, after Longman et al., 1998) illustrating general trends in carbonate content, TOC, clay & sand content, and depth. Study area denoted by the yellow dot.

Piceance basin outcrop south of the study area, near New Castle, Colorado that is approximately at the same longitude as the area for this study. The Fort Hays in Bruchez's section consists of alternating platy chalks and limestones. He does not observe limestone or blocky chalk in the Smoky Hill Member equivalent. Further to the east where carbonate content increases, Bruchez (2013) observes more intervals of platy chalk and blocky chalk in the Smoky Hill Member equivalent than to the west.

There are two basic explanations for the existence of the three more carbonate-rich marl benches: 1) they represent periods of restricted siliciclastic input and/or 2) they represent increased carbonate deposition and/or preservation. Since there is very little localized tectonic movement during the deposition of the Niobrara, it is likely that these two possible mechanisms were controlled by changes in climate, sea level, and/or nutrient supply. A local change to a drier climate in the Sevier orogenic belt may have limited erosion and resulted in decreased siliciclastic input. An increase in temperature may have supported increased carbonate production. If the temperature increase was global then the resulting rise in sea level would have resulted in a transgression pushing siliciclastic deposition further shelfward. Increased oxygen and nutrients from better water circulation may have resulted in more ideal conditions for carbonate production. If the controls were on a larger regional scale, it would support the idea that the marl benches of northwestern Colorado are diluted equivalents of the chalk benches in the Denver Basin. Testing these controls would require a biostratigraphic and more detailed sedimentologic study of the Niobrara interval in northwestern Colorado to determine timing of deposition of each bench. These depositional periods may then be compared with changes in global and local sea level, Milankovitch cycles, and changes in carbonate composition or other bio-indicators of environmental change.

The proximity to the siliciclastic supply to the west coupled with the increased accommodation space resulted in an increase in thickness of the Smoky Hill Member equivalent to the west from less than 100 ft in South Dakota to more than 1,800 ft in west-central Wyoming (Finn and Johnson, 2005). Assuming the pelagic organic matter supply was consistent throughout the foreland basin, the western regions have the potential to produce at least the same amount of hydrocarbons as the equivalent intervals in the Denver basin since the amount of organic matter would be the same.

2.1.2 Niobrara petroleum system

The Niobrara produces self-sourced oil from organic-rich, low-permeability, fractured, carbonate-rich rocks in the Niobrara Formation. A regional overview by Finn and Johnson of the Niobrara in the Southwestern Wyoming and Northwestern Colorado identifies this region as a continuous accumulation based on the following characteristics: (1) no down-dip hydrocarbon/water contact, (2) little or no water production, (3) abnormally pressured, and (4) production independent of structural closure. Since the Niobrara in this region is a continuous accumulation, oil may potentially be produced in any structural setting including anticlines, monoclines, and synclines provided there are sufficient fractures present.

To determine Niobrara kerogen type, Finn and Johnson (2005) analyzed Rock-Eval data from 28 Niobrara samples (USGS Organic Geochemistry Database) of well cuttings from northwestern Colorado and south-central Wyoming. Results were plotted as a modified Van Krevelen diagram, S2 vs. %TOC, and hydrogen index vs. Tmax (Fig 2.6). The plots indicate that the majority of the samples contained Type-II, oil prone kerogen with some Type-III, gas-prone kerogen that likely came from terrestrial sources along the western shoreline and/or cavings from the overlying Mancos shale.

The study area falls between the 0.6-0.8% R_o contour lines in a regional thermal maturity map (Fig. 2.7), placing it within the oil window (Finn and Johnson, 2005). No direct R_o data was available for the Niobrara, so the maturity map was generated from extrapolated R_o values based on best fit R_o vs. depth lines for Mesaverde coal maturity data (Finn and Johnson, 2005). With an estimated R_o range of 0.6-0.8% and Type-II kerogen with TOC's of 1-3%, the Niobrara in the study area is a moderately good source rock for oil. A large regional study of 100 Niobrara samples indicates a clear decrease in TOC from east to west (Landon et al., 2001). The study area falls within the arbitrary north-south compartment with a TOC range of 0.99-3.47% with an average of 1.85% defined by Landon et al. While these TOC values are not high, they are sufficient for unconventional production.

Fractured, more calcareous-rich intervals act as the reservoir rock for the Niobrara petroleum system. High-density fracture zones are often associated with structures formed during the Laramide orogeny (Vincelette and Foster, 1992). These fractures formed during folding, and fracture production has been successful on the crests of anticlinal and monoclinal structures as well as on the steep and gentle flanks of those structures. Since it is a continuous oil

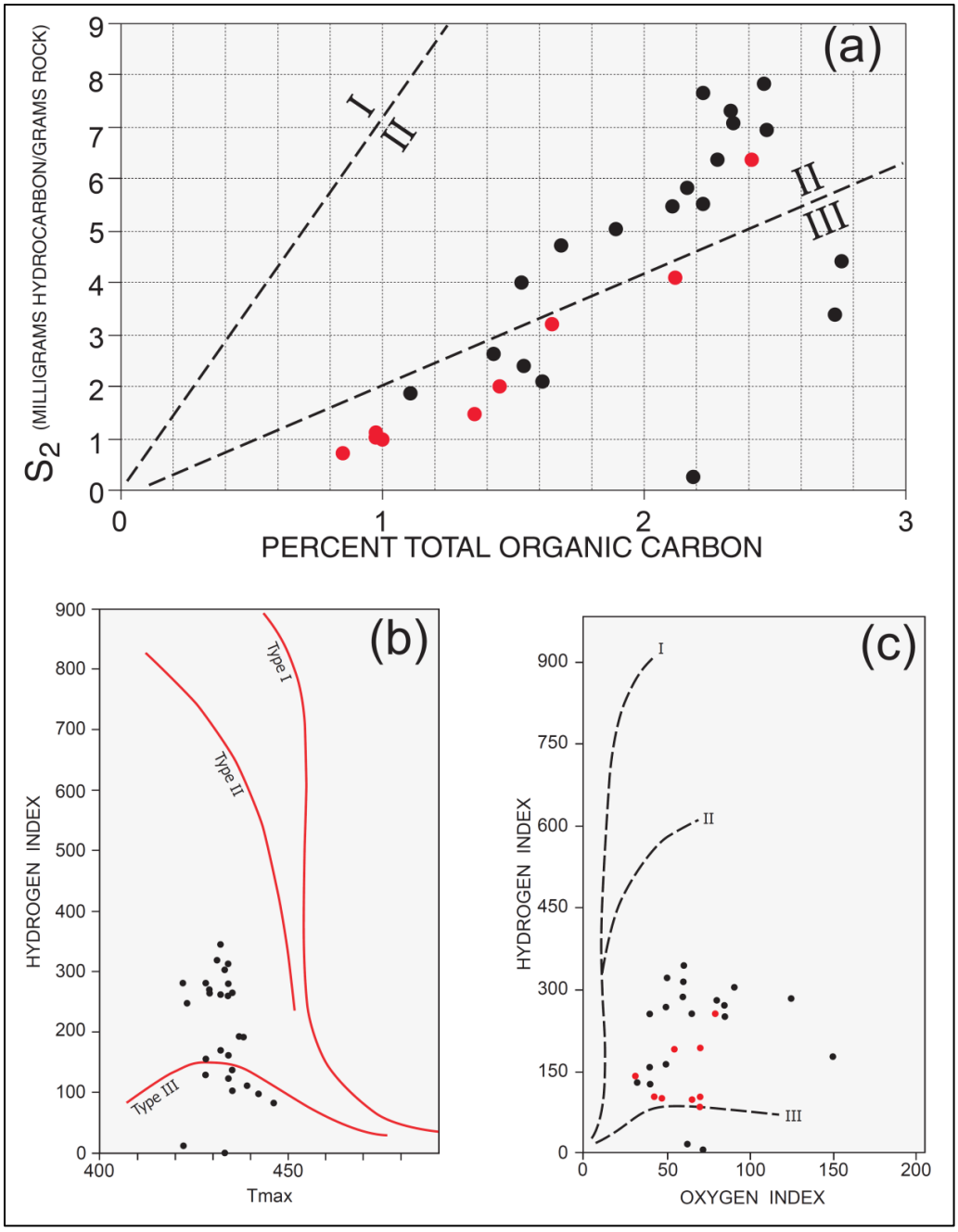

Figure 2.6. Plots of data from Rock-Eval analysis of kerogen of 28 Niobrara Formation samples, USGS Organic Geochemistry Database (Finn and Johnson, 2005). The samples are from well cuttings from northwestern Colorado and south-central Wyoming. (a) S2 vs. total organic carbon, (b) hydrogen index vs. Tmax, and (c) modified van Krevelen diagram. The majority of the samples indicate a Type-II oil-prone kerogen with some Type-III gas-prone kerogen that may have been terrigenous input from the nearby shoreline to the west or cavings from the Mancos Shale above. Black dots represent samples with a Tmax < 435 and red dots represent samples with a Tmax ≥ 435.

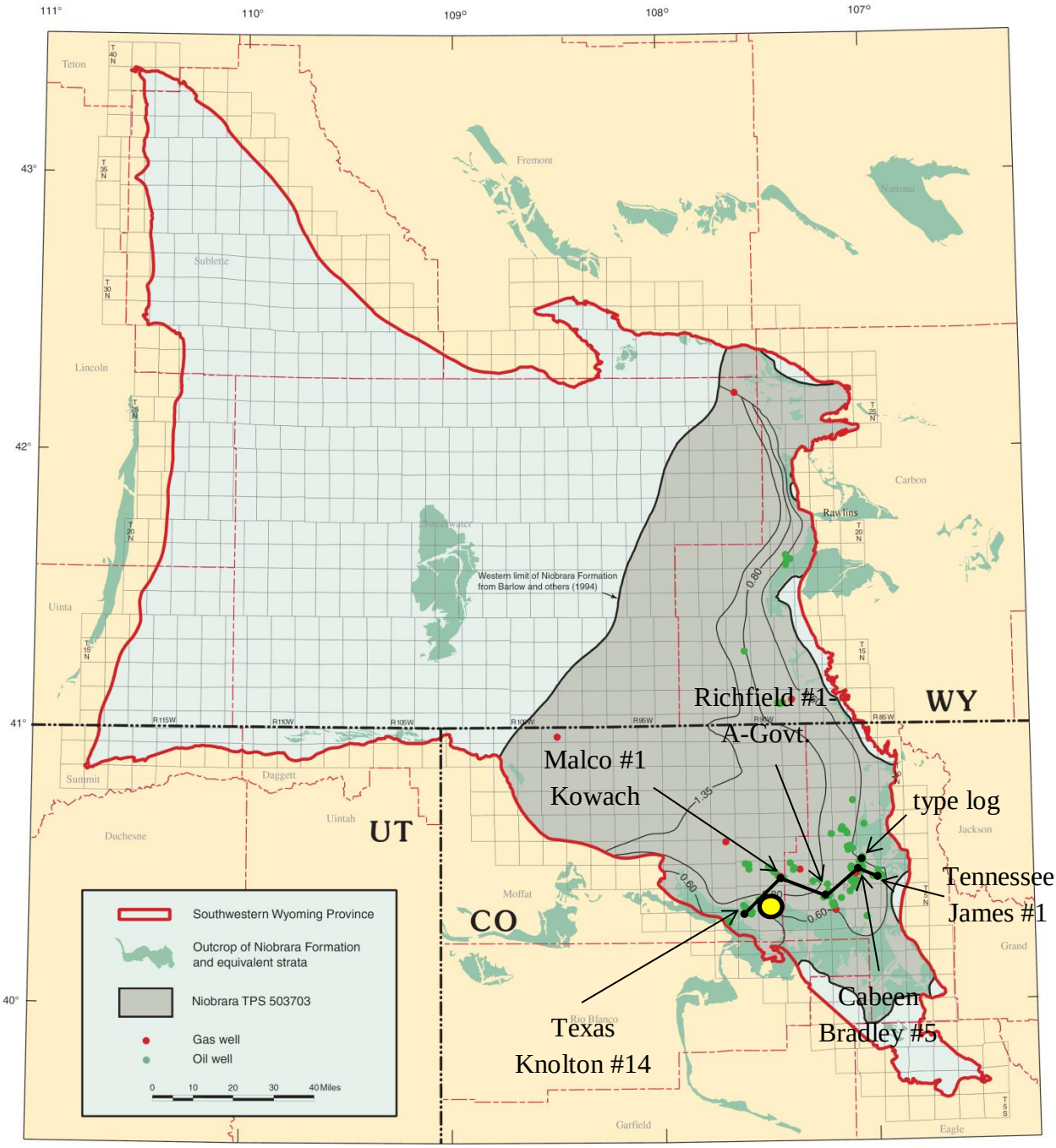

Figure 2.7. Eastern part of the Southwestern Wyoming Province showing variations in levels of thermal maturity based on extrapolated vitrinite reflectance (R_o) for the Niobrara Formation and equivalent rocks (modified Finn and Johnson, 2005). Study area (yellow dot) falls between 0.6 and 0.8% R_o. Nearby oil production primarily occurs within the oil generation window suggesting little to no migration of the oil after it is generated. Location of type log and well log cross section from Figure 2.4 shown as black dots.

accumulation, production may be successful in synclinal structures as well, given a sufficient amount of open fractures.

While Laramide folding is important, Vincelette and Foster have determined that post-Laramide Neogene extension is possibly more important. Most of the fractures associated only with Laramide compression are completely calcite-filled. Fractures that were reactivated by later Neogene extension are lined by a layer of younger calcite but are not completely filled, leaving fracture porosity. Vincelette and Foster suggest that the new influx of meteoric waters after the Laramide uplift diluted the calcium-carbonate content of the pore water, thus retarding the mineralization of calcite. Reactivation of fracture trends may be the reason many of the best Niobrara producing wells cut through or are near normal faults. It is unclear whether Neogene extensional features alone are sufficient for Niobrara production or if reactivation of older Laramide fractures is necessary since the wells studied were drilled near reactivated faults.

Ductile shales that occur above, below, and interfingering with the Niobrara act as the seals for this petroleum system. The thick section of non-calcareous Mancos shale above and the Carlile shale below act as good quality regional seals for the Niobrara Formation. The Mancos also forms a lateral stratigraphic seal toward the west. The brittle reservoir zones within the Niobrara are also overlain, underlain, and/or interbedded with relatively ductile, clay-rich marine shales. These shale zones are less likely to fracture than the more calcareous-rich reservoir zones and thus seal the hydrocarbons within the fractured brittle reservoir rocks (Finn and Johnson, 2005).

The integrity of the siliciclastic-rich shales above and below the Niobrara and the fine-grained lithology of the marls and shales within the Niobrara limit migration of oil (Landon et al., 2001). This is supported by a map of Niobrara oil production that shows production only in areas where the Niobrara is thermally mature with respect to oil generation (0.6 – 1.35% R_o). Few wells produce in areas where the Niobrara is immature or marginally mature (Fig. 2.7).

Having mature source rocks, fractured reservoir rocks, ductile shale seals, structural and stratigraphic traps, and little to no migration, the Niobrara in northwestern Colorado provides optimal conditions for a self-sourced oil reservoir. Vincelette and Foster also noted that underpressuring and large oil columns are typical in the northwestern Colorado region, which supports simple gravity drainage as a method of production. Due to the underpressured nature of the Niobrara reservoirs in this region, it is possible that many potential producing intervals were

bypassed because conventional drilling muds caused formation damage or masked shows in the Niobrara (Finn and Johnson, 2005). This means there are potentially more Niobrara fields to be discovered in the Sand Wash basin. Accurately determining locations of open fracture trends is critical for identifying high quality production.

Vincelette and Foster do not suggest a mechanism for the underpressuring of the Niobrara, however, unconventional tight oil petroleum systems that have not been actively generating oil can become underpressured as oil slowly leaks out of the reservoir and there is no new oil generation or insufficient influx of other fluids to keep the pressure up.

2.1.3 Regional structure

The study area is located in a unique, tectonically complex zone at the southern boundary of the Sand Wash basin. Stone (1986) defines this area as the Ancestral Axial fault zone since it connects the E-W trending Uinta Mountain features in the northwest with the NW-SE trending ancestral Rockies in the southeast. Based on changes in isochore thickness, Stone determined that the faults in this zone, including the major Indian Run Fault that runs through the study area, were active during the same Pennsylvanian-Permian time span during which faults of the Ancestral Rockies were active. Most of the Rocky Mountain region is dominated by NW-SE to N-S trending features that primarily resulted from pre-existing zones of weakness from the Ancestral Rockies and the roughly E-W direction of shortening during the Laramide orogeny. The anomalous E-W Uinta Mountain trend is likely the result of pre-existing fabrics imparted during crustal assembly. Stone suggests that these fabrics were then reactivated during the late Proterozoic rifting associated with the formation of the Uinta Aulacogen.

A simplified map of the Greater Green River basin with SH_{max} superimposed on top is shown in Figure 2.8. The map shows SH_{max} orientations rotating from primarily E-W and WNW-ESE in northwestern Colorado to NNW-SSE in southwestern Wyoming. The SH_{max} orientations also change abruptly to a N-S orientation in the Uinta Mountains due to its anomalous structural trend.

2.1.4 Local structure

Fractures are often associated with structure features, so it is important to understand the past and present tectonic settings of the region. The surface structure map by Morel et al. (1986) shows that the study area covers part of the Beaver Creek Anticline, the plunge end of a smaller unnamed anticline, and the plunge end of the Pagoda anticline (Fig. 2.9). Most of the major

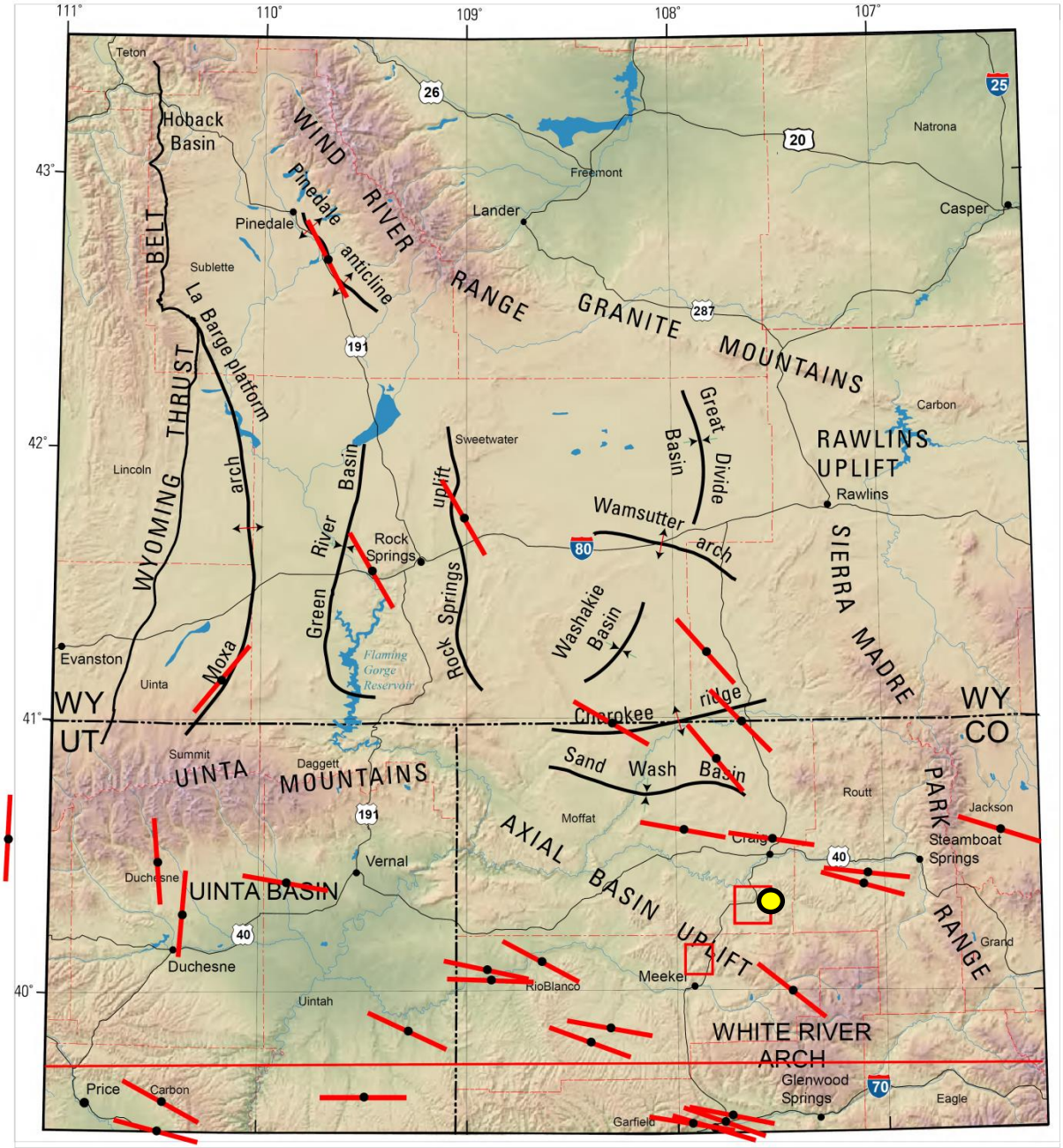

Figure 2.8. A simplified map of the Greater Green River basin with SH_{max} superimposed on the geologic map (S.M. Larson from E.A. Erslev, 2013, personal communication). These orientations were derived from orientations of minor faults and joints at the surface using Compton's (1966) method. The study area is denoted by the yellow dot and lies between a roughly E-W oriented SH_{max} to the north and a NW-SE oriented SH_{max} to the south. If it is assumed that the study area occurs bewtween these two orientations, then the expected SH_{max} orientation would probably be WNW-ESE.

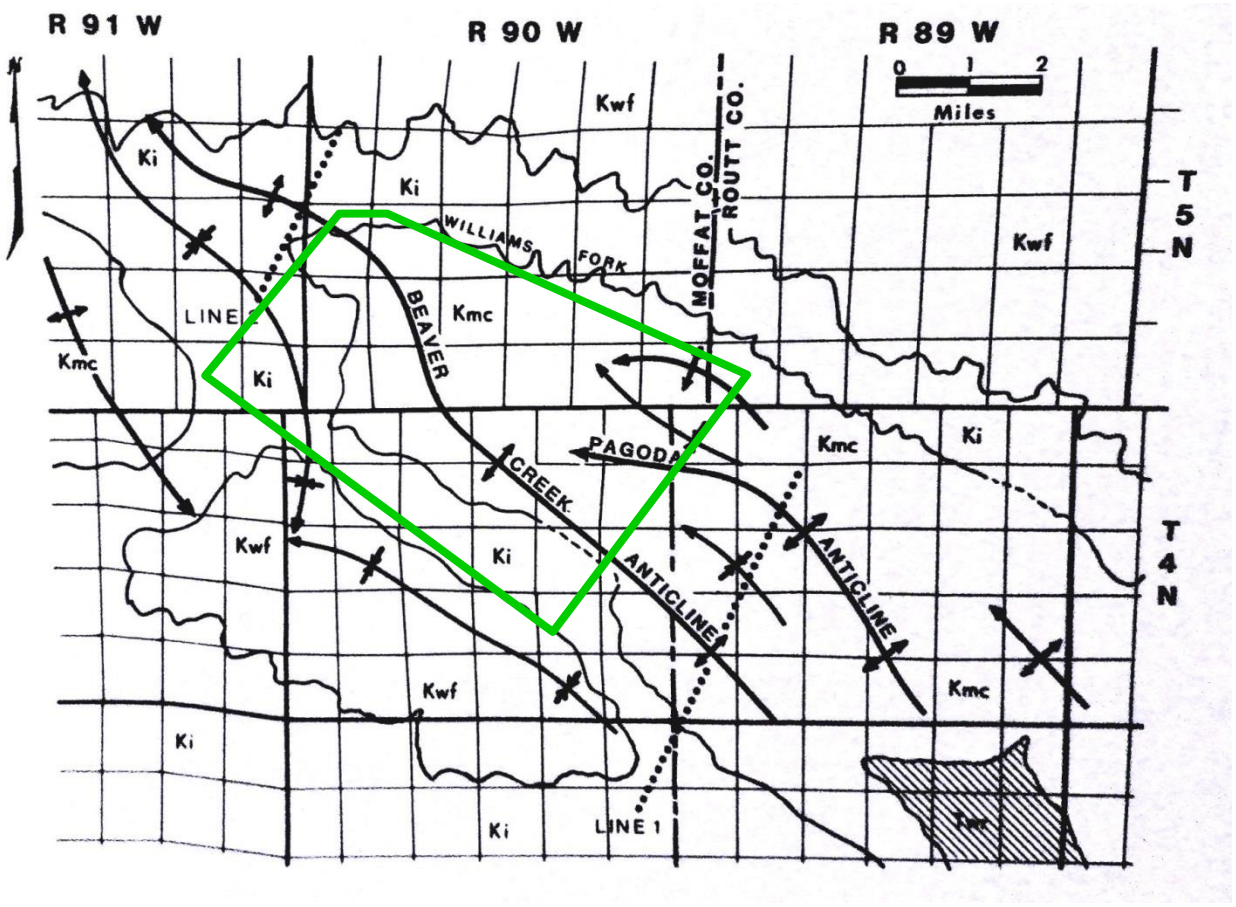

Figure 2.9. Green line outlines the approximate extent of the 3D seismic survey, and encompasses the area of this study. The survey is 4.5 mi by 6.1 mi and covers approximately 25 square miles and images the Beaver Creek anticline, the associated Indian Run fault, the plunge end of the Pagoda anticlince, and a smaller unnamed anticline (modified after Morel et al., 1986). This area likely has complex stresses related to the transition from the NW-SE trending Axial Basin anticline to the N-S trending Grand Hogback toward the east and the E-W trending Uinta Mountains to the northwest.

structures trend to the NW, but the Pagoda anticline changes orientation to E-W at its northwestern plunge end. The Beaver Creek Anticline at the surface appears to curve toward the North in T5N R90W and then continues its trend to the NW.

A 2D seismic line (Fig. 2.10) three miles to the SE of the study area shows that these anticlinal structures are associated with subsurface basement-involved thrust faults. The fault associated with the Beaver Creek Anticline is the largest and is called the Indian Run Fault. Another deep thrust fault is associated with the smaller unnamed anticline. Morel et al. also identify a truncated Precambrian wedge in the hanging wall of the Indian Run fault and suggest that the fault was originally a normal fault that formed after the deposition of the Uinta

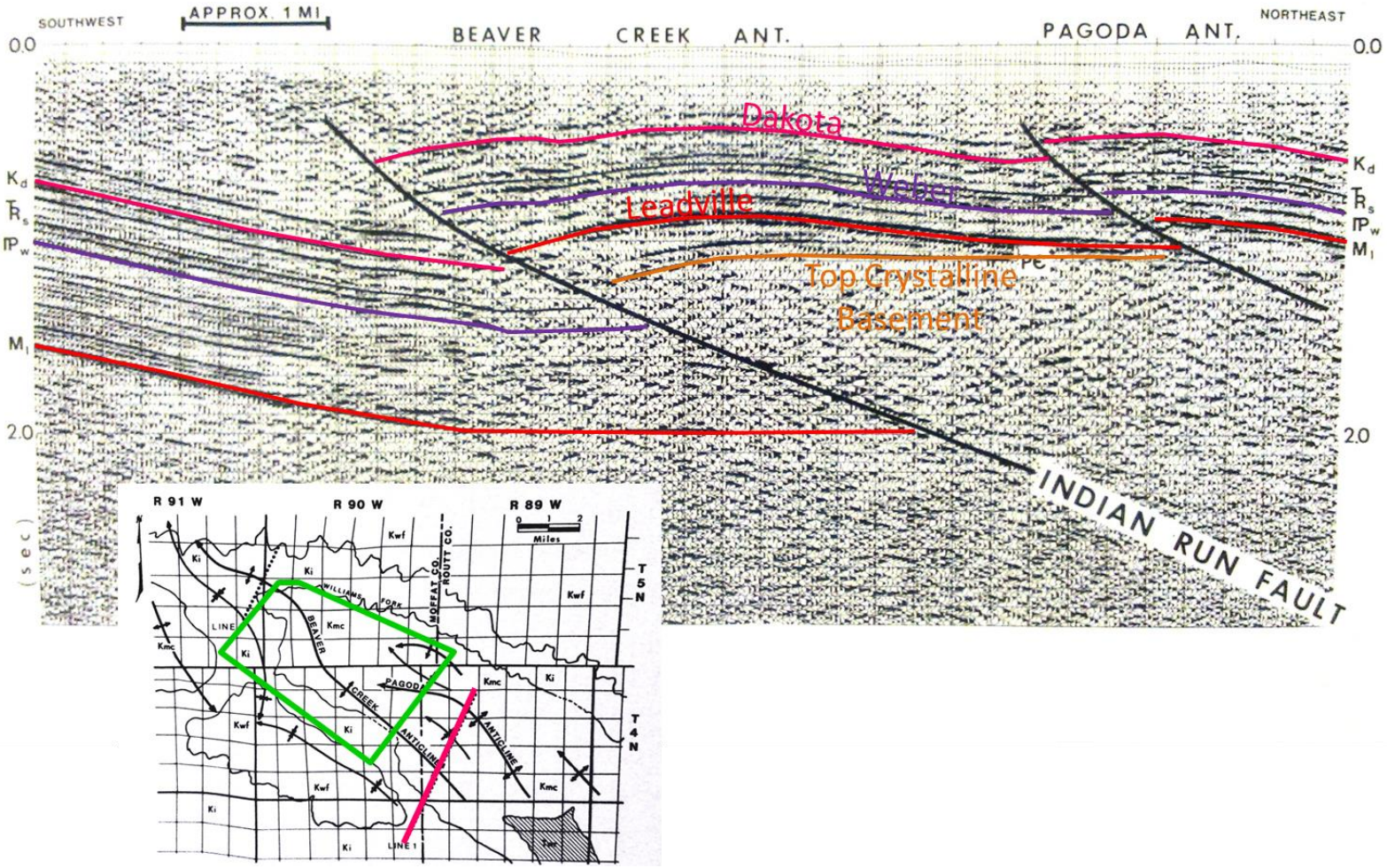

Figure 2.10. Two-dimensional seismic line SE of the study area showing the deep, basement-involved Indian Run fault associated with the Beaver Creek Anticline (Morel et al., 1986). The Precambrian wedge between the top Leadville and crystalline basement may be clearly observed within the hanging wall of the Beaver Creek Anticline fault block but not in the footwall, suggesting that the Indian Run fault was originally a normal fault that was later reactivated as a reverse fault. This is supported by the thinning of the Weber-Leadville interval above the Precambrian wedge relative to the Weber-Leadville interval in the footwall, which indicates that the wedge was inverted during the Pennsylvanian (Morel et al., 1986).

Mountain group, as indicated by the lack of onlap and thickening toward the fault that would indicate syn-depositional tectonics. Truncation of the Precambrian wedge and thinning of the Weber-Leadville interval above the wedge suggest that there was deposition, rotation, and erosion of the strata followed by reactivation of the fault in the reverse direction during the Pennsylvanian (Fig. 2.10). Relatively constant thickness intervals above the Weber sandstone observed on the 2D seismic line suggest little to no local tectonic activity until the Laramide orogeny when the fault was reactivated again as a reverse fault.

Figure 2.8 suggests that the SH_{max} orientation in the study area is roughly WNW-ESE, assuming the orientation lies between the E-W orientation to the north and the NW-SE orientation to the south. A WNW-ESE direction of compression does not match with the NW-SE trending anticlinal structures, which would suggest a NE-SW compressional direction. This disparity indicates that the structural story is more complicated than Figure 2.9 depicts. This complexity is supported by the large variation in fault, joint, and sigma 1 orientations at the surface (Fig. 2.11). The mapped joints are the most "well-behaved." Joint set one trends NW-SE or NNW-SSE with one anomalous joint set 1 trending NE-SW. Joint set two trends NE-SW. Mapped minor faults were more chaotic with trends oriented E-W, NW-SE, N-S, and NNE-SSW. Similarly, sigma 1 orientations range from NW to NE to overburden stress.

2.2 Predicting fracture orientations

To predict where fractures are most likely to occur, fracture models developed for different structural types may be useful. One model, by Zahm and Hennings (2009), illustrates the formation of hinge-parallel and hinge perpendicular fractures along the fold of a high-angle thrust fault (Fig. 2.12). Hinge-parallel fracture intensity in this model is greatest where maximum curvature is greatest in both positive and negative features. Hinge-perpendicular fractures are present throughout the fold regardless of curvature.

Angster (2010) constructed a forward model in 3D Move of the asymmetrical Big Snowy Mountains anticline, similar to the Beaver Creek Anticline in the study area, to determine areas of high strain where fractures may form (Fig. 2.13). Curvature analysis showed elongate high strain in regions with the highest curvature along the fold, which is consistent with the Zahm and Hennings model. Smaller regions of high strain were also observed on the steep wall of the anticline in the Angster model. Some high strain also occurs at the crest of the anticline and some high strain areas were related to a bend in the anticlinal axis.

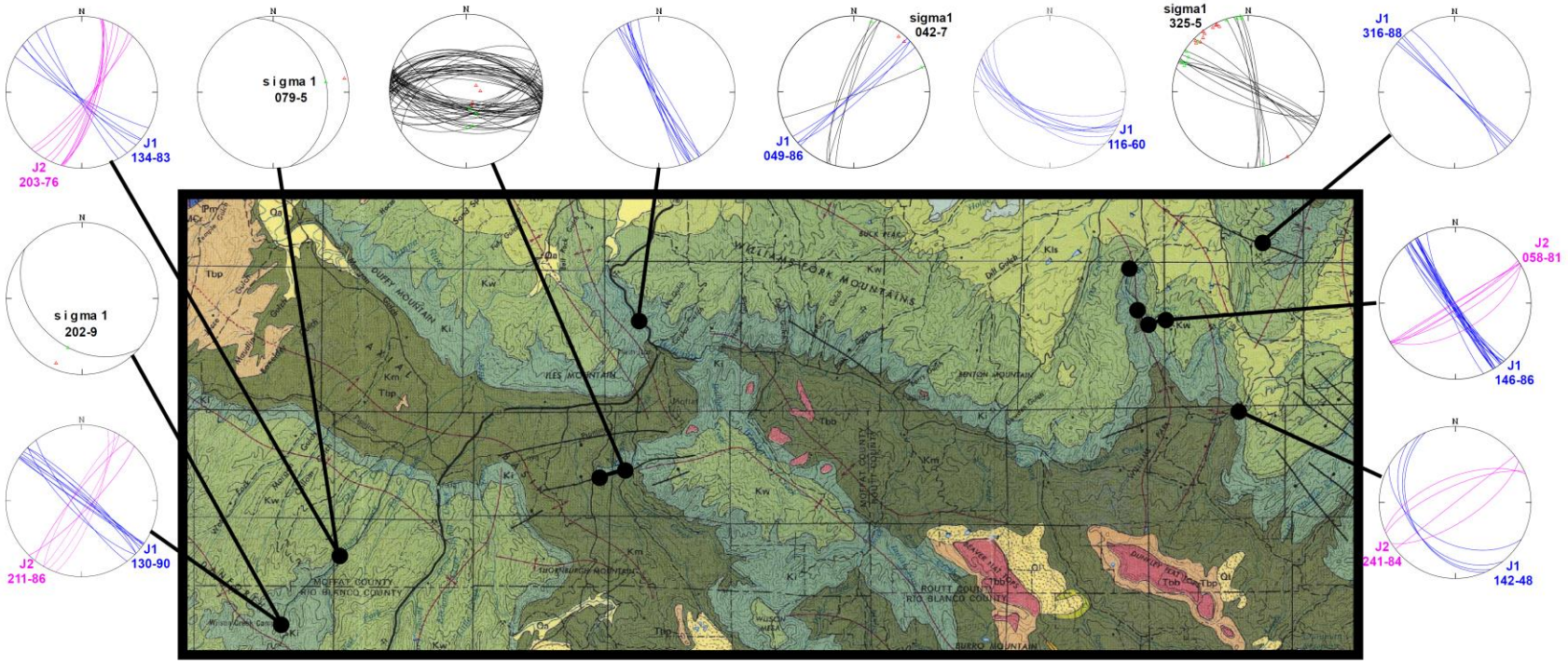

Figure 2.11. Geologic map of Craig with stereonets of joint planes superimposed on the geologic map (S.M. Larson from E.A. Erslev, 2013, personal communication). Joint set one (J1) trends NW-SE or NNW-SSE with one anomalous joint set 1 trending NE-SW. Joint set two (J2) trends NE-SW. Mapped minor faults were more chaotic with trends oriented E-W, NW-SE, N-S, and NNE-SSW. Similarly, sigma 1 orientations range from NW to NE to ENE to overburden stress. The Durham Ranch 3D survey area is in the center of this map.

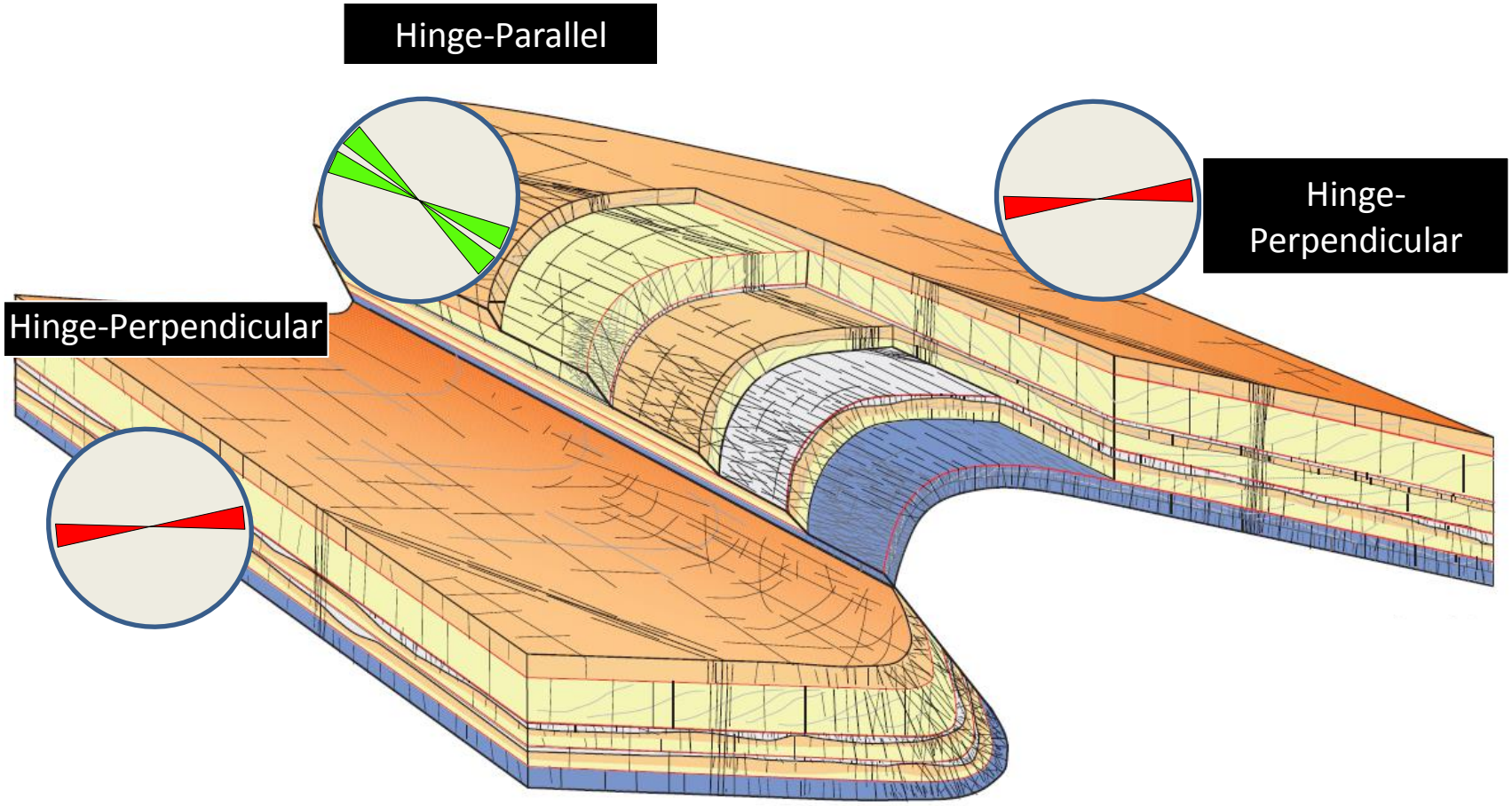

Figure 2.12. Diagram of a fold model for fracture intensity along the fold of a high-angle thrust fault (from Zahm and Hennings, 2009). Model indicates highest density of hinge-parallel fractures in zones of maximum curvature. Hinge-perpendicular fractures seem to exist throughout the fold regardless of curvature.

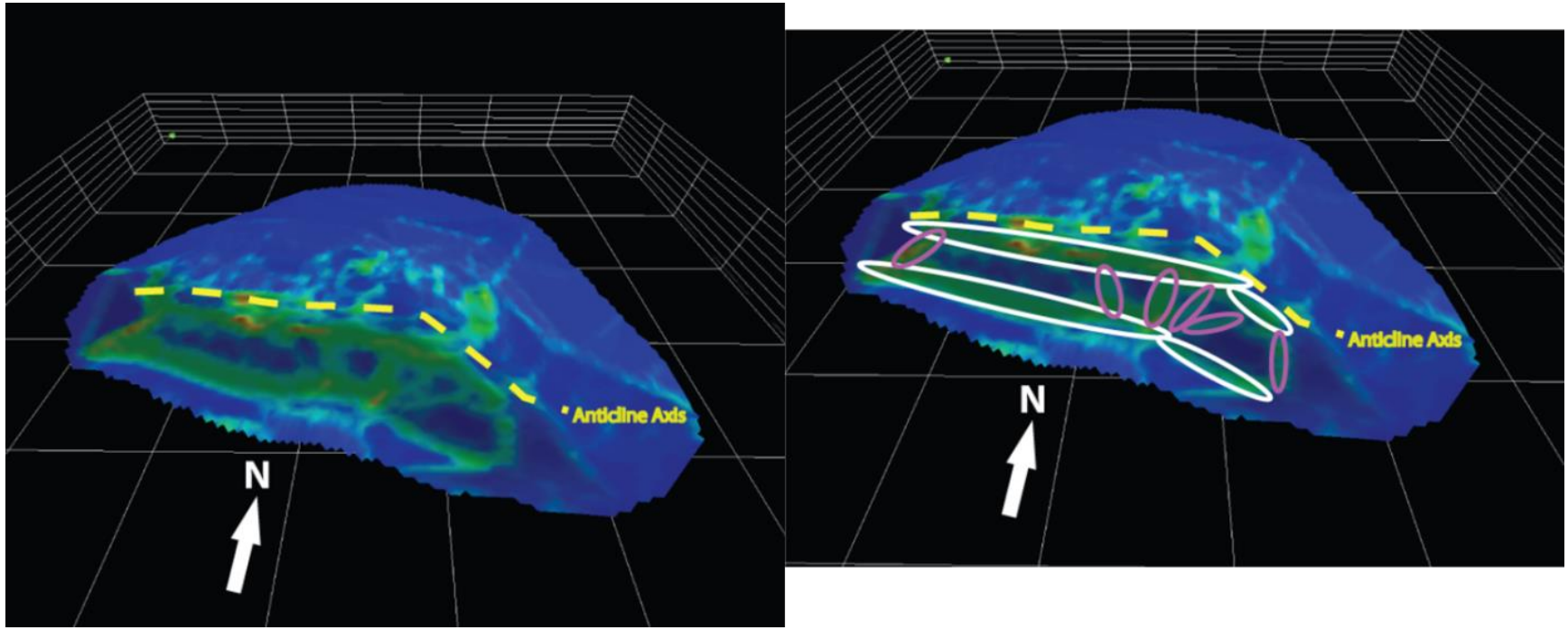

Figure 2.13. Three-D Move model of the Big Snowy Mountains showing high strain (green) in regions with highest curvature, including on the steep wall of the anticline, at the crest of the anticline, and near the bend in the anticlinal axis (Angster, 2010).

These models for predicting fractures related to fold structures are useful but, as was mentioned before, Vincelette and Foster (1992) found that most of the Laramide-related fractures are completely calcite-filled. Understanding the circumstances needed for reactivation of the Laramide-related fractures may be essential to predicting the location of reactivated and potentially open fracture trends. Vincelette and Foster suggest that Laramide fracture trends that are oriented sub-parallel to the direction of later extension are most likely to be reactivated. They also noted that calcite-filled fractures perpendicular to main structural thrust trends in overlying brittle beds were often indicative of open fractures within the Niobrara below.

2.3 Basics of seismic curvature attributes

Klepacki's (2012) seismic curvature attribute analysis of the Bicentennial 3D survey in the Williston basin will be used as a basis for the workflow of the seismic attribute analysis in this study. In his summary, Klepacki explains how to parameterize a 3D seismic volume when calculating curvature attributes in both the Kingdom and Petrel software, both of which will be used in this study. He identifies Kingdom as easier to use but less customizable, and Petrel as more robust but requiring a deeper understanding of the calculations.

Klepacki also reviews the several main types of curvature. Maximum curvature may be used to display duality in fault anomalies. High values of minimum curvature indicate deformation in multiple directions and have been associated with dense faults and fractures. Most positive and most negative curvature highlight positive (peaks and ridges) and negative (bowls and valleys) features respectively. They are two of the best attributes for identifying small faults and folds. Dip curvature may be utilized to image hinge-parallel faults superimposed on a larger structure. Strike curvature would image hinge-perpendicular faults superimposed on a larger structure. All of these can be useful in identifying smaller-scale features in 3D surveys.

CHAPTER 3
METHODOLOGY

3.1 Well log top picks

Forty-six well logs, five of which have sonic logs, were acquired from the IHS database and include wells from the conventional Waddle Creek Oil Field. Most wells had resistivity and/or gamma ray logs. These well logs were interpreted in order to "ground truth" the seismic interpretations by providing well ties and generating structure maps.

All of the top picks were made in the Petra program on raster logs except for the five with sonic logs, which were digitized. Top picks within the Niobrara were first made on the five digitized logs, based on the type log and cross section by Finn and Johnson (Fig 3.1). These picks were then coordinated with the nearby Piceance basin well log picks, which were validated by comparison to several published Piceance basin well logs and petrophysical analysis of a core (M.C. Krueger, 2012, personal communication). Using criteria developed from the above digitized data, the Niobrara Formation intervals were picked on all forty-five well logs available. These criteria include:

1. Top Niobrara: Identified by a rapid cleaning upward in the GR log and a similar decrease in induction up section.
2. Base Niobrara (top Carlile): Identified by an abrupt shift from higher GR readings to lower gamma ray readings that reflect the cleaner nature of the Fort Hays equivalent limestone and chalk interval at the base of the Niobrara. This abrupt gamma ray shift is accompanied by a similar drop in conductivity or increase in induction.
3. Marl benches: Identified by peaks in induction logs and troughs in conductivity logs. Unlike the Buck Peak and Tow Creek benches, which are recognized by a single induction peak each, the Wolf Mountain bench in the study area is identified as two stretched out peaks in the induction logs. The gamma ray pattern varies and the overall pattern is unique for each bench.
4. Marly shales: Identified by relatively low induction log readings. Gamma ray pattern varies and the overall pattern is unique for each shale.

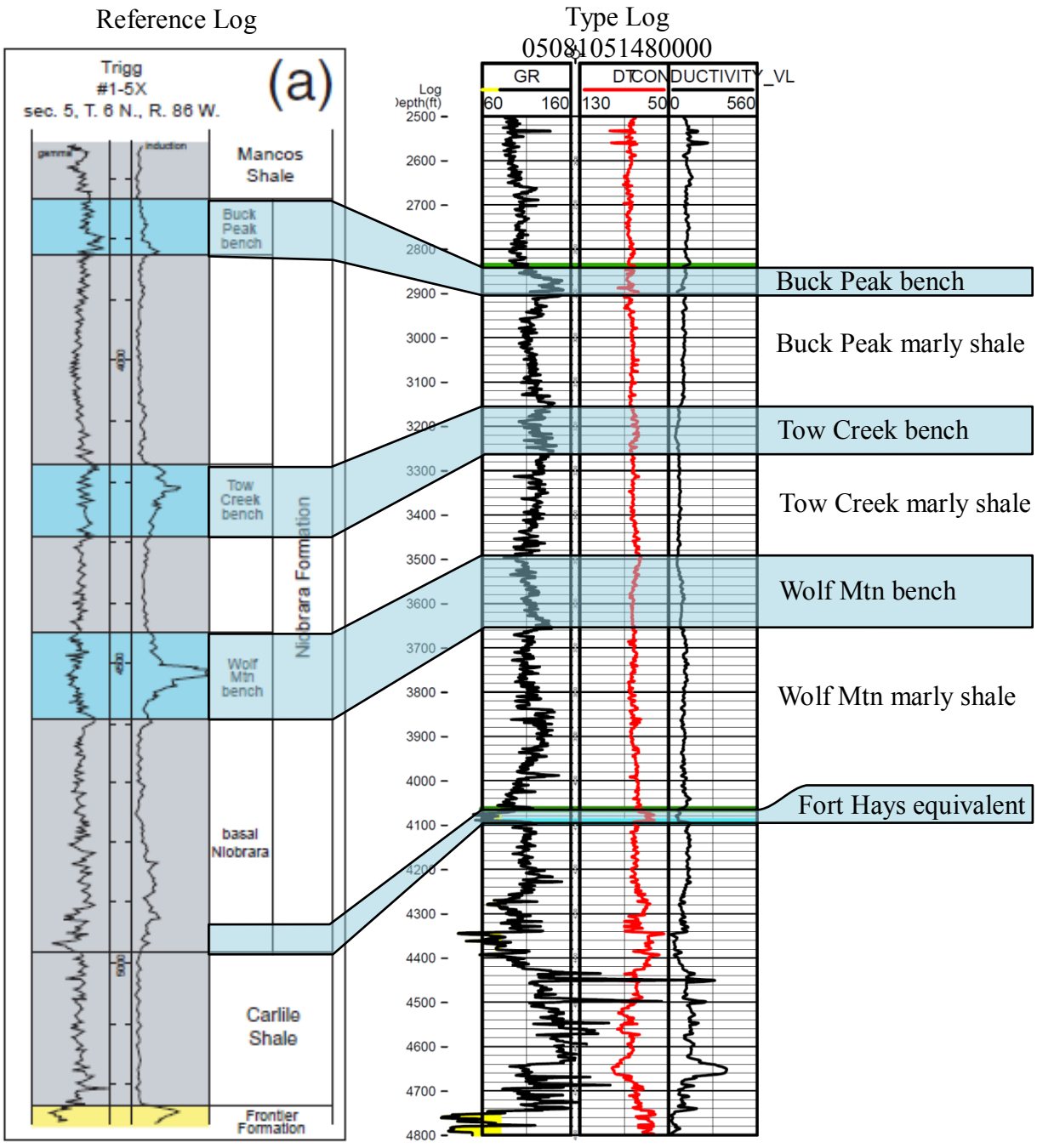

Figure 3.1. Type log picks on right for study area based on reference log on left from Finn and Johnson (2005). The top of the Niobrara is identified by a rapid decrease upward in the GR log and a similar decrease in induction up section. The base of the Niobrara is identified by an abrupt shift from higher GR readings to lower gamma ray readings that reflect the cleaner nature of the Fort Hays equivalent limestone and chalk interval at the base of the Niobrara. This abrupt shift in the gamma ray is accompanied by a similar drop in conductivity or increase in induction. The three marl benches are identified by peaks in induction logs and troughs in conductivity logs. Gamma ray patterns for the benches vary but the overall pattern is unique for each bench.

Other deeper tops were picked using the Wilson Creek Field Texaco Unit 66 well log picks as a reference (Stone, 1986). These tops included Frontier, Dakota, Morrison, Curtis, Shinarump, Moenkopi, Phosphoria, Weber, Minturn, and Leadville although most logs did not reach deeper than Dakota.

Niobrara structure and thickness maps were generated in Petra using the Niobrara tops as a simple check of the structure observed in the seismic data.

3.2 Seismic well tie

After the tops were picked, the five digitized sonic logs were imported into Kingdom Suite and Petrel with the GR log, induction/conductivity logs, and well top picks and tied to the seismic. To accomplish this, synthetic seismic traces were generated for each well and the character of the synthetic was matched with the character of the seismic trace. To help facilitate the tie, an estimated time-depth relationship was developed by inputting two-way time (TWT) estimates for the well tops at each well. Based on the knowledge that the Niobrara is shallow in this area (Chapin, personal communication), and the expected seismic signature of the Niobrara based on lithology changes, estimates were made for where tops would be in two-way time to generate a basic time-depth chart.

In Petrel, the phase of the synthetic was rotated until the pattern seemed to best match the extracted traces from the seismic. In both Kingdom and Petrel, minor bulk time shifts and squeezing/stretching were executed to tie the synthetic to the extracted trace as closely as possible. Using this well tie, the Buck Peak bench, Tow Creek bench, Wolf Mountain bench, and Carlile were digitized in Kingdom and Petrel as horizons (Fig. 3.2). Additionally, Frontier, Dakota, Morrison, Curtis, Shinarump, Moenkopi, Phosphoria, Weber, Minturn, and Leadville horizons were digitized based on the well ties in Petrel only.

3.3 Seismic analysis

The seismic data was used to observe the present day structure, map faults in the study area, and interpret the paleo-tectonics of the area. Structural interpretation was done by integrating mapped horizons, calculated seismic attribute volumes, extracted attributes on key horizons, and construction of isochron maps. Whenever possible, interpretations were supplemented by previous studies in published literature. Faults were also mapped for a clear visualization of the study area and to use in the three dimensional forward model.

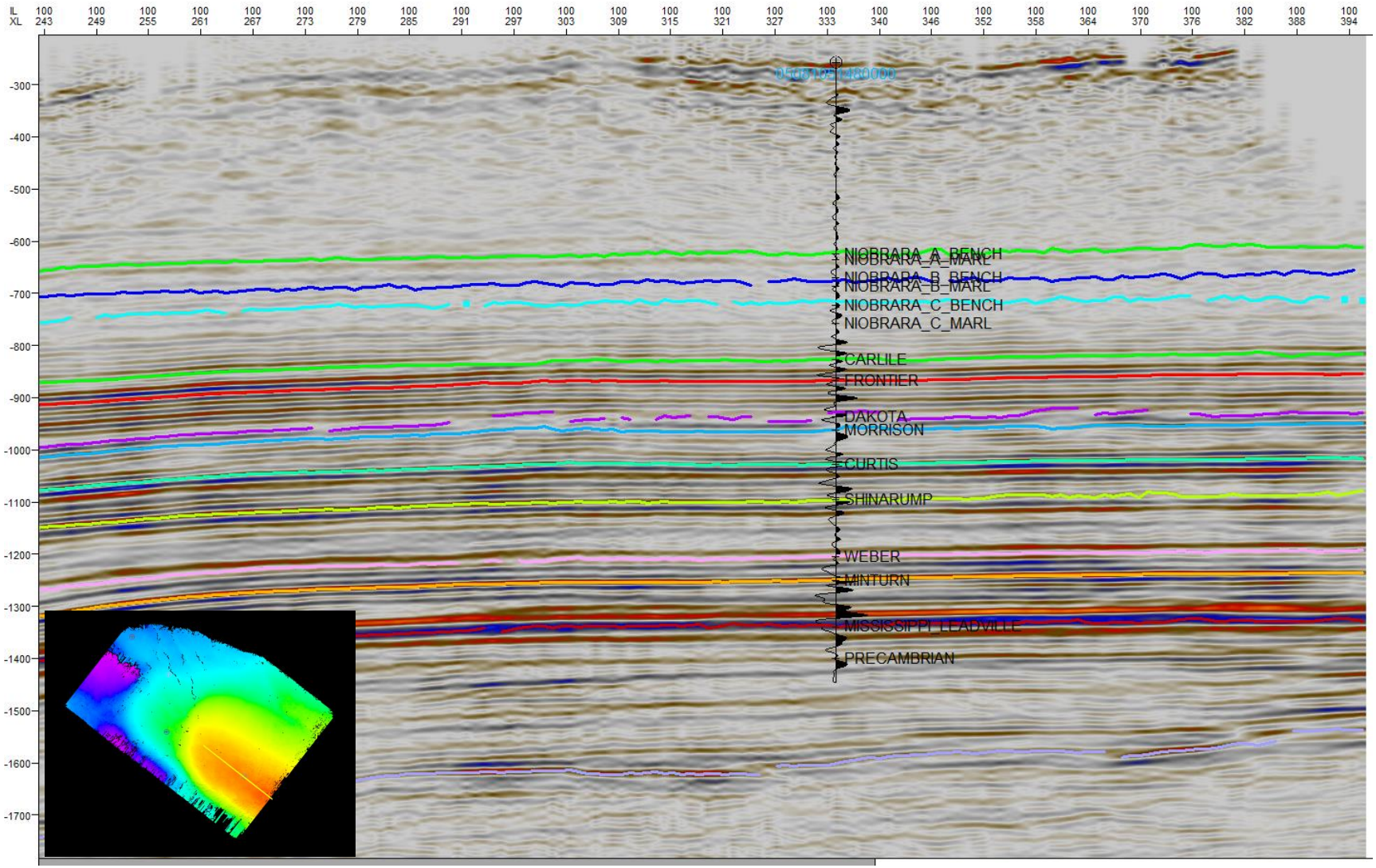

Figure 3.2. Seismic well tie for well 0508105148000, the deepest well drilled in the survey area. The colored lines are the mapped horizons based on the well tie.

3.3.1 Durham Ranch 3D seismic volume dataset

The study area is defined by the extent of the Durham Ranch 3D seismic survey in southeastern Moffat County, CO (Fig. 2.9). The survey covers ~25mi^2 over T4N R90W, T5N R90W, and part of T5N R91W. It was provided by ION Geophysical as a pre-processed volume with a seismic resolution of ~51ft. The processing is listed below:

1) Geometry Assignment, sort out vertical(p-wave) traces, and QC
2) True Amplitude Recovery (t**1.4 Gain)
3) Apply Refraction Statics => Shift to Smooth Floating Datum
4) Trace edits based on trace statistics and limit to 5.0sec
5) Edit trace spikes/noise bursts and air-blast
6) Surf. Cons. Decon (Single Window Spike, 160ms operator lengths, 0.1 operator 'white noise'); bracketed by removable AGC
7) Trace edits based on trace statistics
8) RoGain(tm) (1000ms Median Scaling-400ms smoothing)
    a. 1st Velocity Analysis (1mile x 1mile)
9) One pass of surface consistent residual statics (s1)
10) 2nd Velocity Analysis (1/2mile x 1/2mile)
    a. 2nd pass residual statics (s2) 10B) AZIM(tm) analysis and application
    b. 3rd pass residual statics (s3) and Trim Statics (+/- 9ms)
11) Mute & Stack
12) FXY Decon (3x3 il/xl)
13) Spike to noise burst edit (remove spikes prior to migration)
14) Post-Stk Phase Shift Migration
15) Spectral Whitening (5-10-90-110)
16) Trace Equalization
17) Time-Variant Bandpass Filter (5-10-90-110@0-0.5s;5-10-70-80Hz@1.0-2.0s;5-10-60-70@2.5-3.0s;5-10-40-50@3.5-5.0s;5-10-30-40@6.0-8.0)
18) KxKy
19) RoGain(tm) (1000ms Median Scaling, 400ms overlap)

The seismic volume was bricked (Kingdom) or realized (Petrel) to divide the volume into smaller volumes allowing attribute calculations to be run more efficiently.

3.3.2 Digitizing horizons

Key horizons were mapped using Kingdom and Petrel for better visualization of the structure in three dimensions, to generate isochrones, and to extract seismic attributes on the horizons. The Kingdom program was easier to use whereas the Petrel program was more customizable.

In Kingdom the following workflow was used:

1) Use well ties to determine where to digitize the horizon
2) Use "2D Hunt" to pick the horizon every tenth inline and crossline
3) Manually digitize the horizon where "2D Hunt" is not accurate
4) Run "3D Hunt" on ten by ten grid

In Petrel the following workflow was used:

1) Use well ties to determine where to digitize the horizon
    a. The top crystalline basement horizon was not picked based on well ties, since there were none, but based on the transition from continuous reflectors to discontinuous reflectors
    b. Since the well control for deeper horizons were poor or nonexistent, the Morel et al. (1986) 2D seismic line to the SE was used as reference
2) Use "2D autotracking" to pick the horizon every tenth inline and crossline
3) Use "Fill" when 2D autotracking is overly aggressive
4) Manually digitize the horizon where seismic data is too chaotic for "2D autotracking" and "fill"
5) Generate a structural smooth volume of the seismic with the "Volume attributes" process
6) Run "3D autotracking" with the following parameters:
    a. (Realized) seismic volume as input
    b. Use seeds: Visible points
    c. Check "Seed confidence" and input 25%
    d. Check "Optimize for dipping reflectors"
    e. Check "Use wavelet tracking" and set "Correlation quality" to 0.95
    f. Click "3D Track"

g. Run “3D autotracking” again while decreasing “Correlation quality” by 0.05 each time until you reach 0.75
h. Uncheck “Use wavelet tracking”
i. Run “3D autotracking” again with the structural smooth seismic volume as the input for “Seismic Volume”

7) Manually fix and re-digitize problem areas in the autotracked horizons

By using this workflow for 3D autotracking in Petrel, the well-controlled areas may be autotracked as accurately as possible while still generating an interpretation for the poorly controlled areas using the smoothed volume. There are limitations to autotracking in areas with discontinuous or weak reflectors so manually re-checking the lines is necessary for an accurate horizon interpretation. Since autotracking picks along the highest amplitude, it is expected to highlight faults on the edge of the seismic resolution better along strong reflectors than manual digitization.

3.3.3 Seismic attribute analysis

Generating seismic attributes helps in mapping key structural and fault features in the study area and possibly highlights potential high density fracture zones. A number of different types of attributes were calculated in both Kingdom and Petrel to determine which process would minimize noise and reveal the important features.

In Kingdom the following process was used to generate attribute maps:

1) Run “Rock Solid Attributes…” on the seismic volume with the following parameters (Klepacki, 2012):
    a. For “Correlation Window” input 1/seismic_dominant_frequency
        i. Use the “Spectrum Analysis” to determine dominant frequency for the time interval around the horizon of interest +/- 0.1 sec
    b. For “Maximum Lag” input ½*correlation window
    c. Check “Smoothing (DPS)”
    d. For “Min. Correlation Coef” input 50%
2) Display attributes on horizons with the dropdown menu

In Petrel the following process was used to generate attribute maps:

1) Convert horizons to surfaces via the “Make/edit surface” process
2) Run the “Volume attributes” process

a. Generate a "Structural Smooth" volume as recommended by Klepacki (2012) using the following process
    i. For all curvature attributes use the "Structural Smooth" volume as the input seismic
    ii. For all other attributes use the "(Realized)" version of seismic unless the process requests a different type of volume such as an edge-enhanced volume
b. Pick the attribute to run
c. Select "Dip guided with edge enhancement" as the filter option
d. Set Sigma XYZ to 1, 1, 1
e. Calculate vertical radius using the following equation:
   Vertical Radius = ((1000/seismic dominant frequency)/sample_rate)/2
    i. Use the dominant frequencies collected from the Kingdom workflow to calculate vertical radius
f. For Inline/Crossline radius input 3, which was determined to be the most effective in highlighting features of interest
    i. A value of one images smaller features but also too much noise
    ii. A value of five images larger features that are easily visible on the structure maps
g. Run the process

3.3.4 Convert two-way time horizon to depth horizon

The two-way time horizons were converted to depth horizons to reflect the scale of structural deformation and to make the interpretations more relevant to well planning and production. The following process was used for this time-depth conversion:

1) Collect the two-way times (ms) for well tops in each of the five wells and list them next to the depths (ft) of the well tops
2) Calculate the interval velocities between each well top using this formula:
   $intVel_{1to2}$ (ft/ms) = (depth2-depth1)/(time2-time1)
3) Under "Settings…" for the surface, use the calculator to convert the two-way time surface to depth using the following formula:
   depthSurface2 = ((timeSurface2-timeSurface1)/2*$intVel_{1to2}$) + depthSurface1

3.4 Forward model

A three dimensional forward model was developed to highlight key areas of high strain through time and high curvature in present day structure that may indicate areas of fracture formation. The model was produced in Midland Valley's 3D Move program using the following workflow:

1) Digitize major faults on every 10 inline and crossline in Petrel
2) Export major faults in IESX format
3) Import fault lines into Midland Valley Move
4) Generate a surface in Move using the fault lines as input
5) Transfer the fault surfaces from Move to 3D Move
6) Use "retesselate" and "resample at half" functions in 3D Move to smooth the fault and simplify the model ("Retesselate" converts the point surface into a triangle mesh)
7) Create a horizontal horizon in two way time depth at the expected depth of the undeformed, buried horizon
    a. Based on the constant thickness of the Niobrara interval, it was assumed that the Niobrara was deposited relatively horizontal
8) Cut the horizon with any faults along which there is displacement
9) Open "Strain" window under "Attributes"
    a. Add horizontal horizon
    b. Click Apply
10) Use the "Structural modeling" process to move the hanging wall
    a. Use the "Fault parallel fold" modeling type
    b. Add the fault along which the hanging wall is displaced
    c. Add the horizon
    d. Orient the displacement plane in the direction of movement
    e. Click apply
    f. Adjust the slip until the vertical displacement matches the structure maps from the 3D seismic survey
    g. Repeat for each major fault

i. If the fault did not cut through the horizon but affected it through deformation (folding), slip was moved in the negative direction in order to reflect the correct final geometry

Limitations of the 3D model include the following:

i. Movement along the faults were done separately rather than at the same time
ii. Faults were stationary
iii. Movement along faults was modeled as dip slip when in fact movement was likely at an oblique angle
iv. The faults were smoothed into larger faults even though they were actually fault zones
v. The model does not replicate the main NW-SE trending anticline well due to the limitations of the modeling program

3.5 Production data

Since it is not possible to directly image fractures at the scale of the seismic resolution (51 ft), locations of producing Niobrara wells are used to help support or disprove predictions of open fracture swarms. This will help shed light on areas where structurally formed fractures were sealed, remained open, or were reopened.

The process used to analyze the production data is:

1) Import production data (intial production tests) from IHS Direct Connect in Petra
2) Map IP test data as a bubble map in Petra to show distributions of productive and unproductive Niobrara wells
3) Manually input well locations into Petrel and change well symbol/color to reflect the initial production value
4) Overlay well symbols on attributes to observe any production trends related to attribute features or structure

CHAPTER 4

RESULTS

4.1 Well log results

Based on the criteria listed in Chapter 2, the key Niobrara intervals were picked on all forty-six wells with logs that ran through part or all of the Niobrara within the study area. From these well picks, a structure map was generated in Petra (Fig. 4.1). The map shows the top of the Niobrara dipping steeply to the northwest, gently to the northeast, and dramatically to the southwest. Five major fault locations mapped from seismic work are overlain on the structure map and include the NW-SE trending Indian Run Fault, Major Fault 2 and Major Fault 3 as well

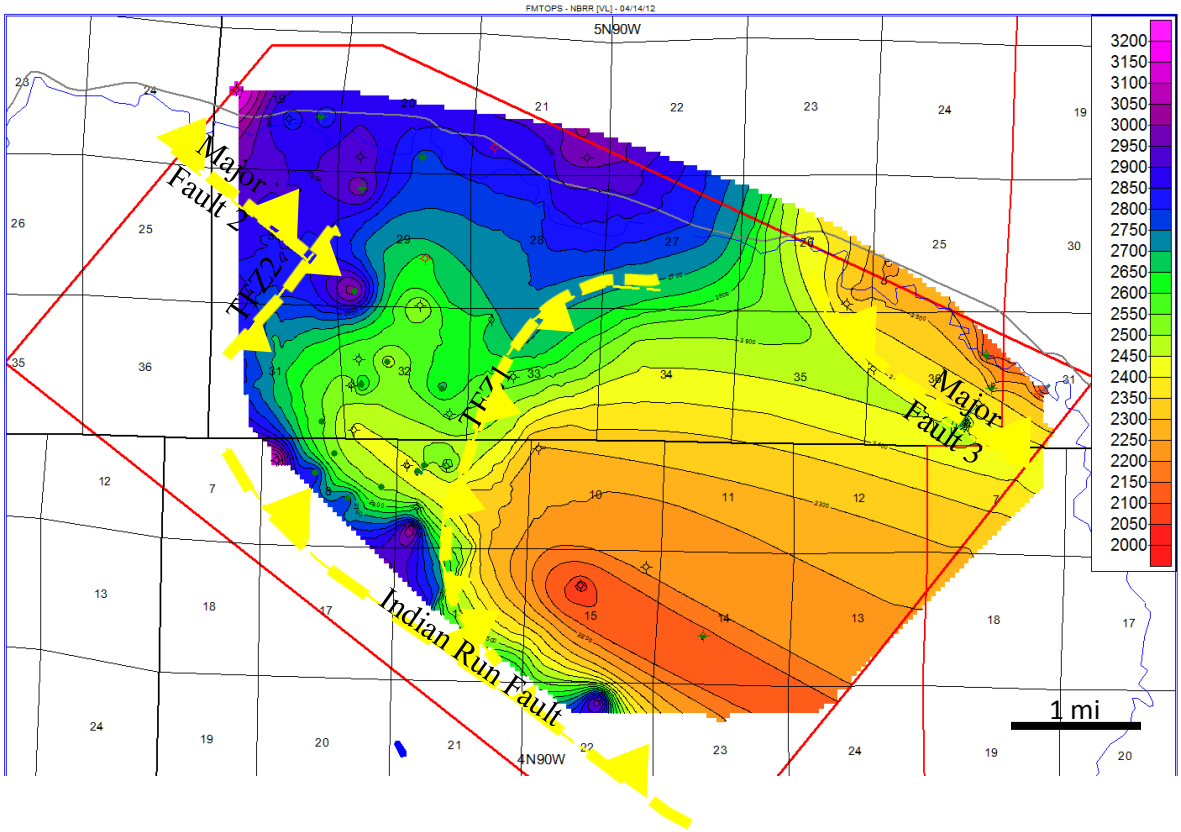

Figure 4.1. Top Niobrara structure map generated from top picks on forty-six well logs in the study area. The map shows the top of the Niobrara dipping steeply to the northwest, gently to the northeast, and dramatically to the southwest. Dashed yellow lines indicate locations of major thrust faults at depth below top Niobrara except for Major Fault 2, which cuts through the Niobrara Formation. Triangles indicate the dip direction of the fault planes.

as the NE-SW trending Transition Fault Zone 1 (TFZ1) and Transition Fault Zone 2 (TFZ2). These five faults are used as structural references in other maps.

A thickness map was also generated between the Niobrara and Carlile well top picks and shows thicknesses ranging from 1070 ft in the southeast to 1200 ft thickness in the northwest (Fig. 4.2). There is a thickness change in the Niobrara of at least 130 ft in the study area. In section 4.3.2, this log-based thickness map is compared with mapped linear features to determine whether the controls on the thickness variations in the Niobrara are depositional or structural. A more detailed seismic isochron maps will also supplement this interpretation. Note that only 23 well logs span the Niobrara to Carlile interval and that this map measures vertical thickness rather than bed thickness meaning increasing dip increases measured thickness.

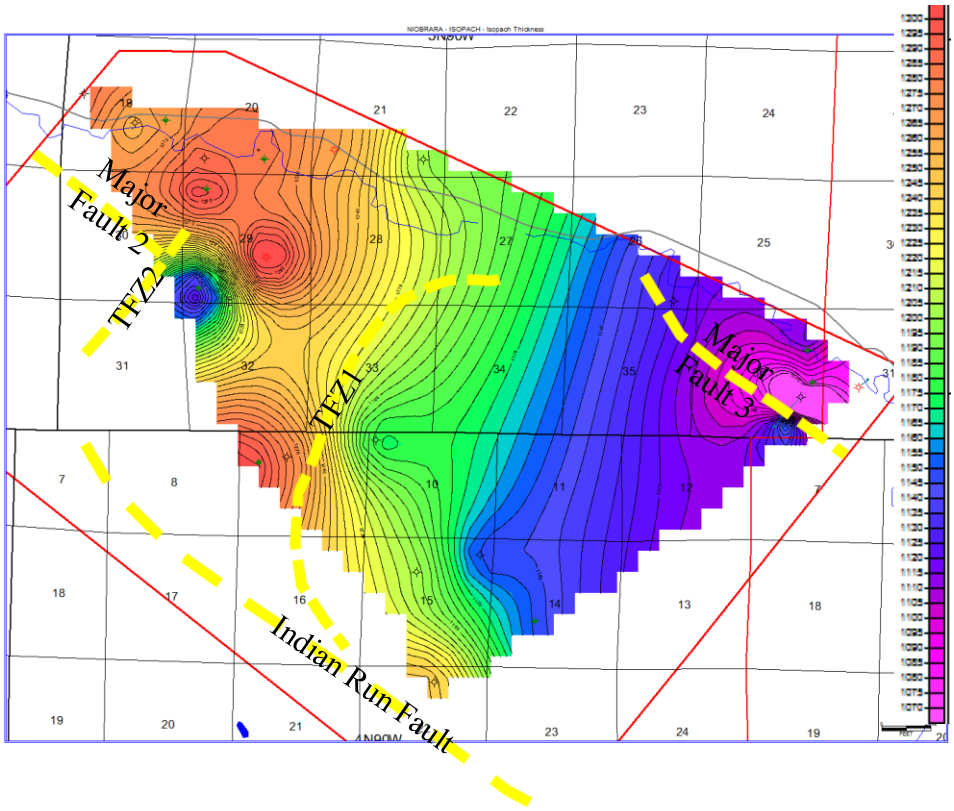

Figure 4.2. Vertical thickness map in feet generated from the top Niobrara to top Carlile top picks from 23 wells. The map shows thicknesses ranging from 1070 ft in the east to 1200 ft thickness in the west.

4.2 Production data

Fifty-six wells in the study area are listed as targeting the Niobrara Formation for production, including several proposed wells. Well information and production data is listed in

Table 4.1. Most of the wells drilled in the Waddle Creek field from the 1960's through 1980's were vertical wells that targeted the both the marl benches and marly shales of the Tow Creek and Wolf Mountain intervals. Only one well targets the upper Buck Peak bench, however, a number of other intervals throughout the Niobrara were also perfed in that well so the production may not be attributed to the Buck Peak bench alone. Figure 4.3 shows all wells within the study areas and the total vertical depth to which the wells were drilled. Not all of these wells had well logs for correlating. The deepest well reached 7,822ft TVD and had a well log data that ran all the way down.

Bubble maps were generated using the IP, cumulative production, and first 12 months' production data (Fig. 4.4, 4.5, and 4.6). The available production data in the study area is sparse and concentrated primarily in one area but by overlaying the well production on structure and attribute maps, the location of producing and dry wells will highlight the features that support production and those that do not. Relationships between production, fault features, and potential fracture zones will be discussed in Chapter 5.

4.3 Seismic data

Evaluating 3D seismic data provides a more holistic view of a study area than one-dimensional well data and two-dimensional seismic lines. The Durham Ranch 3D seismic survey is used in this study to develop a structural analysis and an interpretation of paleo-tectonic controls on fracture formation. To accomplish this, a number of horizon, attribute, and isochron maps were generated. Major and minor faults were mapped based on linear features observed in the attribute maps to emphasize the complex transition zone present in the study area.

4.3.1 Present-day subsurface structure

Mapping key horizons in the seismic survey reveals the present day structure within the study area. Based on this structure, predictions may be made for syn-growth fracture formation based on high curvature and simple fracture models. A look at crosslines and inlines reveal that there are five major thrust faults in the study area and that they may be all linked by the same detachment surface (Figs. 4.7, 4.8, 4.9, 4.10). In the inline, two faults seem to plateau off in a non-balanced section, however, this is due to the fact that the direction of shortening is oblique to the inline plane so the fault surface continues deepening toward the east. This three dimensional view of the major faults illustrate how they interact with each other within the survey area (Fig. 4.11). Two of the faults continue further off the survey area but are assumed to reach the same

Table 4.1. A list of wells targeting the Niobrara formation within the survey area with initial production, cumulative production, and first 12 months production.

UWI/API	SURFX	SURFY	IP (BPD)	Cum Prod (BBLs)	First 12 mo Prod (BBLs)	PERF TOP (ft)	PERF BASE (ft)	COMP DATE	ABAND DATE	Perfed Bench (BP=Buck Peak; TC=Tow Creek; WM=Wolf Mtn; MS=Marly Shale)
05081051710000	1433980.38	369645.45	52	240,784	3,288	3,117	3,431	11/25/1964	10/3/2012	TC
05081051770000	1438080.68	368253.9						6/5/1965		
05081051800000	1436668.61	369042.09	144	118,104	5,255	2,076	3,026	1/6/1964		TC MS
05081051880000	1435668.89	369637.92	102	41,344	2,415	2,754	3,072	8/23/1964		
05081056870000	1435314.81	368624.14	10			3,039	3,259	2/19/1966		TC
05081056880000	1438098.55	369696.11	5			2,910	3,671	11/10/1965		WM
05081060150000	1437744.81	369517.55						6/6/1967		
05081060160000	1435554.01	371348						6/21/1967		
05081062400000	1435838.6	373176.12				3,170	3,335	1/22/1975		
05081062670000	1435578.43	376952.43	4			3,330	4,630	1/5/1976		TC
05081062700000	1437675.13	369953.15						8/29/1978		
05081062710000	1439099.52	373021.15	7			2,908	3,707	1/13/1976		
05081064550000	1432434.92	370127.59						1/29/1981		
05081065250000	1441957	373504.01						10/12/1982		
05081065440000	1440396.95	368631.87		21,120	8,155	2,455	3,273	5/1/1983	10/1/1995	BP MS, TC, WM
05081065440000						2,305	2,455			BP
05081065440000						2,455	3,111			
05081065440000						3,151	3,192			
05081065440000						3,232	3,273			
05081065440001	1440396.95	368631.87								
05081065600000	1438232.9	369625.68	110			2,810	2,825	8/23/1983	10/1/1995	TC MS

Table 4.1. A list of wells targeting the Niobrara formation within the survey area with initial production, cumulative production, and first 12 months production cont'd.

05081065830000	1436793.72	374228.24	390	171,382	63,990	2,919	3,047	5/4/1984		TC
05081065830001	1436793.72	374228.24	50			2,919	3,170	6/12/1996		WM
05081065910000	1435472.08	362987.42						7/25/1985	4/23/1998	
05081065930000	1437756.24	362358.01								
05081065940000	1435439.17	373143.48						11/7/1985		
05081065960000	1435900.39	361759.13						7/25/1985		
05081066180000	1441074.28	375999.12						8/26/1985		
05081066420000	1437886.97	367432.44						1/13/1986		
05081066440000	1439275.2	372114.77						11/22/1985		
05081066450000	1442292.52	375042.35						12/4/1985		
05081066460000	1438212.65	376359.41						12/10/1985		
05081066470000	1435622.83	374379.72						1/12/1986		
05081066580000	1436972.51	371421.93						12/22/1986		
05081066590000	1435618.19	374603.99								
05081069340000	1434507.1	371683.55								
05081069350000	1434775.67	370416.72	71	9,339	3,355	1,512	3,060	5/4/1998		WM
05081069350001	1434775.67	370416.72				1,512	3,300	6/1/2000		
05081069850000	1434272.37	371688.63	100	27,461	9,346	2,810	3,291	2/27/2001		TC, WM
05081072510000	1439928.88	373974.06								
05081072520000	1438194.28	374548.17								
05081072570000	1432842.94	368381.11								
05081072580000	1437391.89	375624.69								
05081072590000	1434155.17	374331.51								
05081075920000	1437392.31	375624.57				3,041	3,896	12/2/2009		
05081076200000	1433162.2	371454.55	206	6,469	6,469	3,002	6,030	1/23/2012		
05081076220000	1433132.6	371496.44	202	521	521	3,134	6,750	1/17/2012		
05081076230000	1437843.45	367444.25								

Table 4.1. A list of wells targeting the Niobrara formation within the survey area with initial production, cumulative production, and first 12 months production cont'd.

05081076670000	1440369.49	368693.05		18,069	18,069	2,315	5,175	10/1/2012		
05081076670100	1440369.49	368693.05								
05081076680000	1440354.49	368645.18		9,245	9,245	2,766	6,543	10/1/2012		
05081076680100	1440354.49	368645.18								
05081076810000	1435427.98	363016.78						6/24/2012		
05081076810100	1435427.98	363016.78								
05081075920100	1437392.31	375624.57	51	564	466	4,661	5,255	7/22/2010		
05081075920100						4,661	4,662			
05081075920100						4,870	4,871			
05081075920100						4,913	4,914			
05081075920100						4,956	4,957			
05081075920100						4,999	5,000			
05081075920100						5,042	5,043			
05081075920100						5,085	5,086			
05081075920100						5,128	5,129			
05081075920100						5,171	5,172			
05081075920100						5,216	5,217			
05081075920100						5,254	5,255			
05081077170000	1441231.54	375096.09								
05081077170100	1441231.54	375096.09								
05081077570000	1441221.58	375062.13								
05081077580000	1441216.04	375044.15								
05081077590000	1441226.06	375079.09								

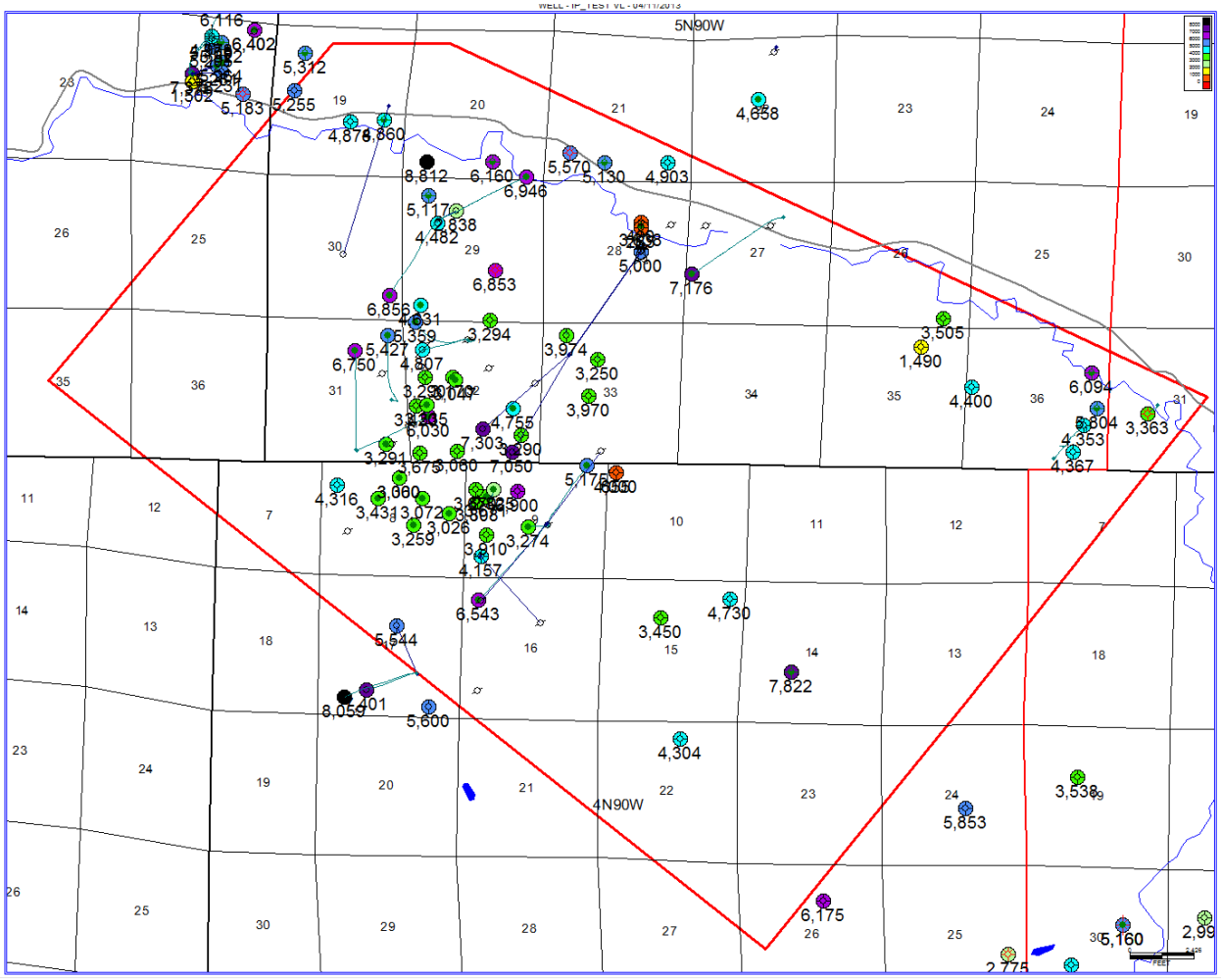

Figure 4.3. True vertical depths of all wells within the Niobrara. The green bubbles indicate wells that are approximately within the Niobrara interval. Not all wells had well logs for correlating. The deepest well reached 7,822ft TVD and had a well log data that ran all the way down. This included a sonic log, which allowed a well tie to be made down to the Leadville horizon.

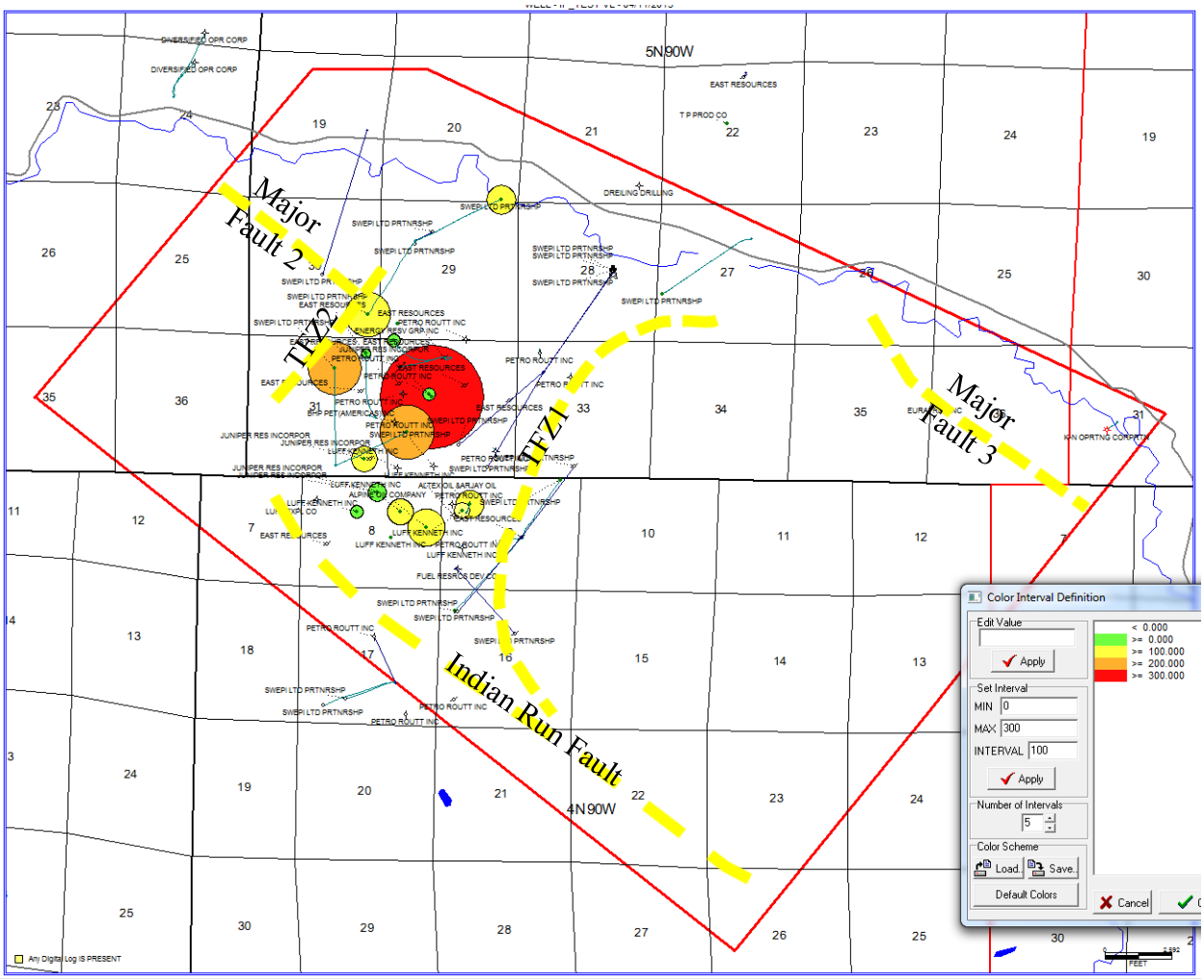

Figure 4.4. Bubble map of the fourteen Niobrara wells with initial production test data. The colors reflect the value range: green = between 0 and 100 bpd; yellow = between 100 and 200 bpd; orange = between 200 and 300 bpd; red = between 300 and 400 bpd.

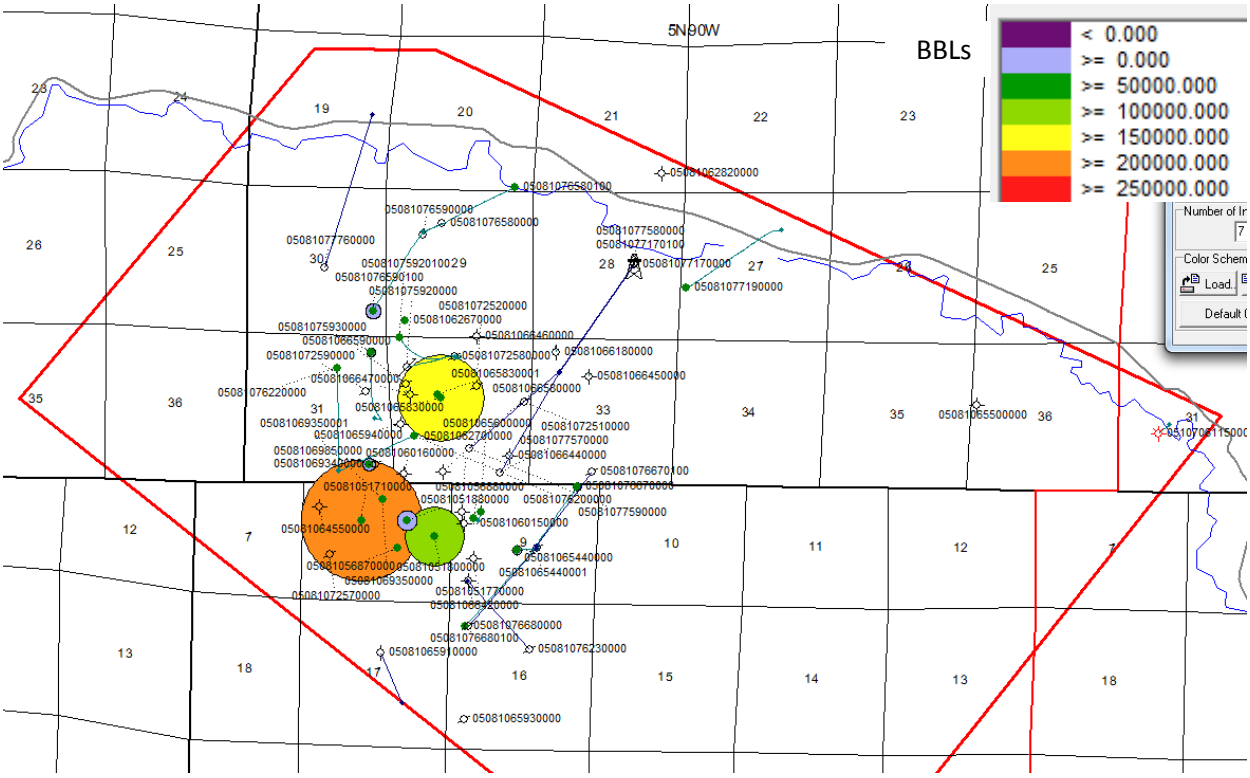

Figure 4.5. Bubble map of cumulative production from the Niobrara.

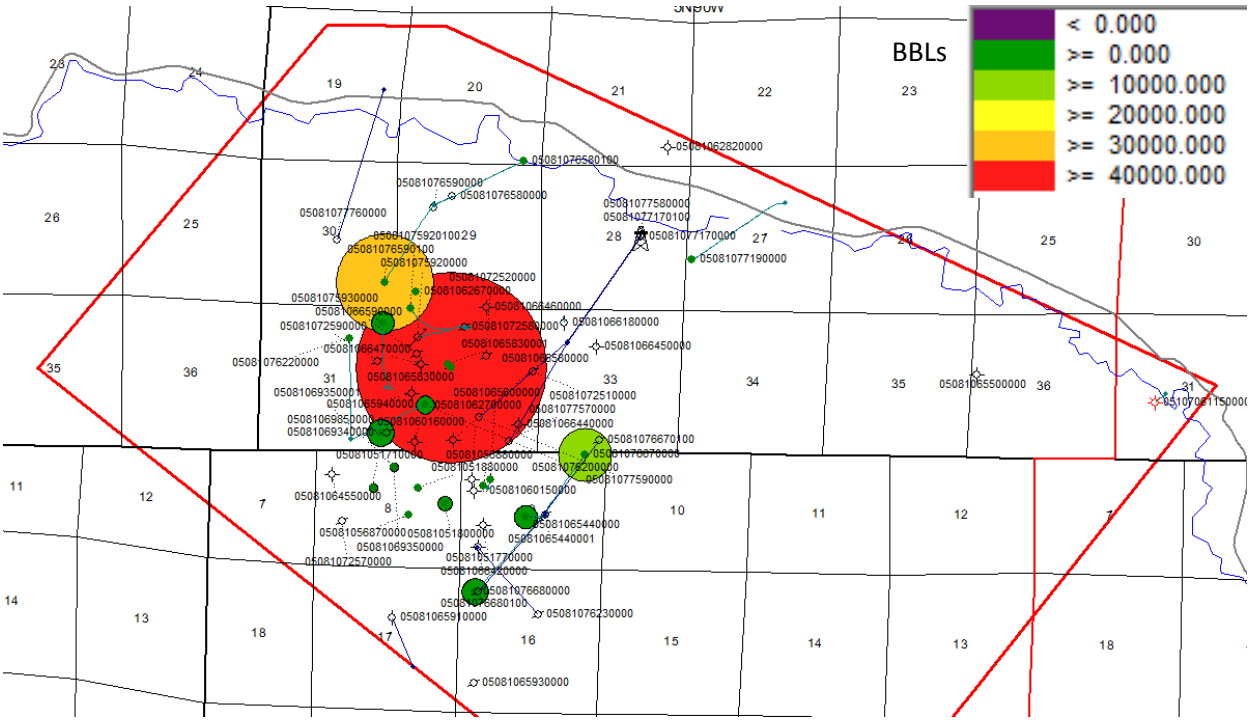

Figure 4.6. Bubble map of first 12 months production from the Niobrara.

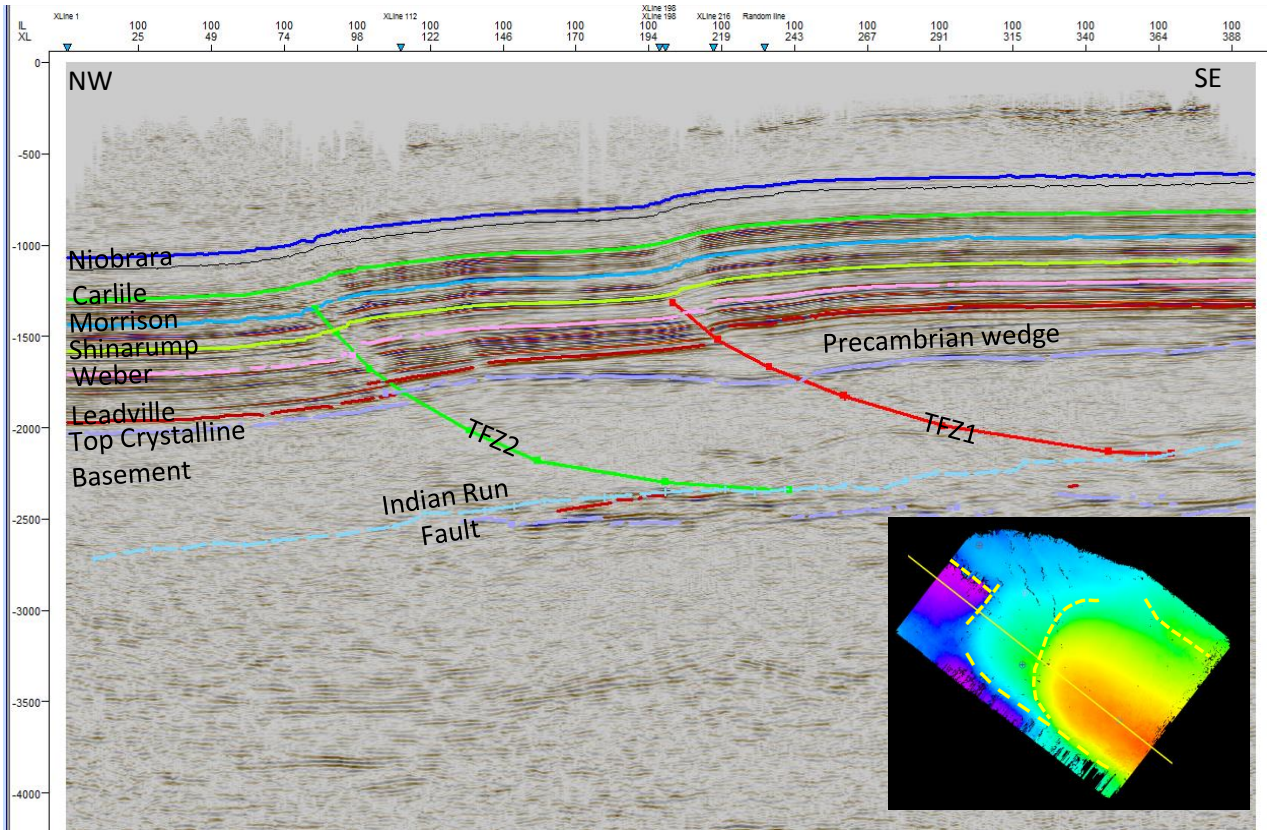

Figure 4.7. Inline 100 showing Transition Fault Zone 1 (TFZ1) and Transition Fault Zone 2 (TFZ2) forming three fault blocks. Both TFZ1 and TFZ2 are thrust faults in this view. TFZ1 and TFZ2 eventually meet up with the Indian Run Fault at depth meaning it is a linked fault system. The inset map shows the location of the inline on the Niobrara structure. There is little offset of the Precambrian wedge across TFZ1 but a distinct thickness change because the hanging wall of TFZ1 was inverted.

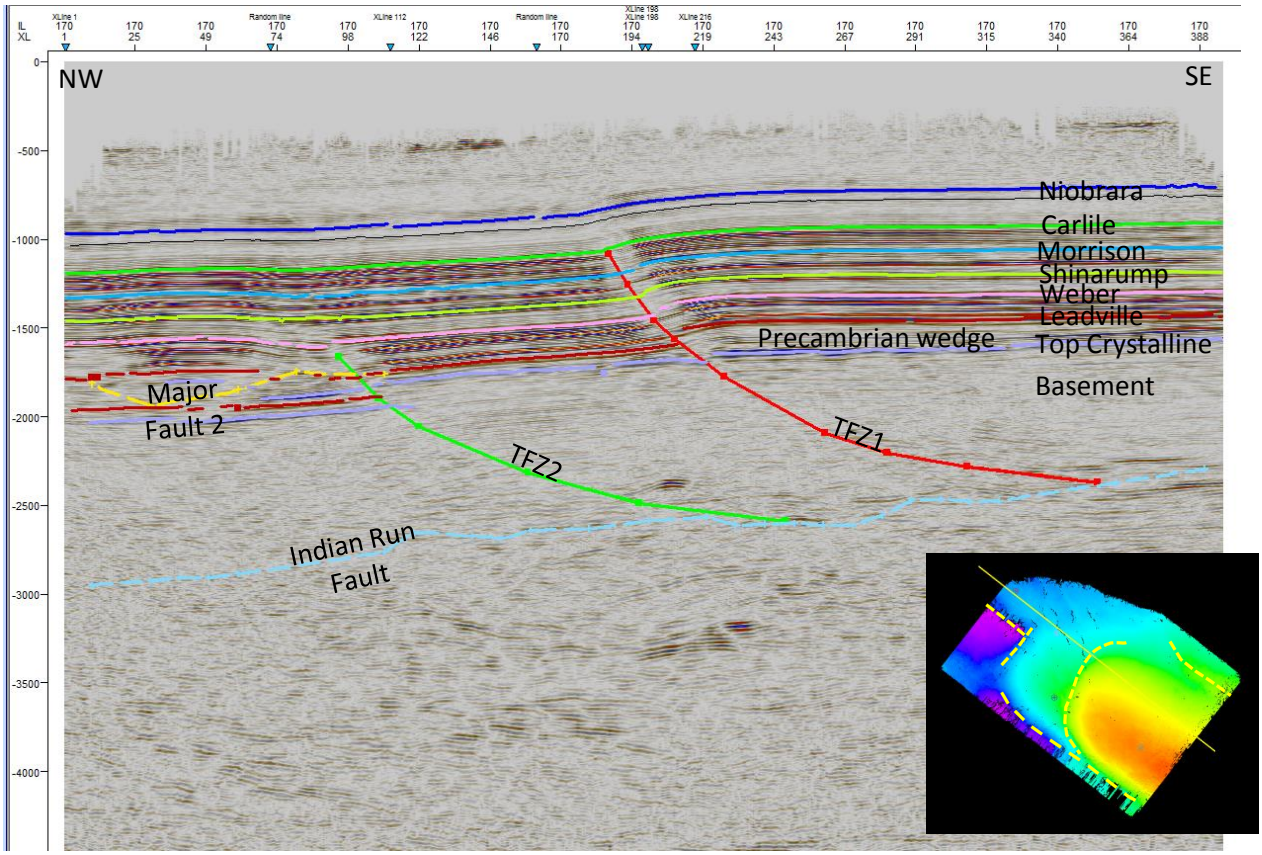

Figure 4.8. Inline 170 showing the complex faulting between TFZ2 and Major Fault 2.

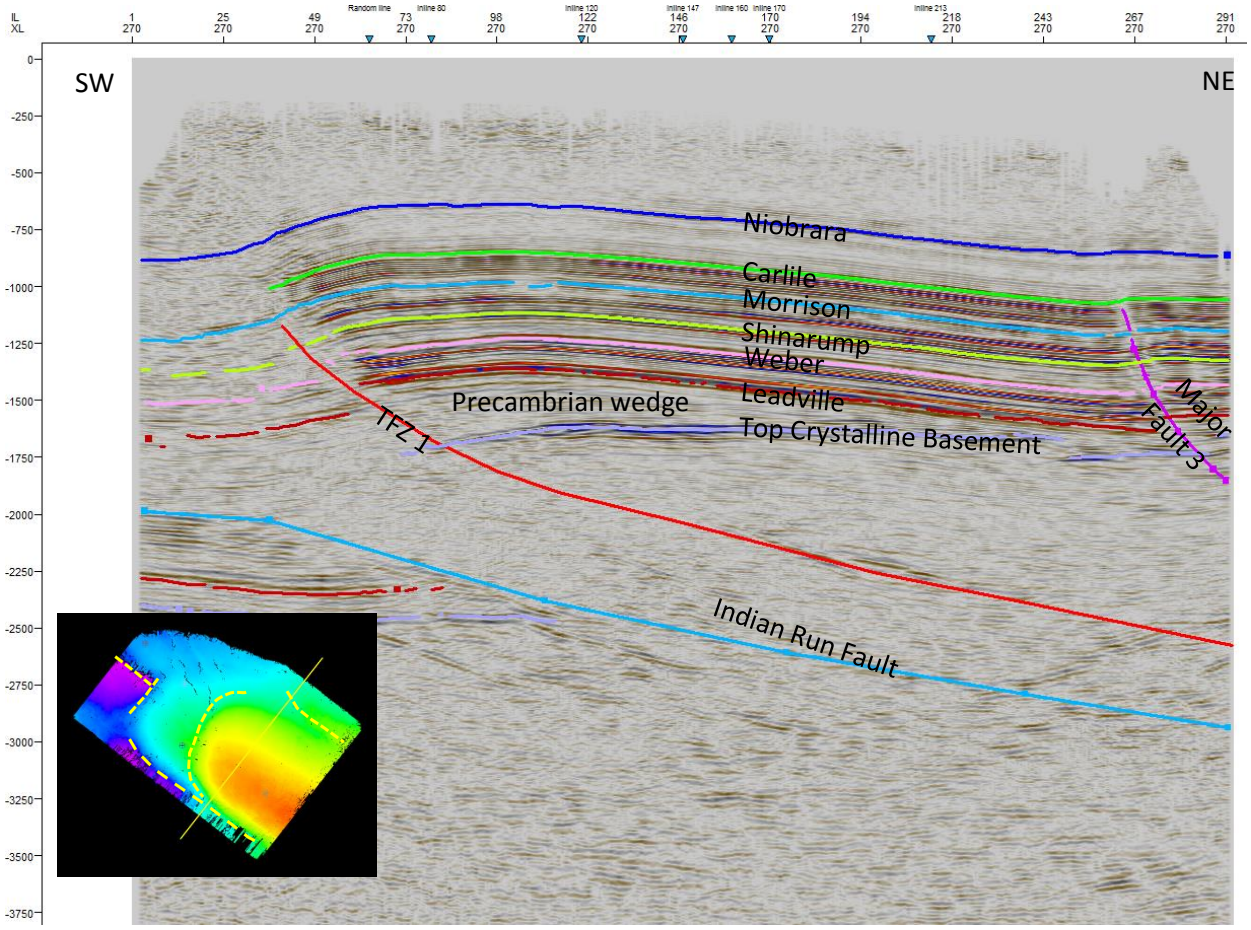

Figure 4.8. Crossline 270 showing the Indian Run Fault, TFZ1, and Major Fault 3. In this crossline TFZ1 has curved around to almost parallel the Indian Run Fault and takes up some of the shortening. The displacement along the Indian Run Fault is large as shown by the offset of the dark red horizon. Major Fault 3 also parallels the Indian Run Fault and takes up some of the shortening in that direction.

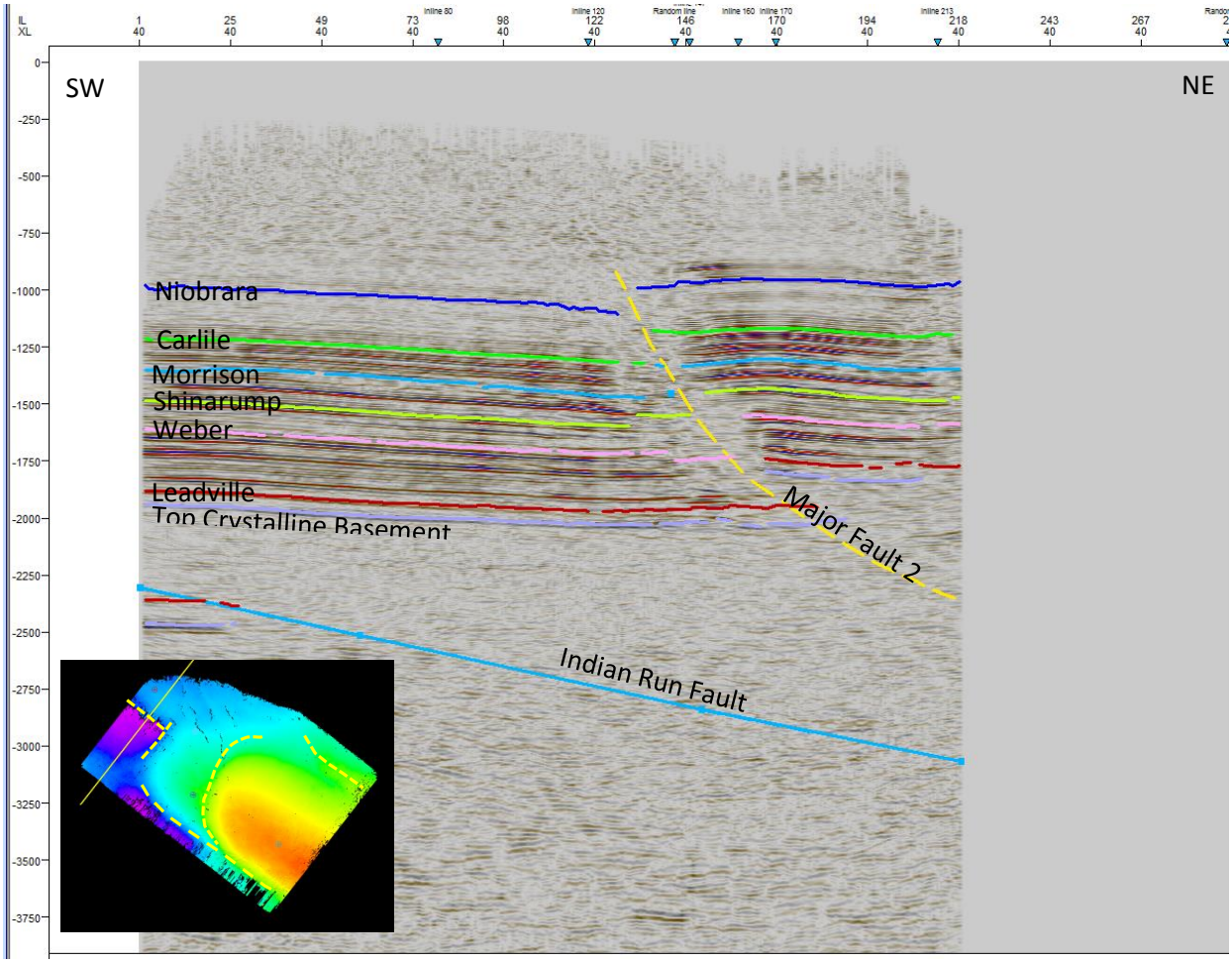

Figure 4.10. Crossline 40 showing the Indian Run Fault and Major Fault 2. They are both thrust faults. Major Fault 2 goes off the survey but it is assumed to detach at the same surface as the Indian Run Fault.

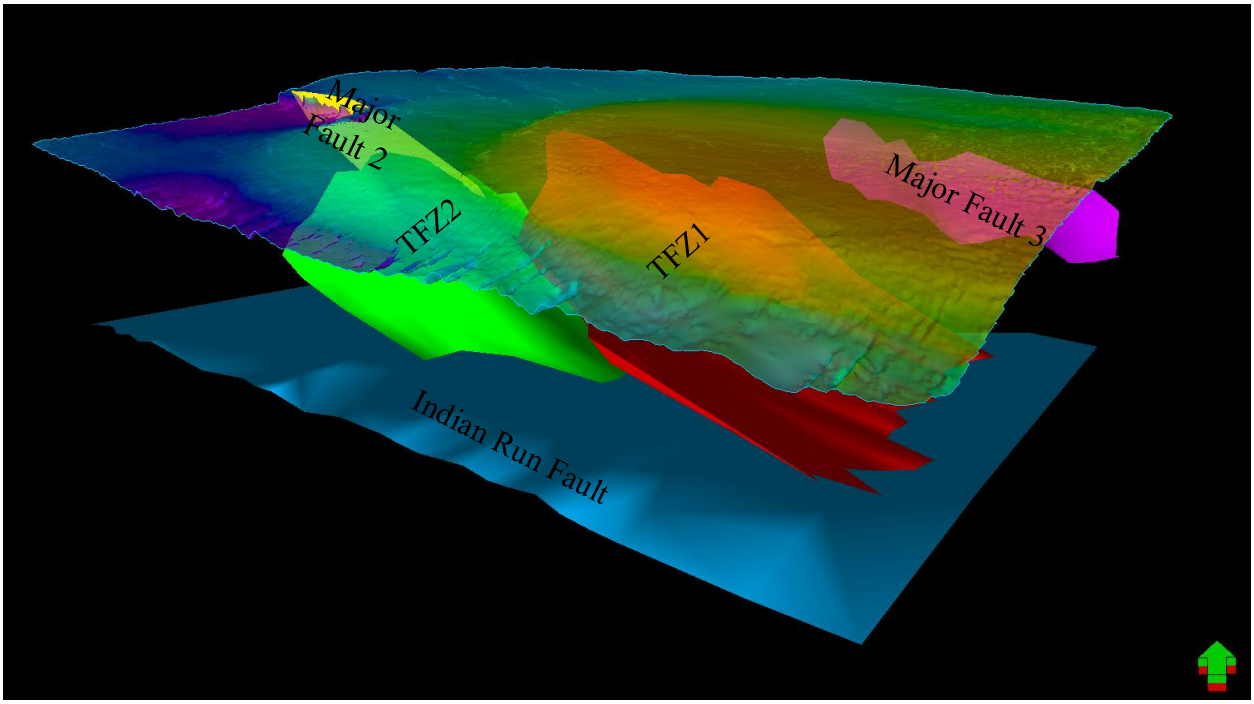

Figure 4.11. Three dimensional view from the south of the five major faults with the transparent Niobrara horizon on top for reference. TFZ1 and TFZ2 are called transition *fault zones* because they consist of a number of faults clustered together, allowing the fault zone to curve in different directions. TFZ1 and TFZ2 both branch off from the major Indian Run fault but the original detachment surface is further downdip.

detachment surface.

The depth converted map of the top Niobrara horizon (Fig. 4.12) reflects the structure of all of the horizons down to top Weber. It shows one large faulted anticline taking up most of the study area and a smaller anticline in the eastern portion of the study area. Both anticlines trend to the NW and are asymmetrical with the steeper limb on the southwest side and the gentler limb on the northeast side. The large anticline is called Beaver Creek Anticline as recognized from surface geologic mapping (Fig. 2.9). The smaller anticline to the east does not have a name but has been identified on surface geologic maps as well.

The Beaver Creek Anticline trends with the basement-involved Indian Run Fault, which trends NW-SE and does not cut through the Niobrara in the study area. The displacement along the Indian Run Fault for the Leadville horizon is estimated to be up to 15,100 ft based on a vertical displacement of 4,400 ft and a horizontal displacement of 14,450 ft in the plane of a crossline. Since the Indian Run Fault was reactivated as a thrust fault once during the formation of the Ancestral Rockies and once during the Laramide orogeny, the displacement of the

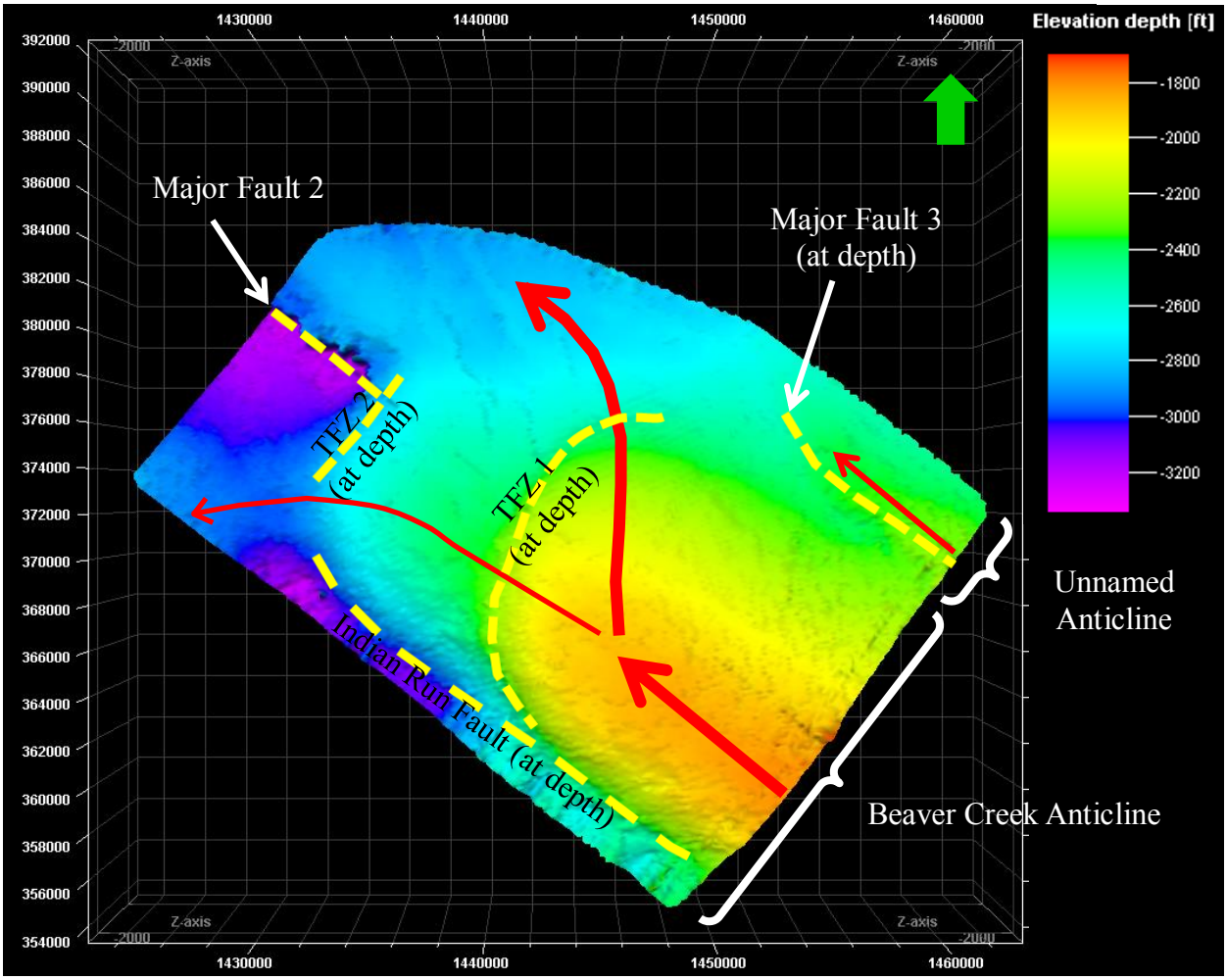

Figure 4.12. Structure map of top Niobrara. The study area covers the NW trending Beaver Creek Anticline and a smaller unnamed anticline trending in the same direction. The red arrows indicate approximate anticlinal axis and show the Beaver Creek Anticline "splitting" to reflect the redistribution of shortening. The five major faults in the area are indicated by the dashed yellow lines. Major Fault 2 is the only fault that cuts through the Niobrara, as shown by the sharp difference in time depth. The Indian Run Fault and the Major Fault 3 at depth both trend in the same direction as Major Fault 2. The NE-SW trending folds result from Transition Fault Zone 1 (TFZ1) and Transition Fault Zone 2 (TFZ2), which are both at depth. All five of these major faults are thrust faults.

Leadville horizon is much more than the estimated 5,800 ft displacement of the Niobrara horizon, which was only affected by the Laramide tectonics and not by Ancestral Rockies shortening. This is supported by the 2D seismic line published by Morel et al. (Fig. 2.10).

Two thrust fault zones branch off of the Indian Run Fault and rotate from a NNW trend to a NW trend. These two fault zones are referred to as Transition Fault Zone 1 (TFZ1) and Transition Fault Zone 2 (TFZ2). TFZ1 and TFZ2 separates the Beaver Creek Anticline into three fault blocks that down step toward the NW as shown by the steep slopes on the Niobrara horizon. TFZ2 runs between the end of the Indian Run Fault and the beginning of another NW trending thrust fault referred to as Major Fault 2 (Fig. 4.12). TFZ2 does not connect the Indian Run Fault and Major Fault 2 completely, leaving a west trending ramp. Displacement along TFZ1 and TFZ2 is at most 300 ft since TFZ1 and TFZ2 are also thrust faults but run at an angle to the Indian Run Fault, it is likely that the direction of shortening is not exactly perpendicular to the Indian Run Fault but rotated clockwise at an oblique angle. This means that movement along all of the major faults in the study area is not pure dip-slip.

While the Indian Run Fault has the largest displacement out of all of the major faults, the Beaver Creek Anticline is defined by the NW-SE trending portions of TFZ1 and TFZ2 and Major Fault 2. These high-angle thrust faults control the shape of the asymmetrical anticline. This distribution of shortening among the major Indian Run Fault and the smaller TFZ1, TFZ2, and Major Fault 2 suggests that movement along the large, relatively low-angle Indian Run Fault was hindered and there was nowhere else for the rock to go but up. This is supported by the fact that TFZ1 cuts through the Precambrian wedge suggesting that TFZ1 was not a pre-existing Precambrian fault. Similarly, the Weber-Leadville interval is roughly the same thickness in both the hanging wall and footwall of TFZ1 meaning the fault zone did not form during the Pennsylvanian. This suggests that TFZ1 and, similarly, TFZ2 formed during the Laramide orogeny.

The fault that forms the unnamed anticline to the east will be referred to as Major fault 3. Major Fault 2 is the only fault that cuts through the Niobrara interval. Since there is only displacement along Major Fault 2 within the Niobrara, the strain would be expected to be the highest between the middle fault block and the underlying footwall because it must account for the largest depth difference in a short distance. The other four major thrust faults are deeper and affect the Niobrara through folding within the study area.

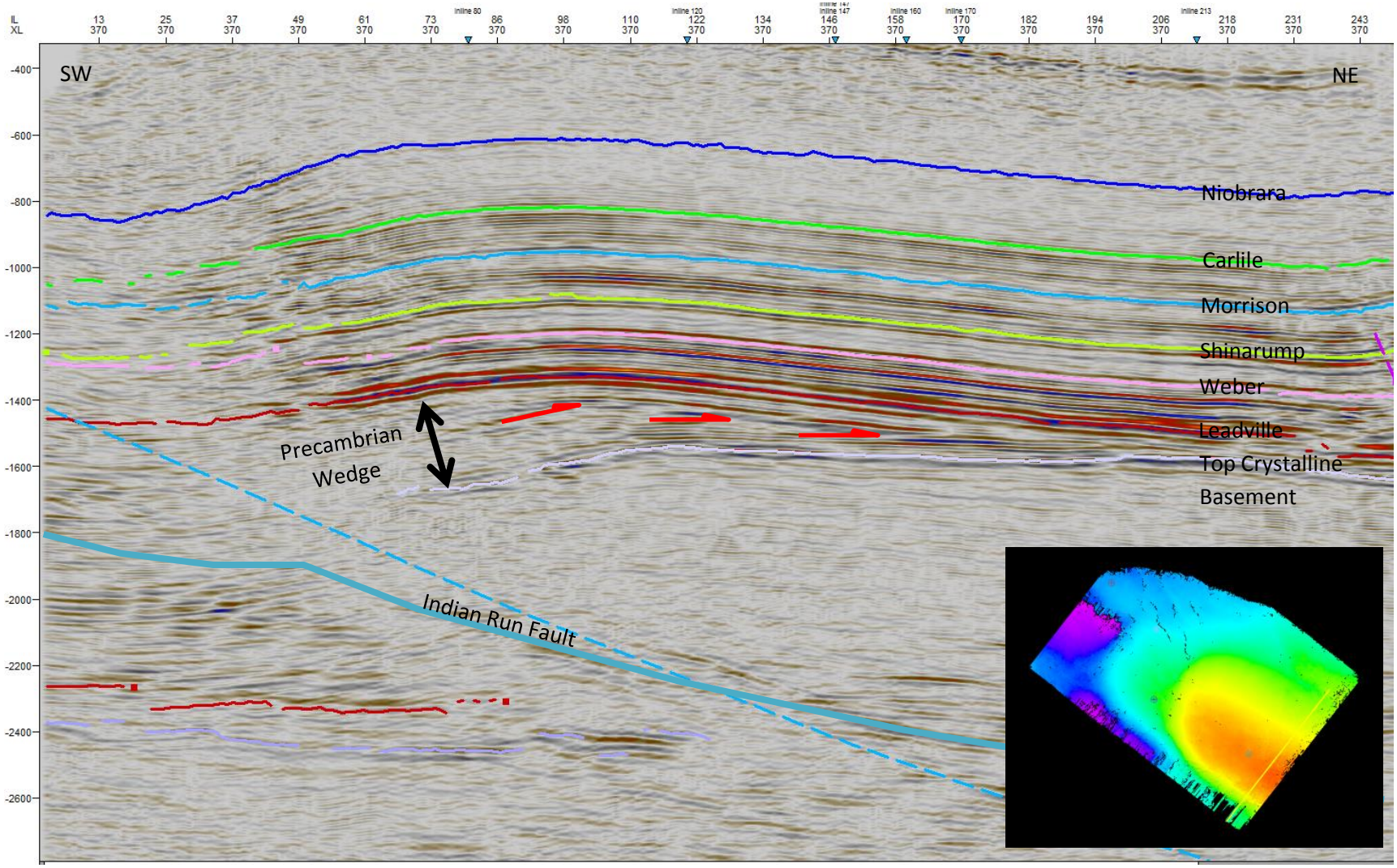

Figure 4.13. Expanded image of crossline 370 showing the truncation of the Precambrian wedge and the rotated parallel bedding in the wedge.

From top Weber and below, the structure is roughly the same but with larger displacements until the Precambrian Uinta Mountain Group, which is preserved as a truncated wedge of parallel strata (Fig. 4.13). The wedge thickens toward the Indian Run Fault and TFZ1 and will be discussed in more detail in 4.3.3.

4.3.2 Seismic attributes

Thirteen curvature attribute volumes were generated from the Durham Ranch 3D seismic survey using different parameters to determine which one produced the most useful results. These attributes were then extracted on four key horizons: top Niobrara (Buck Peak bench), top Tow Creek bench, top Wolf Mountain bench, and base Niobrara (top Carlile).

The resulting curvature and similarity maps in Kingdom enhanced all major discontinuities, making some areas noisy with non-geologic curvature anomalies (Figs. 4.14 and 4.15) The minimum curvature map of the top Niobrara horizon has a lot of noise associated with each of the five major faults. Additionally, it highlights NNW-SSE trending linear features in the northern half of the study area. These will be discussed further below. Other curvature anomalies are visible on the minimum curvature map but due to the amount of noise in the seismic data and limitations in the Kingdom program for determining features on dipping surfaces, it is difficult to determine whether these are true geologic features. The similarity attribute (Fig. 4.15) removes a lot of the noise on the gently dipping surfaces but at the cost of removing all the smaller features as well. The similarity attribute map helps emphasize the NNW-SSE trending linear features, showing that they are sinuous.

The Petrel attribute maps image more features because of its more robust parameterization and maps reflect the size of the features so smaller faults are mapped as smaller anomalies. This results in a cleaner attribute map (Fig. 4.16 and 4.17). All the attribute maps exhibit chaotic anomalies associated with the discontinuous character of reflectors in the seismic. These anomalies are concentrated near the major faults and are associated with deformation from folding. Based on these anomalies, dashed lines were mapped to indicate areas of folding related to the five major thrust faults (Fig. 4.16 and 4.17). There are also curvature anomalies at the crest of the Beaver Creek Anticline that do not reflect geologic features, but emphasize the discontinuous nature of the seismic data at shallower depths. Based on cross referencing the minimum curvature, maximum curvature, most negative curvature, most positive curvature, and the ant tracking attributes, a number of smaller linear features were mapped on the top Niobrara

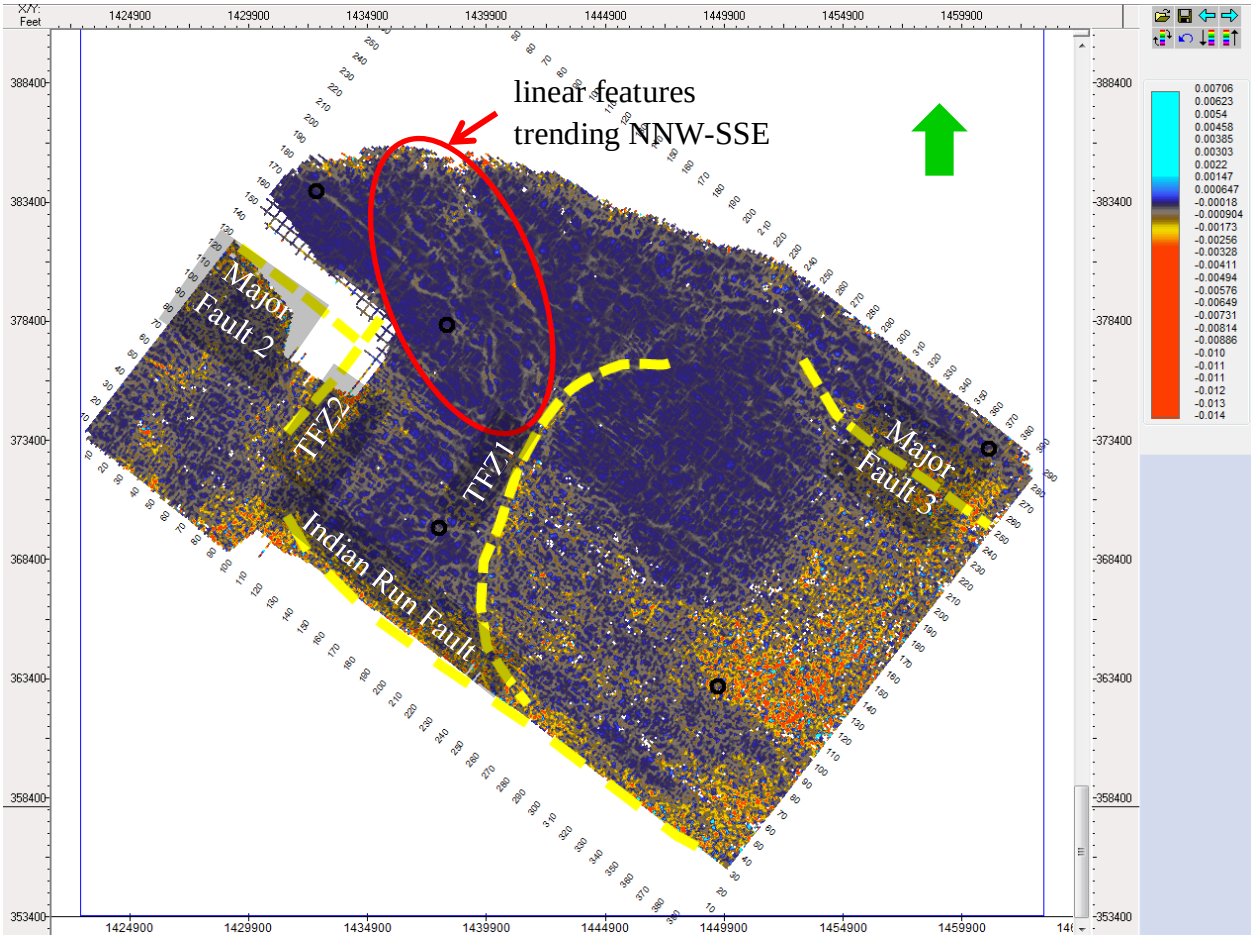

Figure 4.14. Minimum curvature attribute on the Top Niborara horizon extracted using Kingdom. Minimum curvature values are small because it is the value of the curvature in the direction with the least amount of curve. A zero value indicates a flat surface. Positive values indicate positive or anticlinal features. Negative values indicate negative or synclinal features. The minimum curvature map of the top Niobrara horizon has significant noise associated with each of the five major faults. Additionally, it highlights NNW-SSE trending linear features in the northern half of the study area, which are reverse faults. Other curvature anomalies are visible on the minimum curvature map but due to the amount of noise in the seismic data and limitations in the Kingdom program for determining features on dipping surfaces, it is difficult to discern whether these are true geologic features.

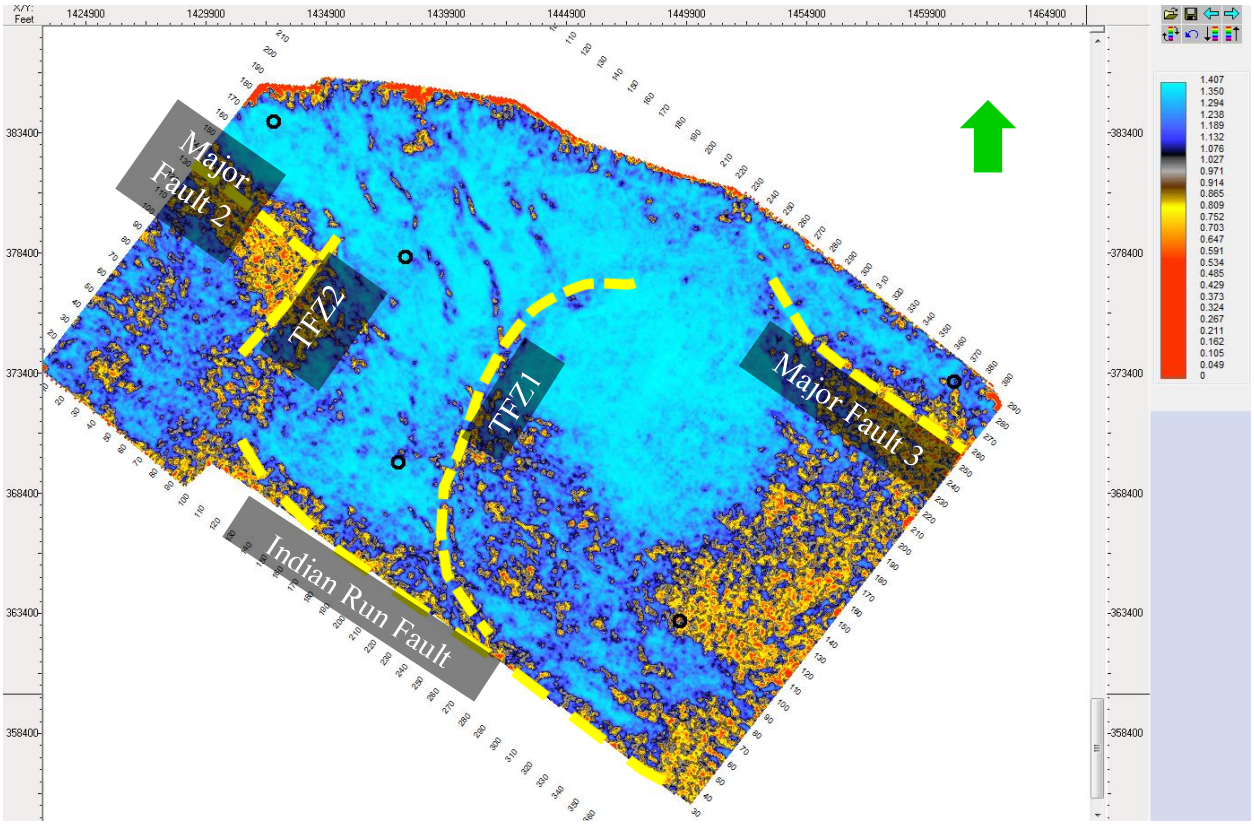

Figure 4.15. Similarity attribute map on the top Niobrara horizon extracted using Kingdom. This map reduces the amount of noise compared to the minimum curvature map but cuts out all smaller features except for those NNW-SSE trending reverse faults in the northern area. The similarity attribute determines how similar the seismic waveform is from trace to trace.

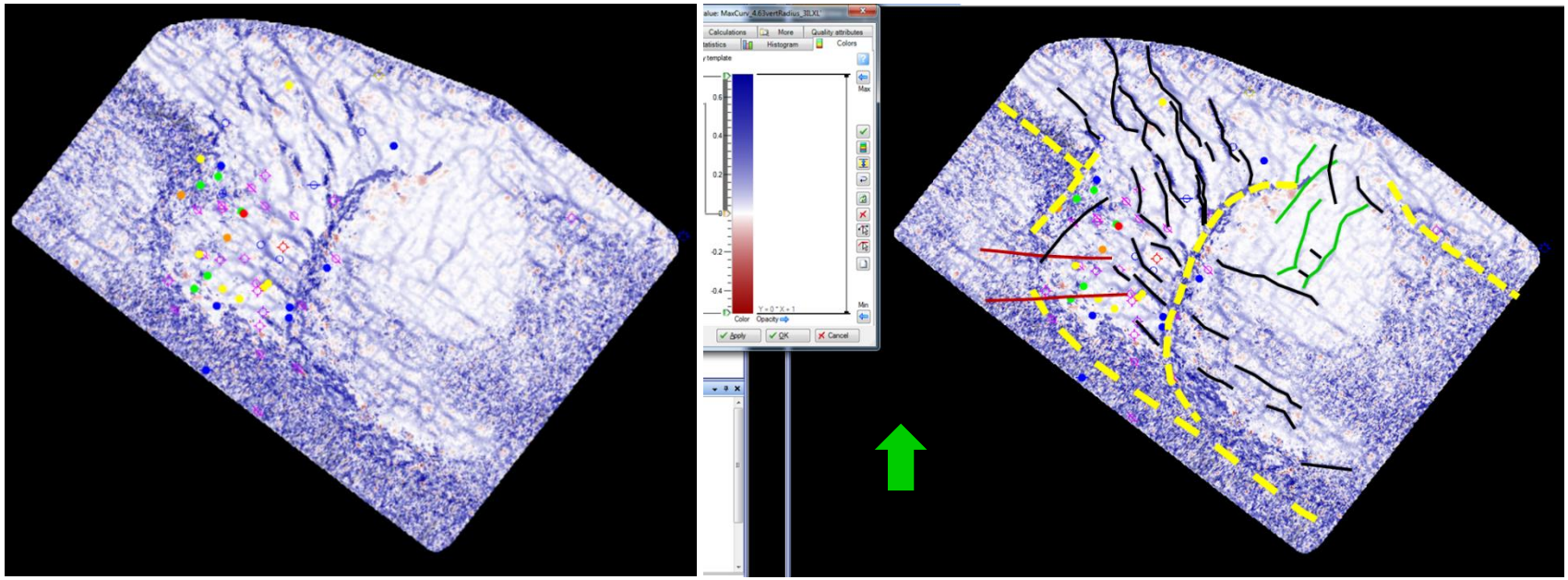

Figure 4.16. Map of maximum curvature on the top Niobrara horizon generated in Petrel. Positive values indicate positive or anticlinal features. Negative values indicate negative or synclinal features. On the left, wells targeting the Niobrara formation are overlain on top of the map. Open pink well symbols represent dry holes. Open pink circles with a slash through it represent abandoned wells. Filled circles represent productive wells and their colors represent the same initial production values listed in Figure 4.4 except for blue, which means the data was not available. Open blue circles represent planned wells. On the right, linear features observed on the maximum curvature attribute were mapped. The picks were supplemented by comparison to the minimum curvature, maximum curvature with different parameters, ant tracking, most positive curvature, and most negative curvature attribute maps on the same horizon. Any features that appeared to parallel the survey boundary were not included to avoid seismic acquisition footprints. Different colors are used for different orientations and do not reflect interpretations of what caused the features to form.

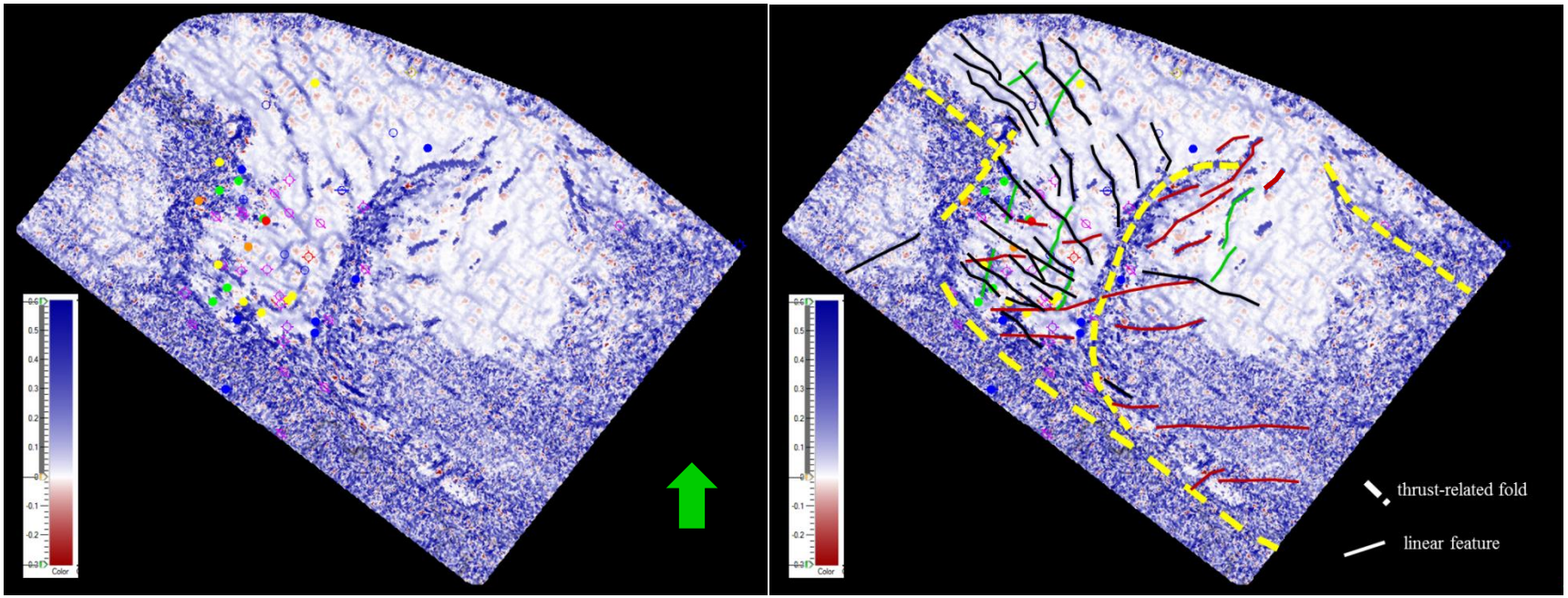

Predicted fracture orientation (red) for left lateral wrench fault rotated to match Tow Creek bench features

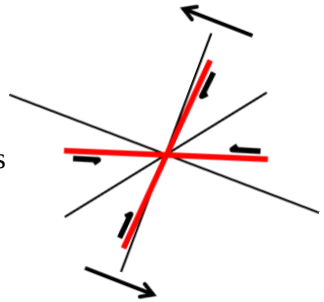

Figure 4.17. Map of maximum curvature on the top Tow Creek bench horizon generated in Petrel with left lateral strain ellipse diagram at bottom. Positive values indicate positive or anticlinal features. Negative values indicate negative or synclinal features. Well symbol description and linear feature mapping explanation same as in caption for Figure 4.16. There are more E-W trending features and NE trending features on this horizon than on the top Niobrara horizon and they match the expected orientations of a left lateral fault system. The SW-NE direction of compression predicted by the left lateral strain ellipse matches the observed larger SW displacement and smaller NW displacement.

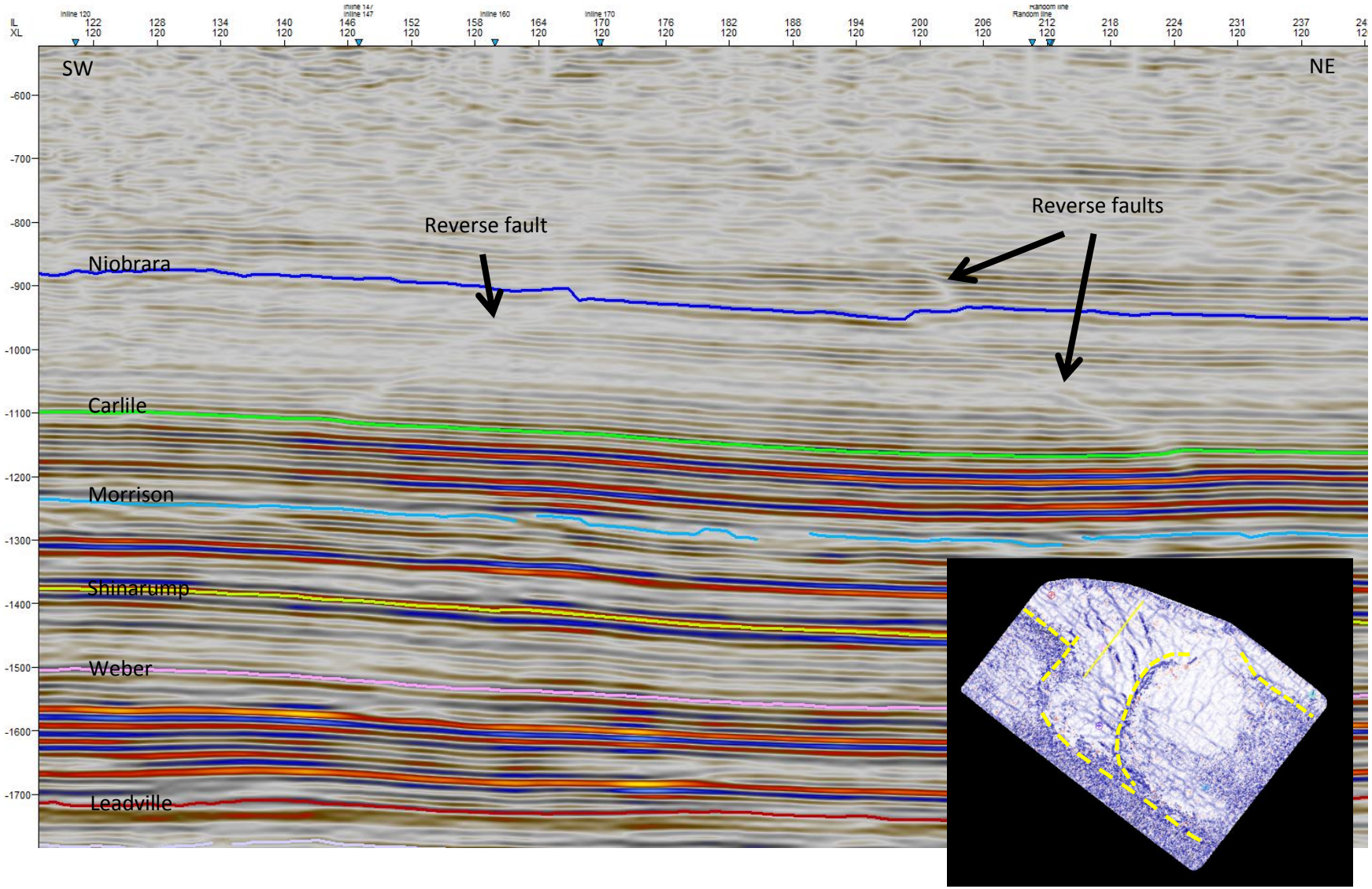

Figure 4.18. Close up of crossline 120 showing that the NNW-SSE trending linear features are reverse faults.

and top Tow Creek bench horizons (Fig 4.16 and 4.17). The sinuous linear features in the northern part of the survey area are still clearly visible and easy to map on the Kingdom attribute maps. A crossline shows that they are reverse faults (Fig. 4.18). The sinuosity of these reverse fault features reflect the transition from a reverse fault dipping in one direction to another dipping in the opposite direction. This alternating dip direction for the sinuous reverse faults may be a mechanism for distributing shortening evenly. Some of these reverse faults remain in the A Bench equivalent of the Niobrara and die out in the A Marl. Some cut all the way through the Niobrara and die out in the Carlile shale. These sinuous linear features seem to curve around the termination of Major Fault 2 and meet up with TFZ1, suggesting that they take up compensational shortening related to the transition from the Indian Run fault to Major Fault 2.

In addition to these sinuous features, there are several NW-SE trending features, a few E-W trending features, and a few NE-SW trending features. The E-W trending features on the top Niobrara horizon colored in dark red (Fig. 4.16) seem to lie between the Indian Run fault and TFZ2 and may be related to the relay ramp that connects the middle fault block to the most down dropped fault block. The NW-SE trending features parallel the Indian Run Fault, Major Fault 2, and Major Fault 3 very well and may be extensional features related to the formation of the Beaver Creek Anticline. The NE-SW trending feature that cuts across one of the E-W features parallels TFZ2 so is likely related to folding associated with that fault zone. The NE-SW features in green are perpendicular to the three major NW trending faults and are likely hinge perpendicular features related to the deformation associated with the formation of the Beaver Creek Anticline.

The mapped linear features on the top Tow Creek bench horizon (Fig. 4.17) shows slightly different feature sets. The sinuous NNW-SSE trending features still curve around Major Fault 2 and NW trending lines exist from the formation of the anticline. Unlike on the top Niobrara horizon, the E-W features on this horizon are much more numerous and do not seem to be related to the relay ramp. The orientations of the dark red E-W features and the green NE-SW features would match the orientations of fracture sets in a left lateral wrench fault at an orientation of 111°. The resulting direction of compression at 239° corresponds well with the much higher amount of displacement in the SW direction than in the NW direction along the five major faults.

The dark red linear features that trend NE appear to be horsetail features related to the

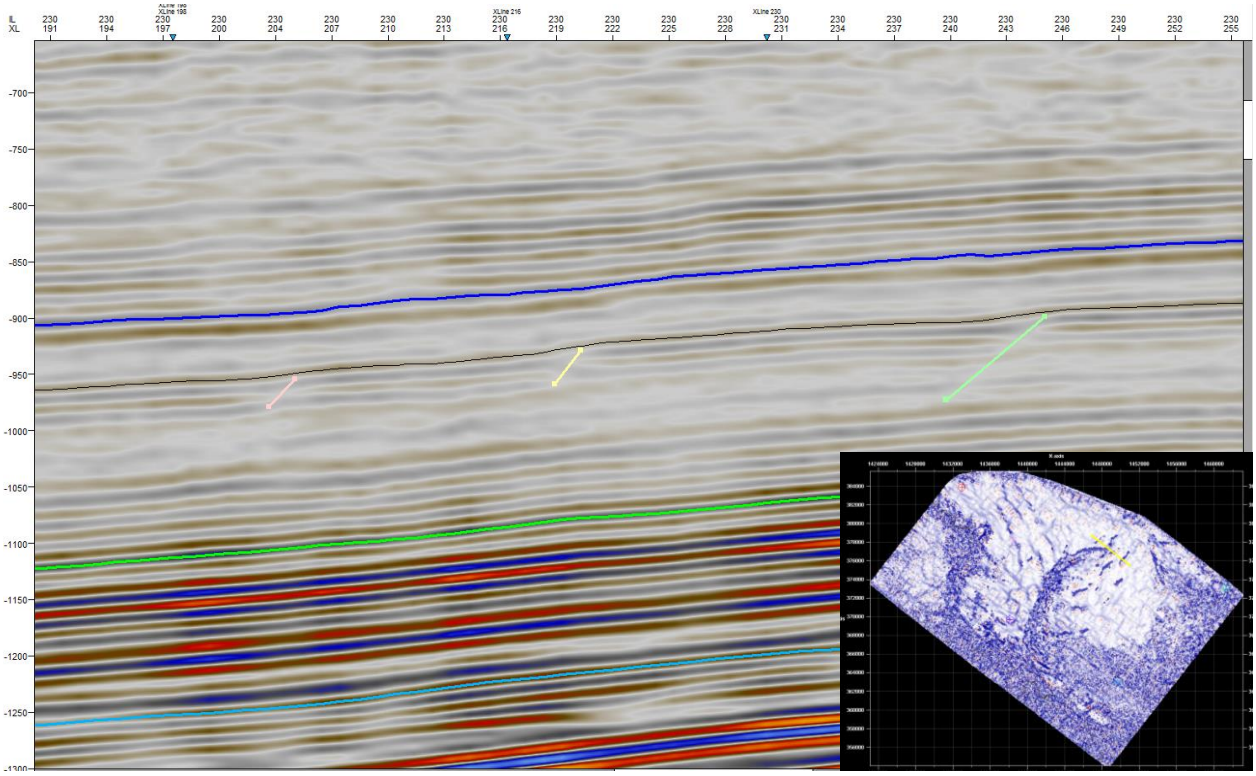

Figure 4.19. Close-up of inline 230 showing that the three linear features at the tip of TFZ1 are normal faults. Since these three linear features are at the tip of TFZ1, which is a reverse fault zone, you would expect the features to be reverse faults if they were formed from the same Laramide compression. Since they are not reverse faults, they likely formed after the end of Laramide compression during some kind of relaxation event. It is possible that any fractures that existed in that area may have been reactivated during the extensional event and would be worth exploring.

termination of the TFZ1 (Fig. 4.17). The horsetail features on the inside of TFZ1 are reverse faults, however, the three faults at the NE tip of TFZ1 are normal faults (Fig. 4.19). Since these three linear features are at the tip of TFZ1, which is a reverse fault zone, the features would be expected to be compressional if they had formed during the Laramide compression. Since they are not reverse faults, they likely formed after the end of Laramide compression during some kind of relaxation event. It is possible that any fractures that existed in that area may have been reactivated during the extensional event and would be worth exploring.

Combining the mapped linear features on Tow Creek bench with the Petra isopach map illustrates that the increase in thickness from 1070 ft in the eastern part of the survey to 1200 ft to the northwest is closely related to the folding and reverse faulting in the area (Fig. 4.20). For example, the thickest part of the well log isopach map coincides perfectly with the reverse faults in the northern part of the survey. Since well log depths are vertical, any dip in the bedding will increase the apparent thickness of the interval. This all suggests that the variations in thickness result from post-depositional shortening rather than from syn-depositional topography.

4.3.3 Isochron maps

To help ascertain the paleotectonic history of the study area, isochrons were calculated for four key intervals: Niobrara-Morrison, Morrison-Shinarump, Shinarump-Weber, Weber-Leadville, and Leadville-basement (Fig. 4.21).

The oldest time interval, Leadville-basement, comprises the Precambrian wedge that thickens toward the Indian Run fault. Note that the wedge is laterally restricted and does not appear to be present in the footwall side of the Indian Run Fault. The wedge also thickens toward the TFZ1 and seismic cross sections show that wedge consists of tilted, parallel beds that dip to the southwest and are truncated to the northwest (Fig. 4.21 Leadville-crystalline basement). The parallel beds and lack of onlap suggest that the Precambrian Uinta Mountain Group was deposited relatively horizontal and tilting occurred post-deposition (Fig. 4.13). The paleo-Indian Run Fault was probably a normal fault that allowed the beds to be rotated toward the fault. Later widespread erosion truncated the wedge and eroded the footwall strata.

Above the Precambrian wedge, the Pennsylvanian Weber-Leadville isochron thickens to the northwest as it crosses the TFZ1 and TFZ2 with an overall thickness change of 150ms (Fig. 4.21). Onlaps are not observed within the seismic in the Weber-Leadville interval and bedding is parallel, meaning that the interval does not have growth strata. The Weber-Leadville interval was

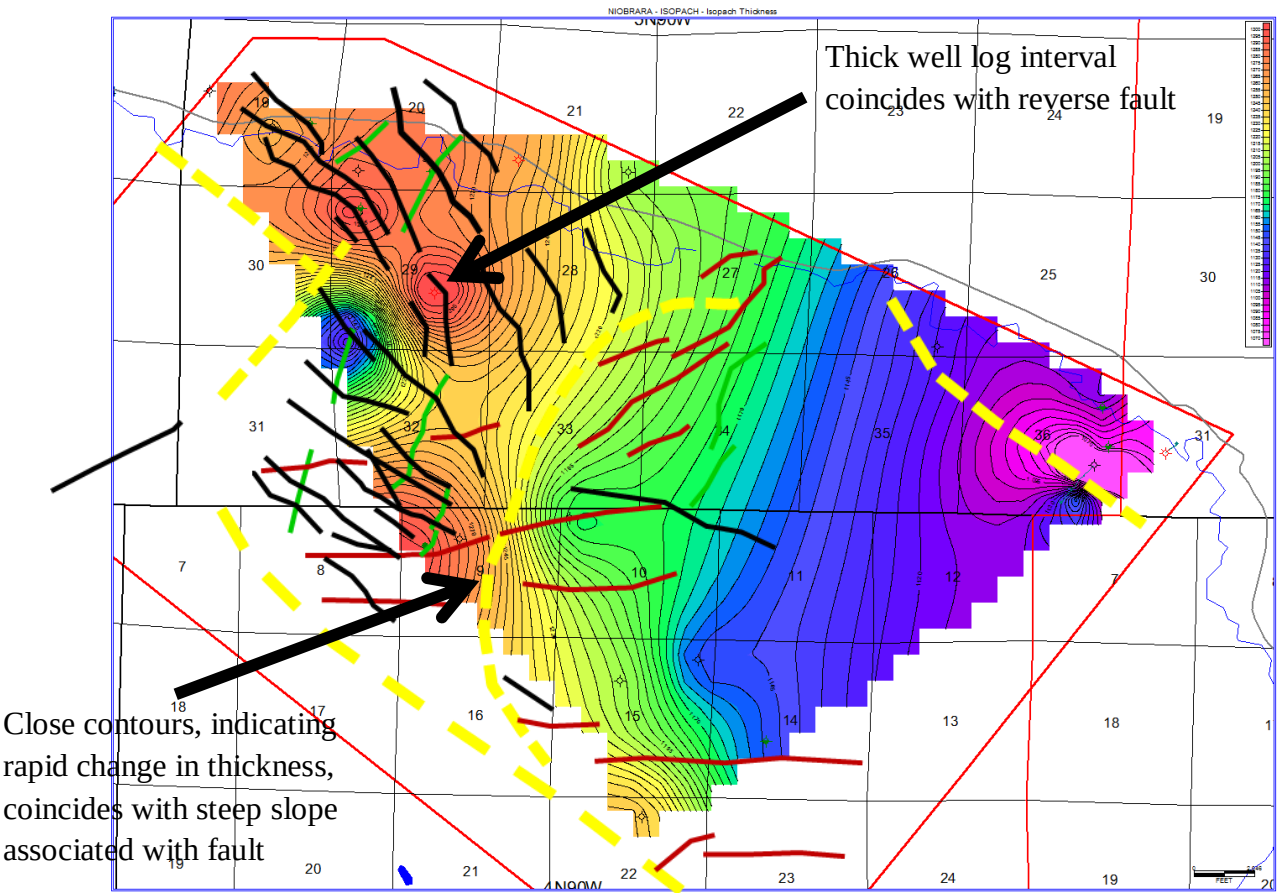

Figure 4.20. Maximum curvature on Tow Creek bench overlain on the Petra isopach map. This illustrates that the increase in thickness from 1070 ft in the eastern part of the survey to 1200 ft to the northwest is closely related to the folding and reverse faulting in the area. For example, the thickest part of the well log isopach map matches well with the reverse faults in the northern part of the survey. Not all reverse faults have thickness anomalies associated with them because well log data in that area is sparse. Since well log depths are vertical, any dip in the bedding will increase the apparent thickness of the interval. This all suggests that the variations in thickness result from post-depositional shortening rather than from syn-depositional topography.

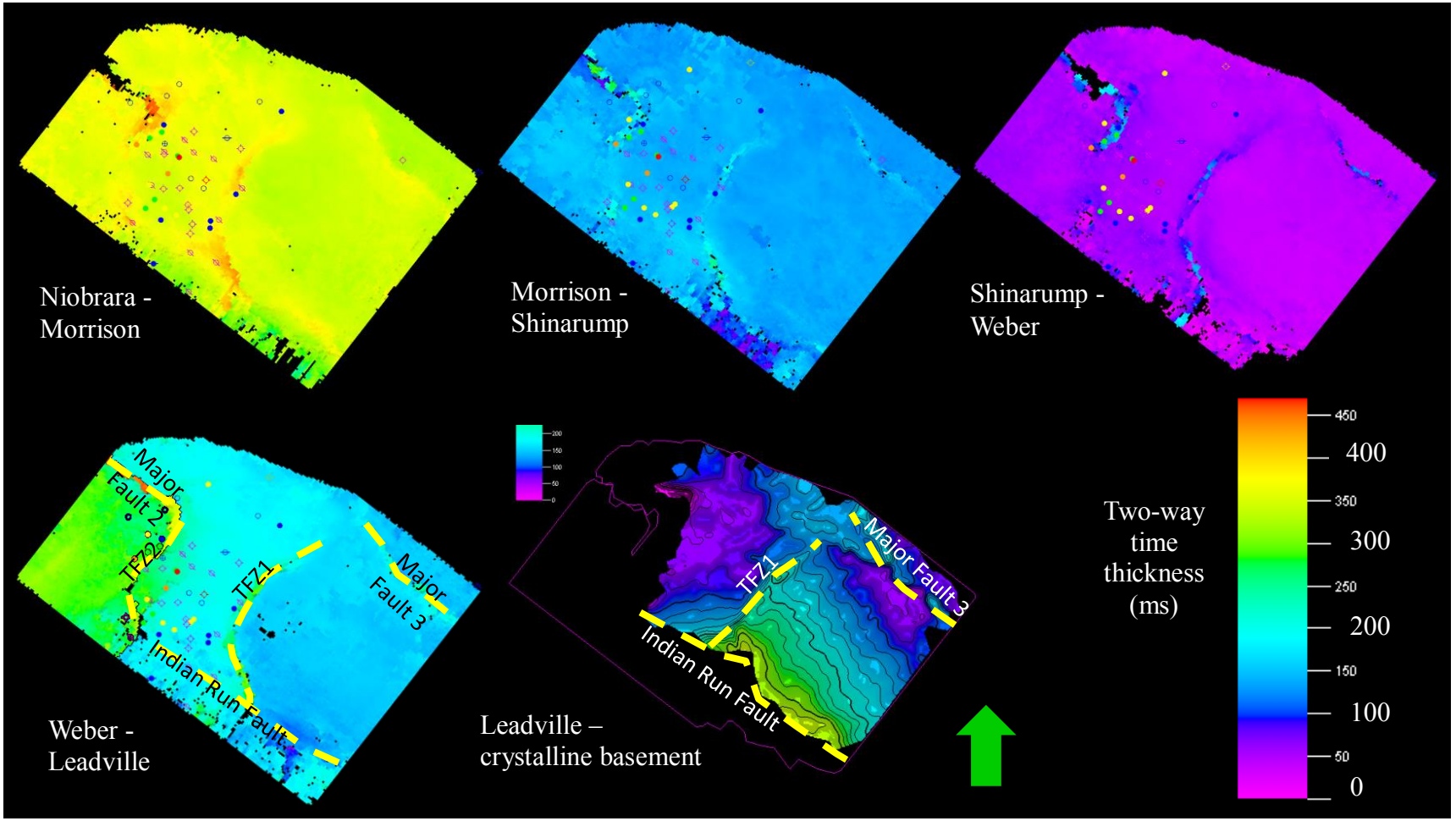

Figure 4.21. Isochron maps of five intervals. The Leadville-basement interval shows a Precambrian wedge thickening toward the Indian Run Fault and the TFZ2. The Weber-Leadville interval shows thickening toward the northwest at each fault block. The remaining three isochron maps show little to no thickness variation. All the intervals are shown on the same color scale for ease of comparison. The locations of the five major faults are mapped on the Weber-Leadville interval for reference. The Pennsylvanian age locations of the Indian Run Fault, TFZ1 and Major Fault 3 are shown overlain on the Leadville-crystalline basement to emphasize that these pre-existing structure did result in zones of weakness along which reactivation occurred to form later structures.

further separated into two isochrons (Minturn-Leadville and Weber-Minturn) to determine whether the paleo-tectonic controls on this thickness change existed throughout the Pennsylvanian (Fig. 4.22). The thickness changes in both the Weber-Minturn and Minturn-Leadville intervals are roughly equivalent suggesting that uplift and erosion occurred throughout the deposition of the Pennsylvanian strata. Since the intervals do not exhibit growth strata and the parallel bedding suggests that they were deposited horizontally, the thickness variations were likely caused by reactivation of pre-Pennsylvanian paleo-structures resulting in erosion of the hanging wall strata during the Pennsylvanian. All thickness changes in these two isochron maps match well with present day location of faults and structure suggesting that the paleo-structure was similar to present day structure. The paleo-faults from the Pennsylvanian and even Precambrian times likely became zones of weakness that were reactivated during later tectonic movement.

The other four key intervals were also separated into smaller isochrons to check if there were subtle paleo-tectonic controls on depositional thickness. All of these isochron maps displayed relatively constant thickness with no more than 10 ms of change except for in the Niobrara intervals. The maximum thickness variation in the Niobrara is 30 ms in the Buck Peak bench to Tow Creek bench isochron and these thickness variations follow the same trends as the mapped minor faults (Fig. 4.23). This suggests that the thickness variations in the Niobrara are related to post-depositional tectonics rather than syn-depositional controls. The Niobrara to Weber interval was likely a period of quiescence during which there was no local tectonic controls on deposition.

A summary of the tectonic history of the study area includes:

1. Relatively horizontal deposition of the Uinta Mountain Group.
2. Rifting and normal faulting that broke up and tilted the Uinta Mountain group deposits.
3. Uplift and widespread erosion of the Precambrian deposits leaving a preserved wedge of sediment.
4. Widespread horizontal deposition of Cambrian, Devonian, and Mississippian strata.
5. Widespread deposition of Pennsylvanian deposits with rapid uplift events and periods of erosion.
6. Long period of quiescence and widespread deposition through the Late Cretaceous.

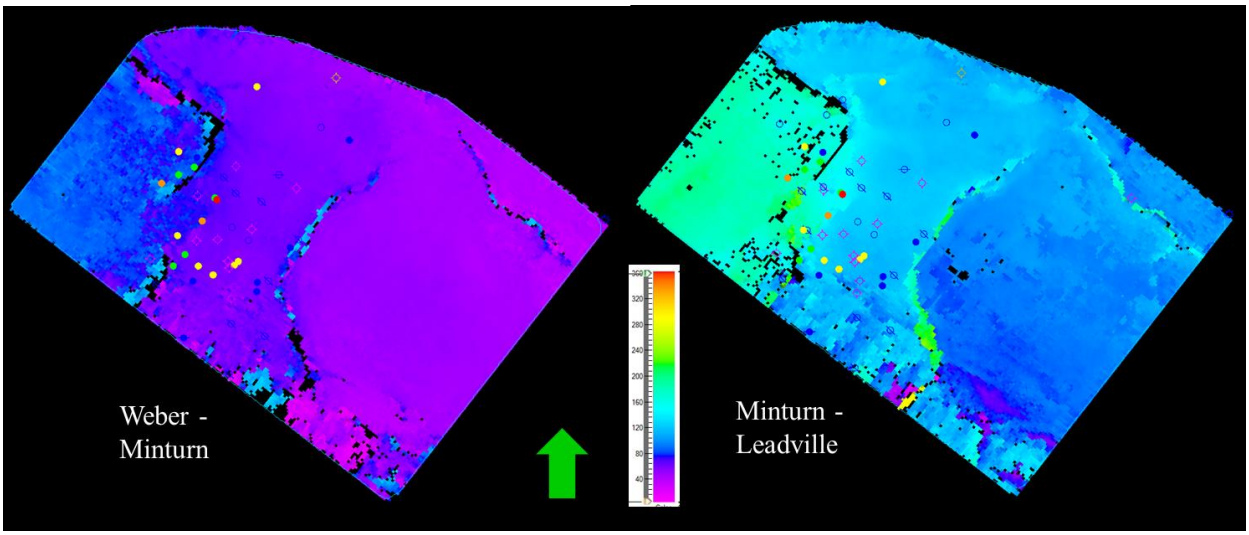

Figure 4.22 Isochron maps in Petrel of the Weber-Minturn and Minturn-Leadville intervals. The thickness changes in both of these intervals are roughly equivalent suggesting that uplift and erosion occurred throughout the deposition of the Pennsylvanian strata. Color scale bar ranges from 0 ms to 360 ms.

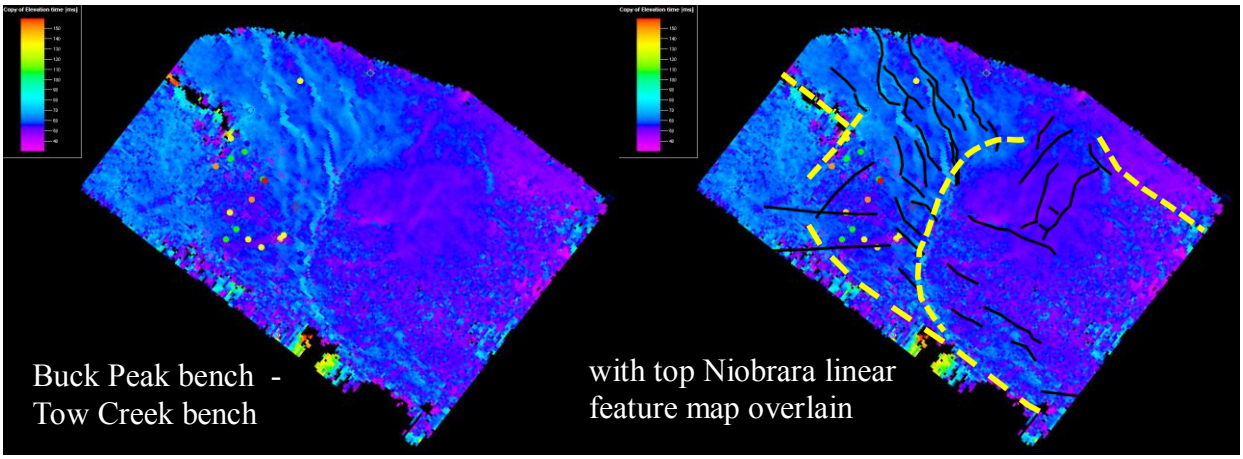

Figure 4.23. Isochron maps in Petrel of the Buck Peak to Tow Creek bench interval. On the right linear features present at the top Niobrara are overlain on the isochron map to illustrate that the thickness variations within the Niobrara are related to post-depositional structural features. Color scale bar ranges from 30 ms to 160 ms.

7. Laramide compression and uplift to present day structure.

4.4 3D Move model

A forward structural model was generated in Midland Valley's 3D Move program to test the viability of the proposed tectonic history, and to determine areas on the top Niobrara horizon that have experienced high strain based on this tectonic history. This could reveal potential high density fracture zones that would not otherwise be recognized based on simple fracture models of present-day structure. As noted in Chapter 3, there were many limitations to the way the model was set up. Additionally the program assumed that strata were translated along faults and does not incorporate any deformation along the fault itself.

Starting from the northwest, the strain analysis map shows strain related to multi-directional compression from Major Fault 2 and TFZ2 (Fig. 4.24). As mentioned before, the largest depth change occurs here in a short distance and high strains would be expected. Next there is a high strain anomaly in the middle fault block that may be related to being wedged between TFZ1, TFZ2, and the Indian Run Fault while being affected by the transfer of shortening from the Indian Run Fault to Major Fault 2. To the southwest there is a complex strain that crisscrosses associated with the mix of strains from the terminations of TFZ1 and TFZ2.

There are also strain anomalies paralleling TFZ1 near the crest of the anticline. To the east there are linear strain features paralleling Major Fault 3. Finally, to the southeast there is an edge effect from the end of where TFZ1 was digitized and this is not a true geologic feature.

Curvature analysis helps to determine the accuracy of the strain model is (Fig. 4.25). Areas of high curvature on the top and middle fault block seem to be slightly offset from where you would expect it to be but overall curvature trends parallel or are constrained by the location of the major faults. There are even E-W trending linear features on the curvature analysis map of the model that match the E-W trending features mapped from the curvature attribute map of the top Tow Creek Bench.

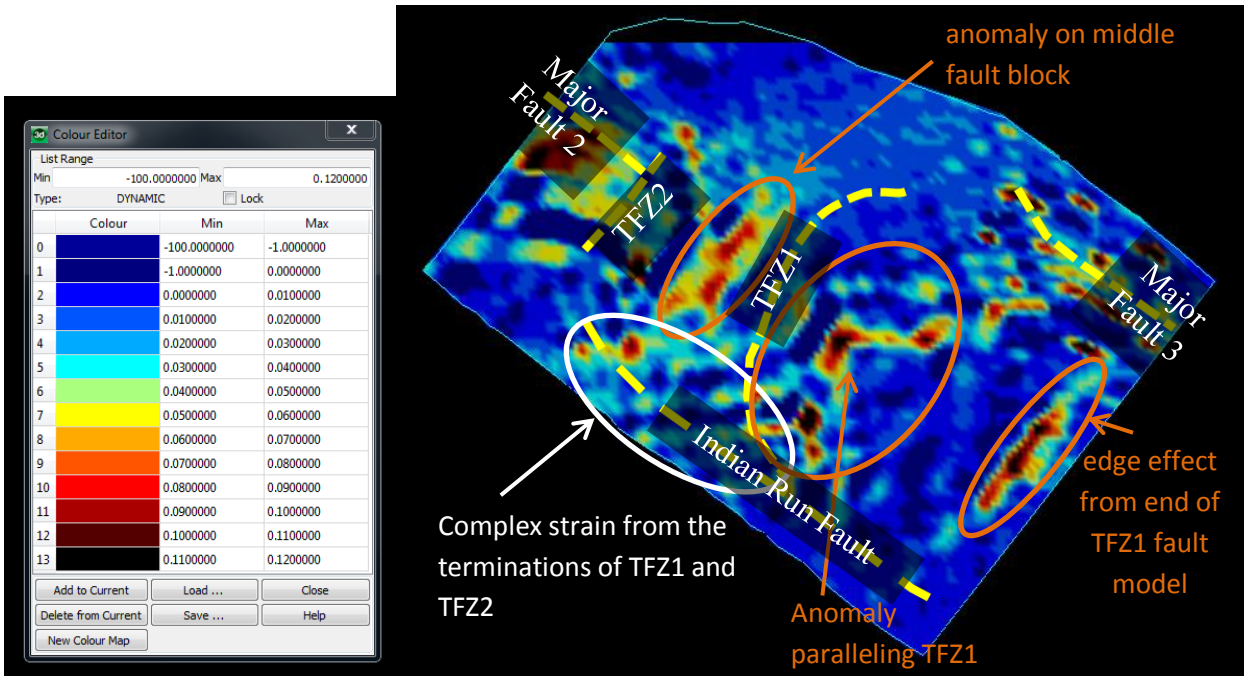

Figure 4.24. Strain analysis run in 3D Move on the forward modeled top Niobrara surface.

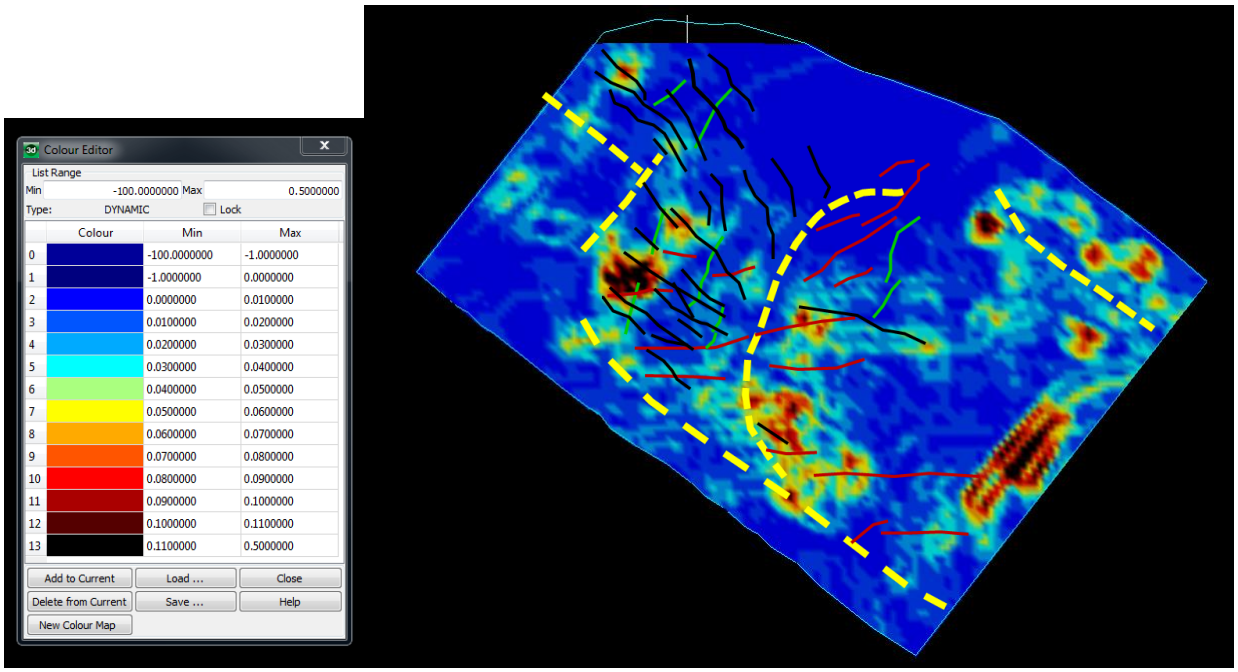

Figure 4.25. Curvature analysis run in 3D Move on the forward modeled top Niobrara surface.

CHAPTER 5
DISCUSSION

5.1 Fracture prediction

This study area is strongly controlled by the pre-existing structures that result in complex stress and strain distributions. In some cases these complex relationships allowed better production and in some cases they resulted in diagenetically cemented fractures. The following section discusses features most closely related with good production and will make inferences about fractures.

5.1.1 Curvature anomalies and production trends

Since the 51 foot resolution of the seismic limits the resolvable structural features to faults, a combination of production maps, models, and structure maps was used to determine areas with high density fracture zones within the study area. Based on the simple fold diagram model by Zahm and Hennings (Fig. 2.12), you would expect fractures to exist in the highest curvature areas of the larger structures. There are two production trends on the southwest and northwest sides of the middle fault block associated with the highest positive curvature from folding above the Indian Run fault and TFZ2 (Fig 5.1). The best producing well (red dot) is in the center of the fault block, offset from the crest, meaning curvature is not the only control on productivity.

Unlike productive wells studied by Vincelette and Foster, the Waddle Creek oil wells are not associated with normal faults formed during Neogene extensional tectonics, although this does not preclude the existence Neogene extensional fractures and their influence on productivity. Fracture formation likely resulted from the complex stresses and strains in the transition zone. Based on the location of productive wells in relation to the mapped linear features (Fig. 4.17), most of the productive wells in the middle fault block lie along the E-W trending dark red features or the NE-SW trending green features. As discussed in Chapter 4, these two trends match the angles expected for fractures formed in a left lateral wrench fault system suggesting that these linear features reflect zones of weakness resulting from the presence of fractures. The overall regional compressional direction during the Laramide orogeny was E-W, but because the study area had pre-existing zones of weakness from the paleo-Indian Run Fault, reactivated

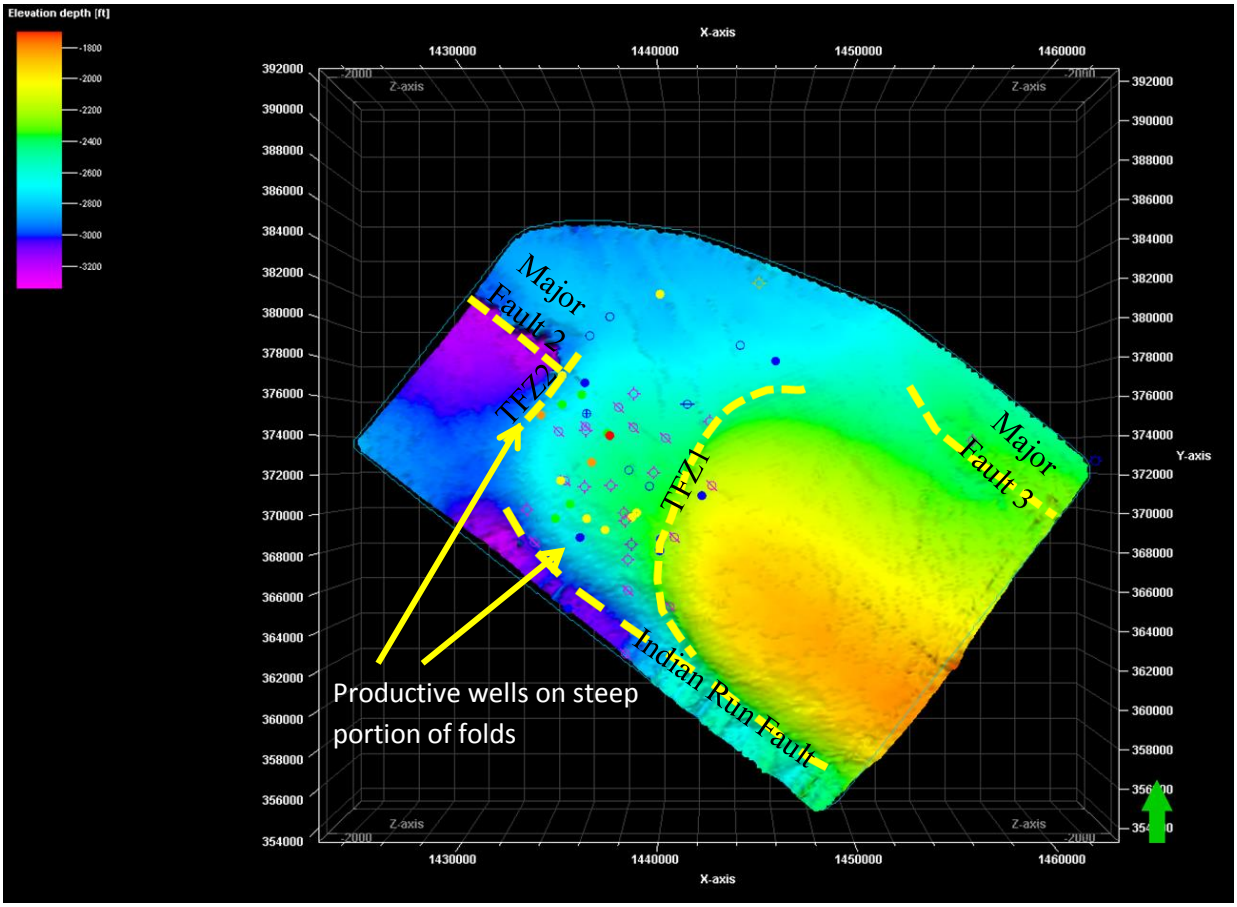

Figure 5.1. Wells targeting the Niobrara Formation superimposed on the top Niobrara structure map with IP data overlain.

movement was transpressional rather than pure dip-slip.

The sinuous NNW-SSE trending features in the northern half of the survey have not been explored much but the one well that was drilled close to one of the features was a dry hole. As discussed in Chapter 4, these features are likely Laramide-age compressional features that take up compensational shortening as part of the transition from the Indian Run fault to the Major Fault 2. A producing well was drilled between two of these reverse fault features but not directly through one and it is closer to one of the NE-trending features that may be fracture-related. While the data is sparse, the lack of productivity along these may be explained by Vincelette and Foster's hypothesis that Laramide-age compressional features are often times cemented because the uplift allowed meteoric waters easy access to the then permeable faults. Similarly the NW-SE trending linear feature that continues along the trend of Major Fault 2 has two dry holes and is likely also a Laramide-age reverse fault that has been cemented.

Three wells drilled along the high curvature anomaly associated with the folding from TFZ1 were oil producers (Fig. 5.1). Three more wells were drilled along the TFZ1 high curvature anomaly although neither production nor well status were reported for those wells. One well drilled along the TFZ1 curvature anomaly was dry however that well is also near the NNW-SSE trending reverse faults that may be Laramide-age reverse faults that Vincelette and Foster (1992) associate with cementation.

If we look at cumulative production and first 12 months production trends in comparison to the mapped linear features (Fig. 5.2 and 5.3), the red and orange wells that have been the most productive do not target the intersection of many linear features but only lie along one dark red linear feature or one green linear feature. In contrast, the purple wells that have been the least productive with only 10-100 bbls of cumulative oil production lie at the intersection of many linear features. The poor production from these two wells and the two dry wells near them may have resulted from intense fracturing that was initially very permeable but cemented up due to increased fluid flow. Wells that were drilled offset from any of the linear features and wells that only penetrated NW-SE features were also dry. Since the NW-SE trending features parallel the Indian Run Fault, the dry holes suggest that the parallel fractures created from the anticline formation are not open in the present day.

Some areas that have not yet been explored but may be worth pursuing include the horsetail feature at the northeast end of TFZ1. While the linear features on the inside of the TFZ1 curve are all reverse features and may have been cemented up, the three northeastern-most features at the end of TFZ 1 are all normal faults. Vincelette and Foster noted that normal faults related to post-Laramide Neogene extension typically had better production as a result of reactivated fractures. For this reason, these three normal faults may be worth exploring.

Similarly, the long E-W trending feature that cuts across the TFZ1 is a normal fault. There is production along this fault in the portion that lies in the middle fault block. Since normal faults have been identified as features that reopen fractures, exploration companies should consider following this normal fault up onto the top fault block to the east. This is risky since the productive wells are all in the complex transition zone and have other cross cutting features that may affect their productivity.

It may also be worth extending exploration of the production trend along TFZ2 further down dip (northwest). The existing production trend likely benefits from the complex interaction

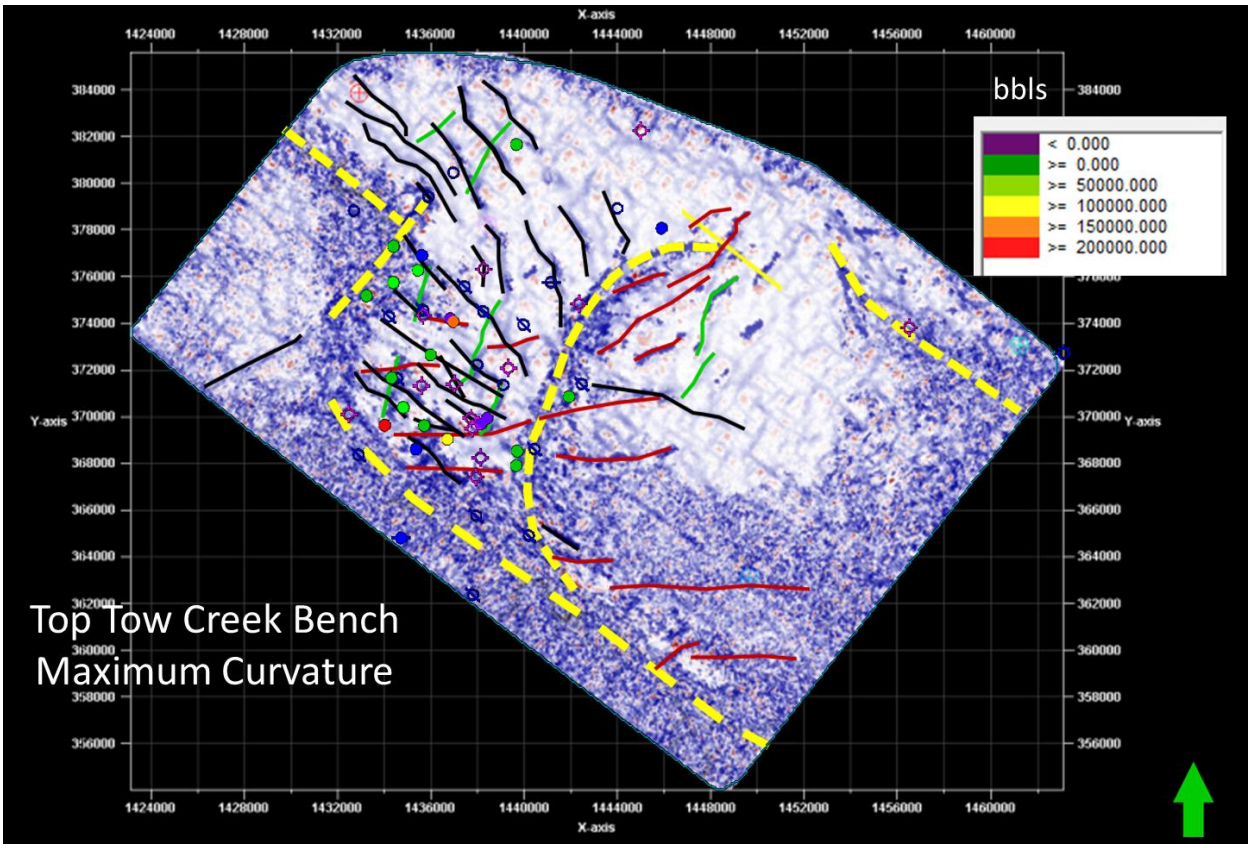

Figure 5.2. Cumulative production (bbls) mapped on top of the Top Tow Creek Bench maximum curvature attribute map with mapped linear features. Wells with the highest cumulative production only pass through one linear feature whereas non-productive wells pass through only the NNW-SSE and NW-SE trending features that may be cemented, the intersection of many linear features, or no linear features at all. This suggests that there must be a balance between too much and too little structuring.

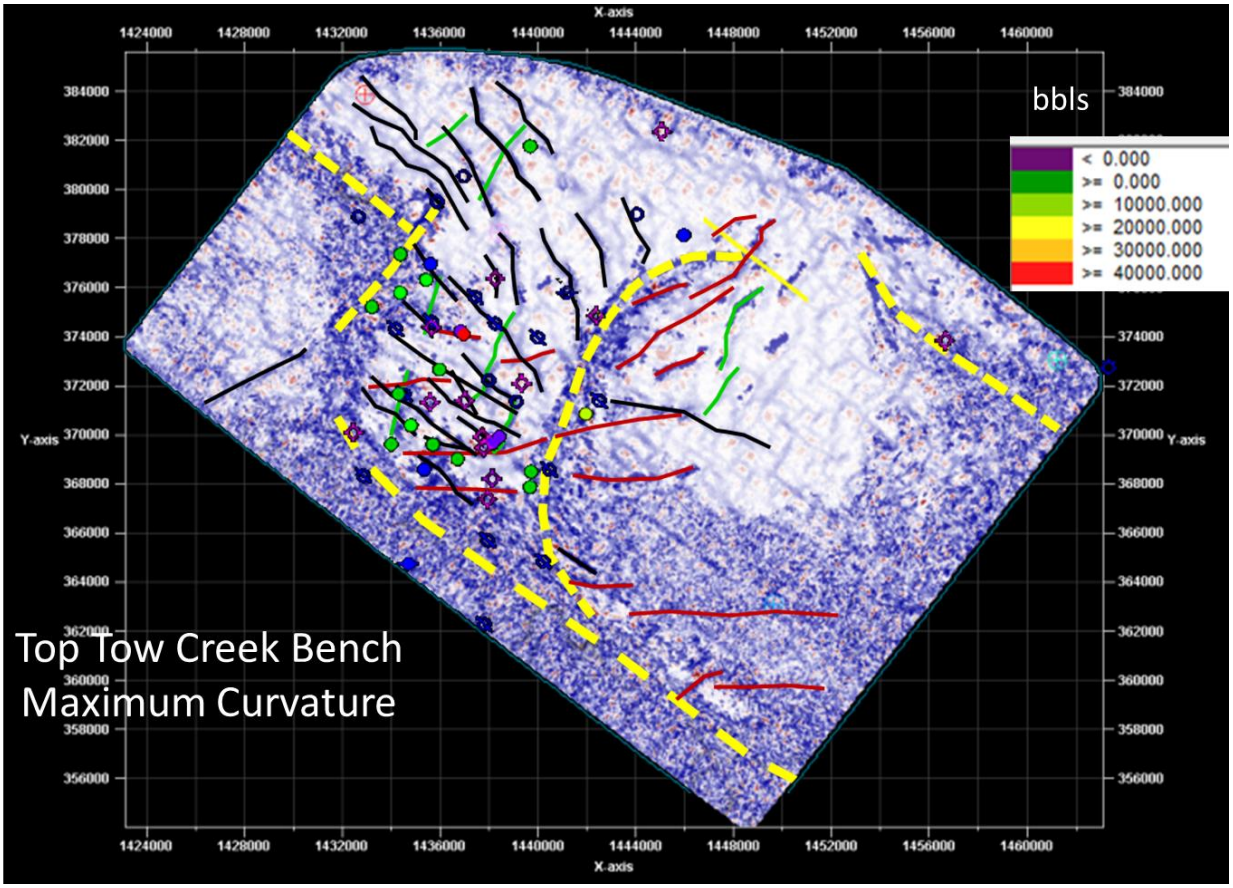

Figure 5.3. First 12 months production (bbls) mapped on top of the Top Tow Creek Bench maximum curvature attribute map with mapped linear features.

between TFZ2 and Major Fault 2 that may have formed fractures and due to the lack of larger through-going faults they do not seem to have been cemented. Since this is a continuous oil accumulation, extending exploration down dip would be a logical next step.

5.1.2 Strain analysis

Since curvature analysis of present-day structure does not reflect potential fracture zones from past structures, it is important to produce a forward model that will help capture fracture formation in the past. The strain map with the Niobrara wells superimposed on top helps shed light on the importance of past strain on production (Fig. 5.4). Based on the relationship observed on this map, the following may be concluded:

- wells drilled in areas with very high strain (orange to red) were dry
- wells drilled in areas with little to no strain (medium to dark blue) were also dry

- wells drilled in areas with mild strain (blue) produced but with lower initial production values
- wells drilled in areas with moderate strain (yellow) produced with higher initial production values

These are, of course, generalizations but very high strain areas should be avoided. High strain areas may fracture the reservoir too severely, allowing water flow resulting in cementation and poor production. Based on these results and the results of the curvature analysis, it seems that the best fracture zones are those generated from strike-slip stresses and strains. Features directly related to compression may have resulted in intense fracturing and faulting that accommodated sustained, strong water flow causing cementation. Less intense fracturing allows enough permeability for hydrocarbon production but not enough for diagenetic cementation.

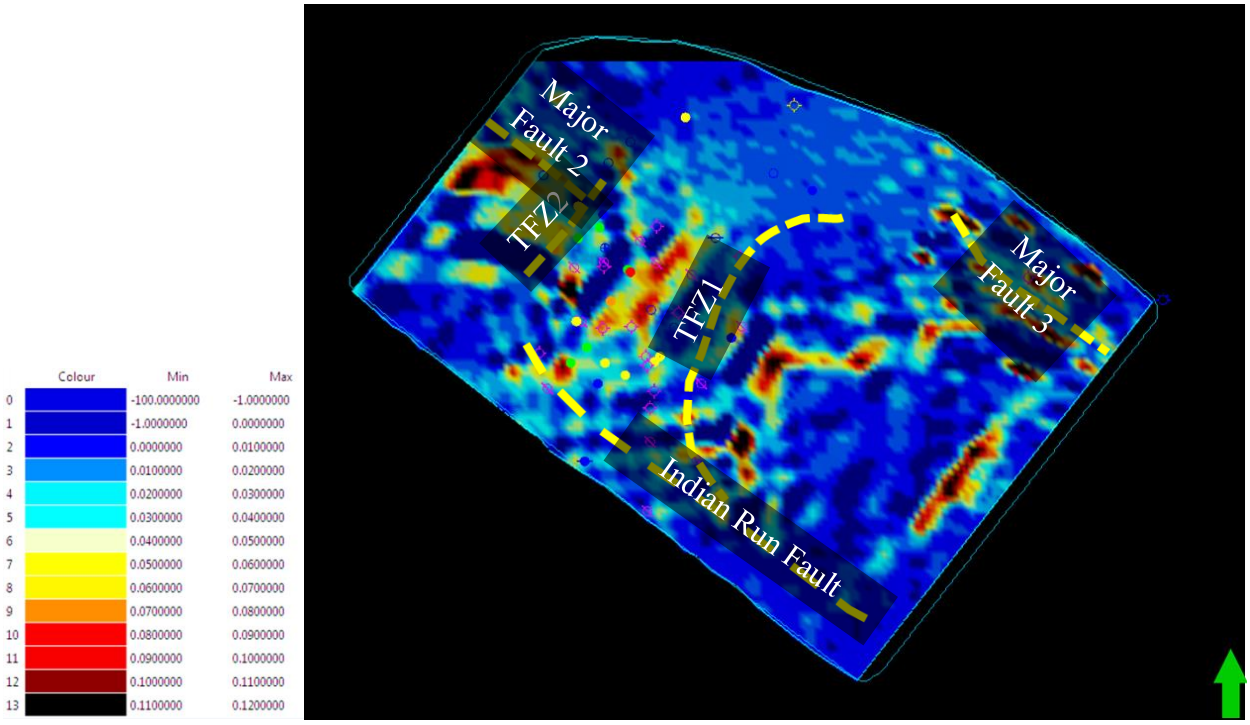

Figure 5.4. Wells that targeted the Niobrara Formation superimposed on the 3D Move strain analysis map.

5.2 Paleo-tectonic history

In Chapter 4, a basic paleo-tectonic history was developed based on isochron thickness and observation of geometric relationships in seismic cross-sections. In table 5.1, the simple

interpretation of "extension, quiescence, compression, etc." is coupled with regional tectonic activity to determine the events that caused these local variations.

Table 5.1. Comparison of the local tectonic events within the larger regional structural history.

Time interval	Local tectonics/geometries	Regional event
Neogene	Not observed at seismic resolution	NE-SW extension
Late Cretaceous-M. Tertiary	Reactivation of previous structures with more strike-slip component	Laramide Orogeny
Permian-Late Cretaceous	Widespread deposition	Quiescence (craton followed by widespread marine transgression)
Pennsylvanian	Widespread deposition with uplift and erosion (no growth strata observed)	Ancestral Rockies: reactivates NW-SE fabric
Cambrian-Mississippian	Widespread deposition	Quiescence
Precambrian	Horizontal deposition of Uinta Mountain Group, extension and tilting of Uinta Mountain group deposits, widespread erosion	Rifting during formation of Uinta aulacogen forms NW-SE fault

The larger change in structural depth toward the northwest in present day structure than in thickness changes in the Weber-Leadville interval suggests that the NW-SE component of shortening is much greater in present day than during the Ancestral Rockies orogeny. This suggests that there was a larger strike-slip component during the Laramide orogeny than during previous tectonic events, which were more dip-slip.

The joint set orientations from surface mapping around the study area (Fig. 2.11) suggest that there is a SW-NE compressional component and a NW-SE compressional component that is governed by the pre-existing fault orientations. This would fit with the interpretation of the study area if the overall E-W compression from the Laramide orogeny were split into two vector components that are perpendicular to the pre-existing faults and stress was distributed accordingly.

During the Laramide orogeny, the NW-SE features formed during the Proterozoic rifting and Ancestral Rockies uplift were likely enhanced by the northeast edge of the rigid Colorado Plateau as it was pushed toward the east. The Colorado Plateau may have acted as a buttress for the pre-existing features allowing compression to be distributed in one vector perpendicular to the Major Indian Run Fault and one vector parallel to the Major Indian Run Fault accounting for both NE-SW compression that formed the Beaver Creek Anticline and left lateral strike slip movement that broke the anticline into fault blocks.

CHAPTER 6
CONCLUSIONS

6.1 Conclusions

1. The study area experienced three main tectonic events: 1) rifting from the Uinta Aulacogen, 2) Pennsylvanian uplift and erosion related to the Ancestral Rockies, and 3) the more recent Laramide Orogeny. Between each tectonic event were periods of quiescence during which widespread, horizontal deposition occurred.
2. The direction of compression in the study area is estimated to be 239° (WSW) based on the direction of the potential strike-slip fracture features. Compression is interpreted to be split into two components that are perpendicular to the major pre-existing faults in the area allowing for strain partitioning. This was reinforced by the rigid Colorado Plateau as it was pushed toward the east and acted as a buttress for the pre-existing NW-SE trending features.
3. Laramide-age reverse fault features likely resulted in cementation of nearby fractures and would not be conducive to oil and gas production.
4. The predicted best producing linear features visible in attribute maps are features that line up with predicted conjugate fracture sets from left lateral strike-slip. The southern edge of the Sand Wash basin, which runs along the axial anticline, should have transpressional movement similar to this study. This is possibly a result of the more rigid Colorado plateau being pushed to the east and reinforcing the NW-SE fabric that would not typically be expected from the E-W direction of compression.
5. Unexplored portions in the survey area that are worth pursuing include down dip of TFZ2 and the tip of TFZ1.

6.2 Recommended future work

1. Conduct surface fracture mapping over the study area to help validate or disprove the conjugate fracture set from the left lateral wrench fault model presented in this study.
2. Produce a regional correlation of the Niobrara to determine whether the three benches in the Sand Wash basin are time equivalent to the three chalk benches in the Denver basin.

3. Analyze a core of the Niobrara in or near the study area to check the top picks, determine whether fractures are open or closed, and to better understand the mechanical properties of the rock based on lithology.
4. Incorporate new production data as companies continue to explore the area and conduct a more detailed analysis of well and production data in the area to better understand the controls on productivity
5. Analyze fluid inclusions to determine whether excessive fracturing may have resulted in increased flow and ultimately cementation of the fractures.

REFERENCES CITED

Angster, S.J., 2010, Fracture analysis of the Bakken Formation, Williston basin, field studies in the Little Rocky Mountains and Big Snowy Mountains, MT, and Beartooth Mountains, WY, and 3D seismic data, Williston Basin, Master's thesis, Colorado School of Mines, Golden, Colorado, 85 p.

Bruchez, K., 2012, Regional outcrop correlation of the Niobrara Formation northwestern Colorado, Master's thesis, Colorado School of Mines, Golden, Colorado, 108 p.

Finn, T. M. and R.C. Johnson, 2005, Niobrara total petroleum system in the southwestern Wyoming province, *in* USGS Southwestern Wyoming Province Assessment Team, Petroleum Systems and Geologic Assessment of Oil and Gas in the Southwestern Wyoming Province, Wyoming, Colorado, and Utah: USGS Digital Data Series DDS-69-D, Ch. 6, p. 1-23.

Klepacki, D., 2012, Application of seismic volumetric curvature - a summary of attribute definitions, attribute equivalency, and parameterization in common industry software: The Bakken – An Unconventional Petroleum and Reservoir System Project, DOE DE-NT0005672, 28 p.

Landon, S.M., M.W. Longman, and B.A. Luneau, 2001, Hydrocarbon source rock potential of the Upper Cretaceous Niobrara Formation, Western Interior Seaway of the Rocky Mountain region: The Mountain Geologist, v. 38, no. 1, p. 1-18.

Longman, M.W., B.A. Luneau, and S.M. Landon, 1998, Nature and Distribution of the Niobrara lithologies in the Cretaceous Western Interior Seaway of the Rocky Mountain Region: The Mountain Geologist, v. 35, no. 4, p. 137-170.

Morel, J.A., P.H. Bursk, and D.L. Dlouhy, 1986, An interpretation of the subsurface structural style of the Beaver Creek Anticline, Moffat and Routt Counties, Colorado, *in* Stone, D.S., and K.S. Johnson, eds. New Interpretations of Northwest Colorado Geology, p. 195-201.

Robertson, G.C., D.W. McDermott, and R.L. Tang, 1995, Model-based, 2-D seismic definition of subthrust structure in the Uranium Peak area, northwest Colorado, *in* Ray, R.R., et al., eds., High-definition seismic: 2-D, 2-D swath, and 3-D case histories: Denver, Colorado, Rocky Mountain Association of Geologists, p. 47-57.

Stone, D.S., 1986, Seismic and borehole evidence for important pre-Laramide faulting along the Axial Arch in northwest Colorado, *in* Stone, D.S., and K.S. Johnson, eds., New interpretations of northwest Colorado geology, p. 19-36.

Strasen, J.L., 2012, Petrologic analyses of core samples-Laramie Energy, Fletcher Gulch Federal 04-24-2H well, Rio Blanco Country, Colorado: Houston ATC Job File No. 120499G, Core Laboratories, Inc, 35 p.

Tweto, Ogden, 1979, Geologic map of Colorado: U.S. Geological Survey, scale 1:500,000.

Vincelette, R.R., and N.H. Foster, 1992, Fractured Niobrara of northwestern Colorado, *in* Schmoker, J.W., E.B. Coalson, and C.A. Brown, eds. Geological studies relevant to horizontal drilling-Examples from western North America: Rocky Mountain Association of Geologists Guidebook, p. 227-239.

Zahm, C.K., and P.H. Hennings, Complex fracture development related to stratigraphic architecture: Challenges for structural deformation prediction, Tensleep Sandstone at the Alcova anticline, Wyoming: AAPG Bulletin, v. 93, no. 11, p. 1427-1446.